AD-A156 693 THE ATCHAFALAYA RIVER DELTA REPORT 10 WAVE HINDCASTS MAIN TEXT AND APPEND.. (U) ARMY ENGINEER WATERWAYS EXPERIMENT STATION VICKSBURG MS HYDRA.. R E JENSEN 1/2

UNCLASSIFIED MAR 85 WES/TR/HL-82-15/10 F/G 8/3 NL

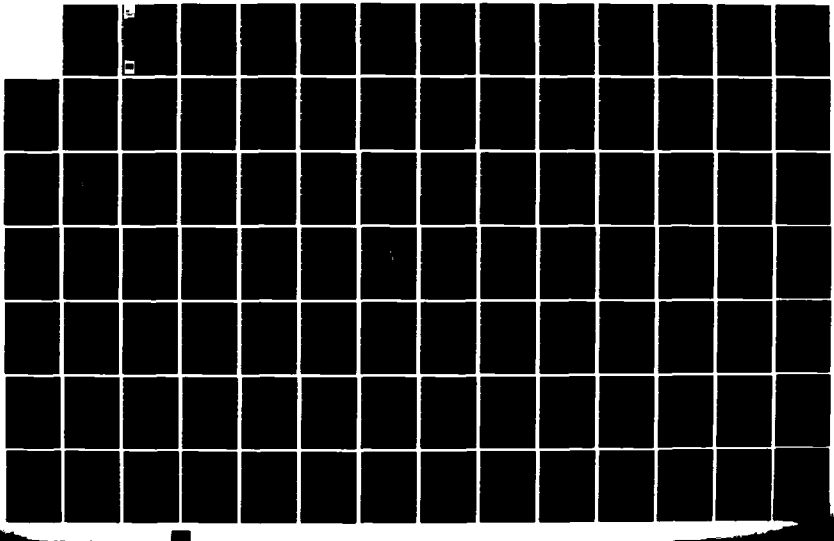

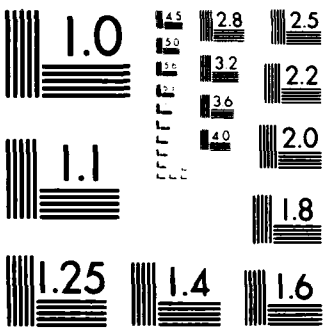

TECHNICAL REPORT HL-82-15

THE ATCHAFALAYA RIVER DELTA

Report 10
WAVE HINDCASTS
MAIN TEXT AND APPENDICES A AND B

by

Robert E. Jensen

Coastal Engineering Research Center

DEPARTMENT OF THE ARMY
Waterways Experiment Station, Corps of Engineers
PO Box 631
Vicksburg, Mississippi 39180-0631

March 1985
Report 10 of a Series

Prepared for US Army Engineer District, New Orleans
New Orleans, Louisiana 70170

Monitored by Hydraulics Laboratory
US Army Engineer Waterways Experiment Station
PO Box 631
Vicksburg, Mississippi 39180-0631

Destroy this report when no longer needed. Do not return it to the originator.

The findings in this report are not to be construed as an official Department of the Army position unless so designated by other authorized documents.

The contents of this report are not to be used for advertising, publication, or promotional purposes. Citation of trade names does not constitute an official endorsement or approval of the use of such commercial products.

Unclassified

SECURITY CLASSIFICATION OF THIS PAGE (When Data Entered)

REPORT DOCUMENTATION PAGE

READ INSTRUCTIONS BEFORE COMPLETING FORM

1 REPORT NUMBER: Technical Report HL-82-15

2 GOVT ACCESSION NO: AD-A156 693

3 RECIPIENT'S CATALOG NUMBER:

4 TITLE (and Subtitle): THE ATCHAFALAYA RIVER DELTA; Report 10, WAVE HINDCASTS--MAIN TEXT AND APPENDICES A AND B

5 TYPE OF REPORT & PERIOD COVERED: Report 10 of a series

6 PERFORMING ORG. REPORT NUMBER:

7 AUTHOR(s): Robert E. Jensen

8 CONTRACT OR GRANT NUMBER(s):

9 PERFORMING ORGANIZATION NAME AND ADDRESS: US Army Engineer Waterways Experiment Station, Coastal Engineering Research Center, PO Box 631, Vicksburg, Mississippi 39180-0631

10 PROGRAM ELEMENT, PROJECT, TASK AREA & WORK UNIT NUMBERS:

11 CONTROLLING OFFICE NAME AND ADDRESS: US Army Engineer District, New Orleans, PO Box 60267, New Orleans, Louisiana 70160

12 REPORT DATE: March 1985

13 NUMBER OF PAGES: 108

14 MONITORING AGENCY NAME & ADDRESS (if different from Controlling Office): US Army Engineer Waterways Experiment Station, Hydraulics Laboratory, PO Box 631, Vicksburg, Mississippi 39180-0631

15 SECURITY CLASS. (of this report): Unclassified

15a DECLASSIFICATION/DOWNGRADING SCHEDULE:

16 DISTRIBUTION STATEMENT (of this Report)

Approved for public release; distribution unlimited.

17 DISTRIBUTION STATEMENT (of the abstract entered in Block 20, if different from Report)

18 SUPPLEMENTARY NOTES

A limited number of copies of Appendix C were published under separate cover. Copies of this report and Appendices A and B are available from National Technical Information Service, 5285 Port Royal Road, Springfield, Virginia 22161

19 KEY WORDS (Continue on reverse side if necessary and identify by block number)

Atchafalaya Bay
Measured wave data
Shallow water spectral wave modeling
Wave hindcast statistics

20 ABSTRACT (Continue on reverse side if necessary and identify by block number)

A wave-measurement system was deployed in Atchafalaya Bay, Louisiana, for the purpose of determining the wave climate within the bay [illegible] meters or less in length. The wave data were then used as the basis for development and verification of a shallow water wave hindcast model. The hindcast model along with 1 year of measured wind information was used to generate 1 year of climatological wave information for 13 locations in the bay.

DD FORM 1 JAN 73 1473 EDITION OF 1 NOV 65 IS OBSOLETE

Unclassified

SECURITY CLASSIFICATION OF THIS PAGE (When Data Entered)

PREFACE

This report documents the processes by which the US Army Engineer Waterways Experiment Station (WES) Shallow-Water Wave Model (SWWM) was applied to the Atchafalaya River Delta Study to simulate a 1-year wave climate. The work described herein was funded by the US Army Engineer District, New Orleans.

The study was conducted under the direction of Messrs. H. B. Simmons and F. A. Herrmann, Jr., former and present Chiefs of the Hydraulics Laboratory; R. A. Sager, Chief of the Estuaries Division; W. H. McAnally, Jr., Project Manager; and J. V. Letter, Jr., Task Coordinator. This study was performed by Dr. Robert E. Jensen, formerly of the Wave Dynamics Division (WDD), Hydraulics Laboratory, under the direct supervision of Dr. R. W. Whalin and Mr. C. E. Chatham, Jr., former and present Chiefs, WDD. The WDD and its personnel were transferred to the Coastal Engineering Research Center (CERC), WES, on 1 July 1983, under the direction of Dr. R. W. Whalin, Chief of CERC. A special acknowledgment is due E. M. Seeley, M. J. Kasper, and E. C. Stiles for typing the original manuscript, and B. F. Vavra and M. B. Habeeb for coordinating all activities with the final publication of this report.

Commanders and Directors of WES during the study and the preparation and publication of this report were COL John L. Cannon, CE, COL Nelson P. Conover, CE, COL Tilford C. Creel, CE, and COL Robert C. Lee, CE. Technical Director was Mr. F. R. Brown.

A-1

CONTENTS

* A limited number of copies of Appendix C were published under separate cover. Copies are available from National Technical Information Service, 5285 Port Royal Road, Springfield, Va. 22151.

CONVERSION FACTORS, US CUSTOMARY TO METRIC (SI)
UNITS OF MEASUREMENT

US customary units of measurement used in this report can be converted to metric (SI) units as follows:

Multiply	By	To Obtain
feet	0.3048	metres
feet per second	0.3048	metres per second
knots (international)	0.514444	metres per second
miles (US nautical)	1.852	kilometres
square feet per second	0.09290304	square metres per second

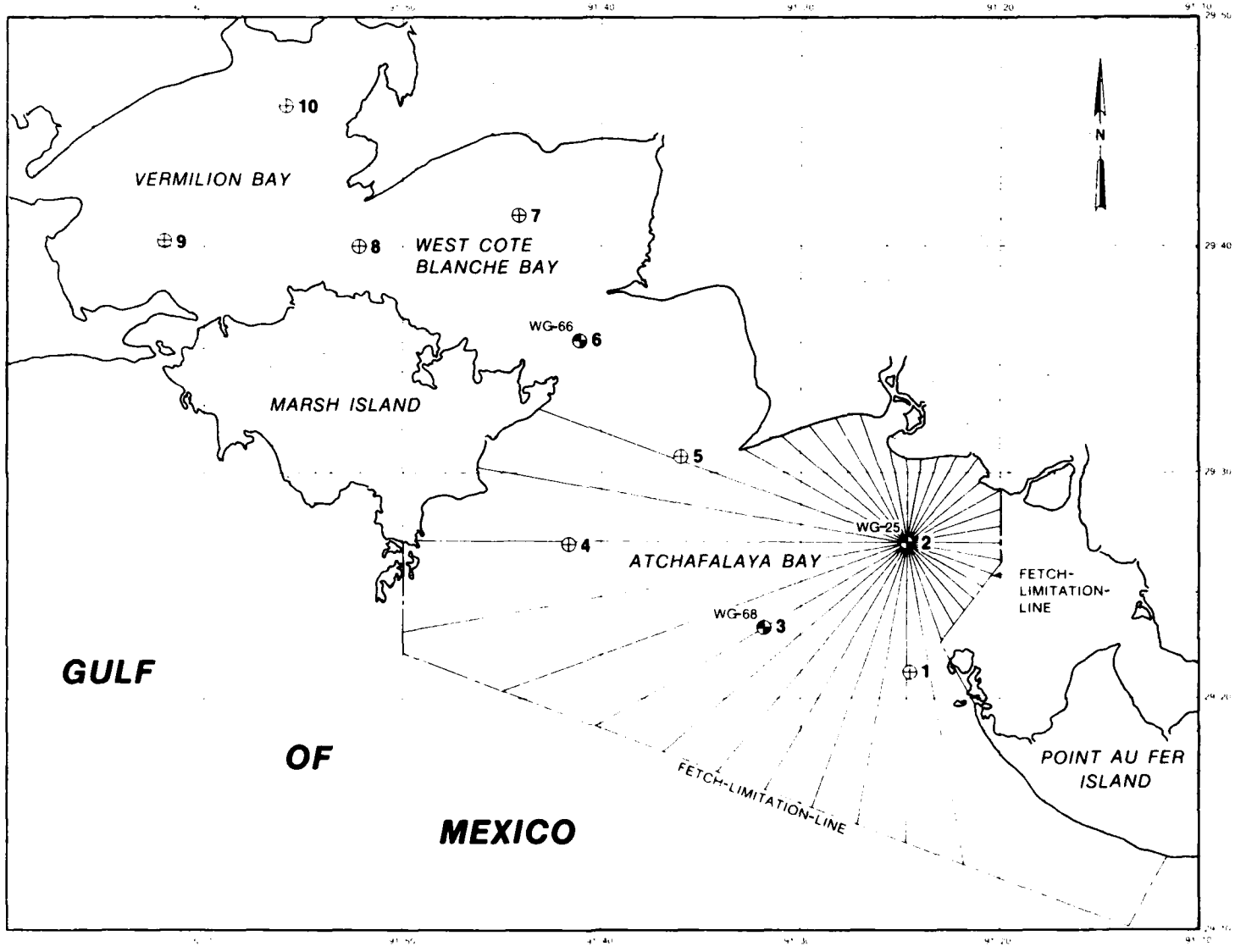

Figure 1. Wave hindcast study area displaying station and wave gage locations

THE ATCHAFALAYA RIVER DELTA

WAVE HINDCASTS

PART I: INTRODUCTION

Background

1. Wind-driven water-wave motions in Atchafalaya Bay are thought to provide the energy necessary to place bottom sediments into suspension where they can then be transported by wind-driven or tidally induced currents. Within a shallow-water bay or estuary, where wind-driven currents are a major contributor to the hydrodynamics, wind-wave motions become more important. Therefore quantification of the wave climate in Atchafalaya Bay becomes a critical element in the overall objective of the Atchafalaya River Delta investigation.* A 1-year wave hindcast at 10 locations was performed to determine the climatic variability. This information will be employed in a two-dimensional numerical model for sediment transport to compute deposition and resuspension of bottom sediments.

2. Results from the wind-field analysis task of the Atchafalaya River Delta investigation indicated that winds measured in the bay during the period 1981-1982 were very typical for the area (Ebersole 1985); hence it is reasonable to assume that during this time the wave climate should be characteristic of those which normally occur. With the wave conditions estimated for a typical year, it can be inferred that historical changes in the bay can be based on the 1-year wave climate. The extreme wave events, such as the 10-, 20-, or 50-year event would not be identified because of the limited data source of 1 year.

3. A wave monitoring program was established to estimate existing wave conditions at three locations in Atchafalya Bay (Figure 1). These results were used to verify an existing finite water depth spectral wave model. Once verified, the model was employed to compute wave information in the bay for a 1-year period using prototype wind estimates as a forcing function. The final

---

* W. H. McAnally, Jr., and S. B. Heltzel. 1978. "A Plan for Predicting the Evolution of Atchafalaya Bay, Louisiana" (unpublished), US Army Engineer Waterways Experiment Station, Vicksburg, Miss.

functions for a given station. Although this formulation removes all temporal variations in the wave climate, it presents the information in a more manageable form. The time-histories of the wave conditions (wave height, period, and direction of wave propagation every 3 hr) at each station location have been saved on magnetic tape for future analysis.

Objective

4. The objective of the overall project is to develop a set of tools to predict the evolution of the Atchafalaya River delta and the effects of that evolution. One of those effects is discussed in this report. The objectives in quantification of the wave climate are:

a. Primary objective. Develop and employ an accurate spectral wave model that includes wave growth and the mechanisms involved in finite water depth wave transformations. Calibrate and verify the spectral wave model based on prototype results. Once verified, generate a 1-year wave climatology for the Atchafalaya Bay area.

b. Secondary objectives.

(1) Analyze measured wave information to establish a baseline to estimate the confidence limits in the computed wave results.

(2) Determine from existing measured wind and wave information the extent of the effect the Gulf of Mexico has on the Atchafalaya Bay wave climate.

(3) Evaluate growth rate relations based on prototype wave information in finite water depths.

PART II: MEASURED WAVE DATA

5. In the fall of 1981, a wave gaging program was initiated in the Atchafalaya Bay area. Three pressure-type wave gages were deployed at the positions shown in Figure 1. The wave gages were self-contained pressure-sensing instruments (SEA DATA Model 635), mounted on the legs of existing offshore platforms as close to the bottom as possible. The gages were synchronized, thus measuring wave conditions at virtually the same time.

6. The sampling interval for all gages was set at 1.0 sec, and the total sample record was 1,024 sec, obtained every 3 hr. The Nyquist folding frequency for a sampling rate of 1 sec is 0.5 Hz (2.0 sec); for waves with periods slightly above 2.0 sec, aliasing of spectral energy can become a problem. However, water depths in which the gages were placed acted as low pass filters and only frequencies greater than 0.6 Hz remained unresolvable, reducing the problem of aliasing to a minor effect.

7. Data tapes were retrieved from the gages and returned to the US Army Engineer Waterways Experiment Station for processing. Wave spectra were computed via a discrete Fast Fourier Transform (FFT) and converted from a dynamic pressure spectrum to a free surface spectrum according to linear wave theory. The spectral energy density* of the sea surface is related to the pressure spectrum in the following manner:

$$E_s(f) = \left[\frac{\cosh(kd)}{\cosh(kh)}\right]^2 E_p(f) \qquad (1)$$

where

$E_s(f)$ = free surface energy density spectrum

k = wave number (equal to $2\pi/L$ where L is the wavelength) defined at each frequency f, at a given local water depth d

d = height of the pressure sensor above the bottom

$E_p(f)$ = pressure spectrum

The computed spectra ($E_s(f)$) are only approximations to the wave conditions that exist at a given period of time and become dependent on the selection of a particular analysis procedure. If a uniform technique is used for wave data

* In actual application, the term E does not have the units of energy but rather of length squared. This will apply to all variables called energy found in this report.

analysis, variation in $E_s(f)$ will reflect the variation in the wave climate.

8. The characteristic wave height H_{mo} can then be computed where

$$H_{mo} = 4\sqrt{\int_{1/T}^{1/2\Delta t} E_s(f)df} \tag{2}$$

where

Δt = sampling interval equal to 1.0 sec

T = record length equal to 1,024 sec.

The peak spectral wave period is defined by

$$T_p = \frac{1}{f_m} \tag{3}$$

where f_m = frequency at which the maximum spectral energy occurs.

9. Certain criteria were established to determine the validity of the measured wave information derived from the pressure gages. During periods of time when extremely low energy levels were recorded, the FFT routine employed in the analysis would indiscriminately place 90 percent of the spectral energy density into the first finite frequency band (0.0044 Hz). A peak spectral wave period of approximately 227 sec would signify "bad" or nonrepresentative wave information. These results were set to zero and ignored in the remaining analysis.

10. The transformation from a dynamic pressure spectrum (determined from the time-history) to a free surface spectrum can also lead to erroneous results. A measure of the uncertainty is found by an energy ratio given by

$$E_r = \frac{\overline{E_s(f)}}{\overline{E_p(f)}} \tag{4}$$

where the overbar signified a weighted average over the frequency domain. The bracketed term in Equation 1 becomes very large for certain water depths and frequencies. Any error found in $E_p(f)$ would be amplified in $E_s(f)$, based on

$$\left[\frac{\cosh\ (kd)}{\cosh\ (kh)}\right]^2 \tag{5}$$

The cutoff between "good" and "bad" wave information can be related to the validity of the wave theory employed to transform $E_p(f)$ to $E_s(f)$. A value

of 20.0 or greater would indicate that nonlinearities exist and the present techniques would not be adequate to resolve the free surface spectrum from pressure measurements. Although there was a certain amount of subjectivity associated with the selection of the cutoff limit, it did provide a uniform standard to reduce the number of potentially invalid wave results.

PART III: WAVE HINDCASTING TECHNIQUE

11. To accurately describe the wave climate within Atchafalaya Bay, two types of techniques can be employed--wage gaging and wave hindcasting. Although a network of wave gages eventually would provide a good data base, the expense involved to provide detailed coverage over the entire Atchafalaya Bay region would be prohibitive.

12. A viable alternative to comprehensive wave gaging within the bay is to hindcast the wave climate throughout the region of interest. Given enough measured wave data within the area, a wave model can be calibrated and verified. Once the verification process is complete, the model can be applied to other locations within the full extent of the study area (assuming that the physical processes affecting one location are similar at other locations). Since three wave gages were deployed in different regions and sufficient wave data were obtained at each, it was expected that model replication of results at the three sites would infer accurate results throughout the bay. The only assumption governing the model is that wind conditions remain uniform in both speed and direction over the entire Atchafalaya Bay. Results from the wind field analysis indicate that this assumption is valid (Ebersole 1985).

13. Many different techniques are presently available to hindcast wave characteristics. These techniques can be subdivided into three categories: (a) empirical, (b) parametric, and (c) numerical. A detailed description of these techniques can be found in Hsiao (1978) and Vincent (1982). A new wave model, the Shallow Water Wave Model (SWWM), has been successfully employed in two previous studies (Garcia and Jensen 1983, and Jensen 1983a). The key to this new approach is that the resulting wave conditions are generated by transformation mechanisms rather than transforming wave conditions during wave propagation. Computationally, it is more efficient to transform wave conditions from one location to the next rather than simultaneously propagating and transforming sets of wave conditions from point to point in a rectangular grid system as is done in numerical methods (for example, Resio 1981). The SWWM includes wave growth, nonlinear energy transfers, wave shoaling, energy dissipation resulting from wave decay, bottom friction effects, and wave breaking. Most transformation mechanisms are evaluated parametrically, while the remaining mechanisms are determined from empirically derived relations. The theoretical development of the SWWM is briefly presented below.

14. Hasselmann et al. (1976) introduced a parametric model of wind-wave generation relating the rate of energy growth to nondimensional characteristics of the wind field. The energy growth (in space or time) is governed by a self-similar process and verified through extensive prototype data (Hasselmann et al. 1973, 1976). In these studies, the dominant energy input to the forward face of the spectrum is related to convergence of energy flux due to nonlinear, resonant wave-wave interactions (Figure 2) of the form described by

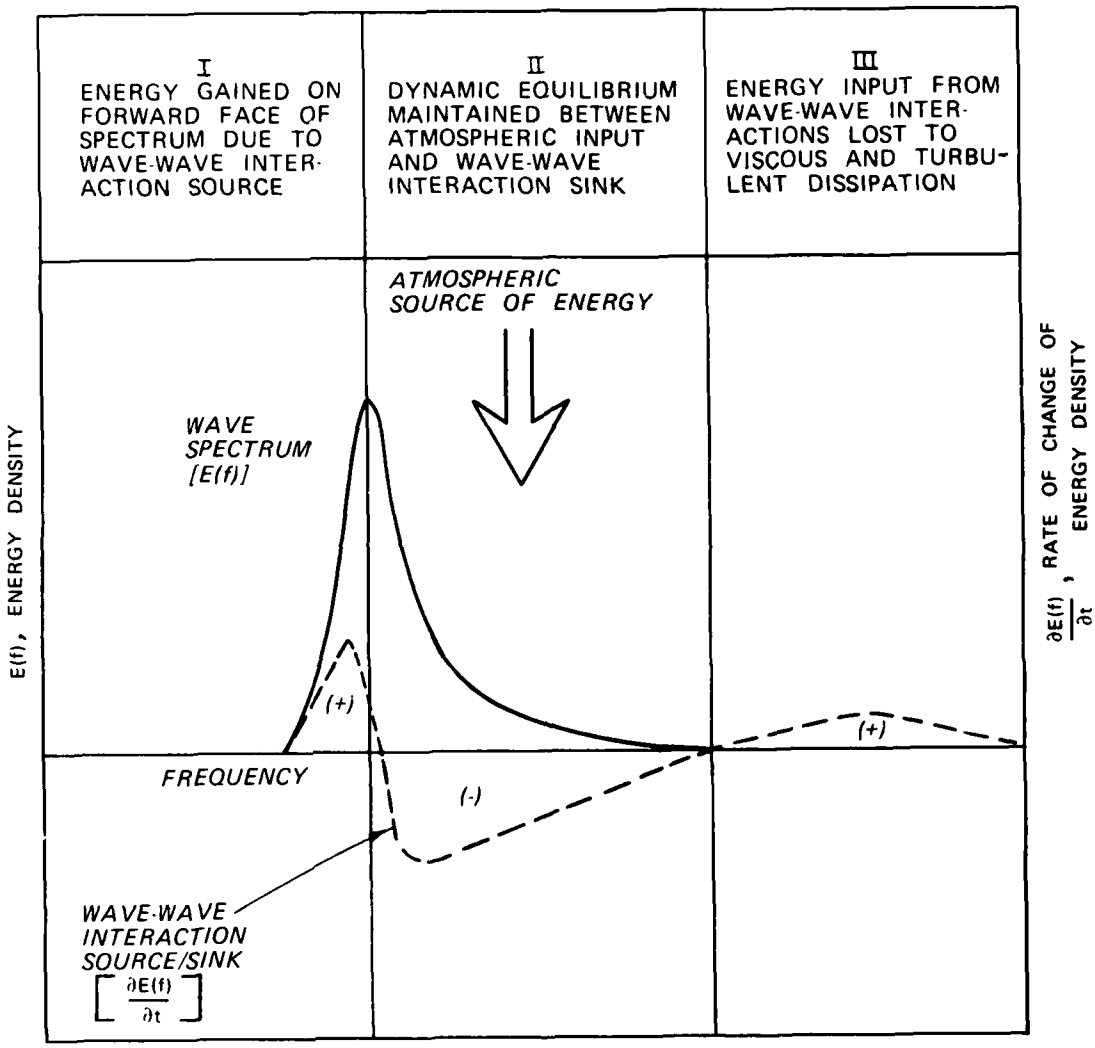

Figure 2. Schematic representation of the nonlinear wave-wave interaction

Hasselmann (1962). Studies by Mitsuyasu (1968, 1969) and Kitaigordskii (1962) also displayed similar results. Although these formulations were developed for deepwater wave conditions, they are used in the SWWM because the only

formulations of the nonlinear transfers are based specifically on JONSWAP type wave spectra.

15. The rate of wave growth under ideal conditions of fetch or duration limitations and a stationary wind field can be computed (Hasselmann et al. 1976). For growth along a fetch, the solution is

$$E_o = 1.6 \times 10^{-7} U^2 \frac{F}{g} \tag{6}$$

and for growth through time, it becomes

$$E_o = 4.3 \times 10^{-10} U^{18/7} g^{-4/7} t^{10/7} \tag{7}$$

where

E_o = total energy resulting from a wind speed U (assumed to be over-water wind conditions adjusted to 33-ft* elevation), blowing over a given fetch length F

g = gravitational acceleration

t = time since the wind began to blow

16. Additional information required to quantify the distribution of E_o given in the form of an energy density spectrum is the nondimensional peak frequency $\tilde{f}_m$ and the Phillips equilibrium constant α (Phillips 1957), as shown in Figures 3 and 4. These parameters are written as

$$\alpha = 0.076 \tilde{X}^{-0.22} \tag{8}$$

and

$$\tilde{f}_m = 3.5 \tilde{X}^{-0.33} \tag{9}$$

where $\tilde{X}$ is the nondimensional fetch length

$$\tilde{X} = \frac{gF}{U^2} \tag{10}$$

17. Although Hasselmann et al. (1976) found that wave growth followed the parametric forms defined in terms of distance and time, it is shown that for all wave-generating conditions in Atchafalaya Bay, wave growth is adequately described only by spatial variations. Therefore it becomes a matter

* A table of factors for converting US customary units of measurement to metric (SI) units is presented on page 3.

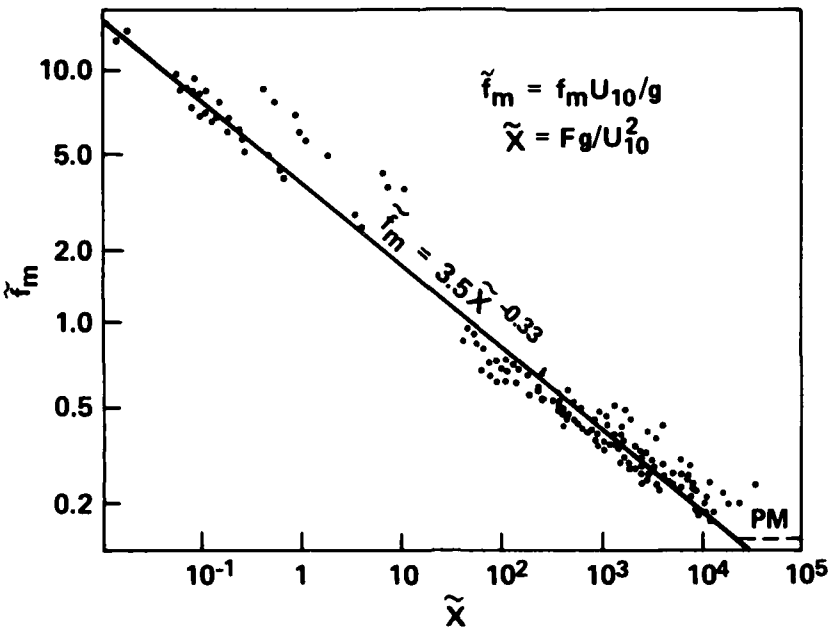

Figure 3. Nondimensional peak frequency $\tilde{f}_m$ as a function of nondimensional fetch length $\tilde{X}$ (from Hasselmann et al. 1976)

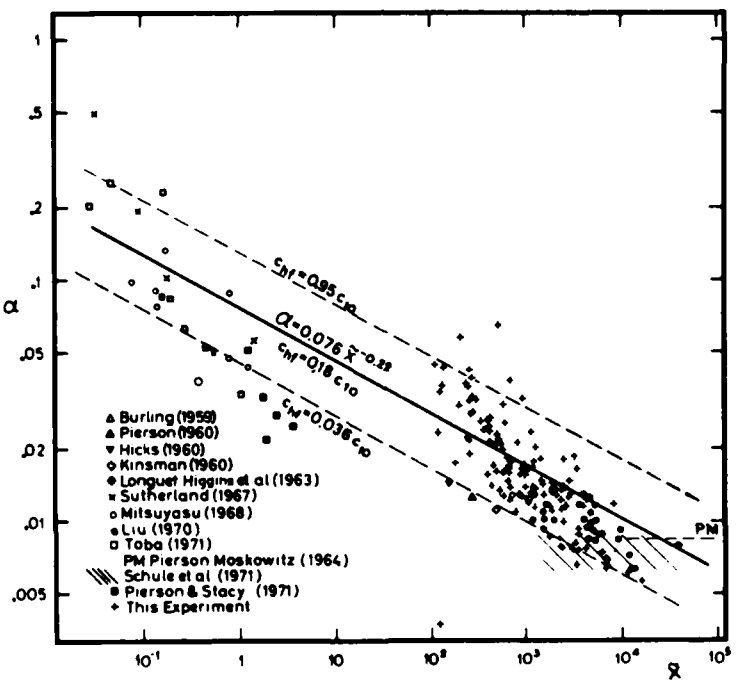

Figure 4. Phillips' equilibrium constant α as a function of nondimensional fetch length $\tilde{X}$ (from Hasselmann et al. 1976)

of comparing the prototype results (H_{mo}, T_p, and $E(f)$) with the hindcast model that employs Equations 6, 8, and 9.

18. The parameterization of the wave growth is somewhat restricted so that when the nondimensional peak frequency attains a value of 0.13 or less, a fully developed sea state is achieved and wave growth is halted. Over long fetch lengths and low wind speeds, this condition can occur to some degree of regularity. Thus Equations 6, 8, and 9 are then redefined by

$$Q = K \sum_{i=1}^{10} \zeta_i \tag{11}$$

where

Q = dependent parameters

K = nonvarying parameters (and constants)

i = increment counter parameter

ζ_i = independent parameters (F and $\tilde{X}$) found in Equations 6-10

After each discrete fetch length F_i, the nondimensional peak frequency is evaluated to determine if $\tilde{f}_m < 0.13$. If this occurs, wave growth is terminated; and wave decay is initiated for the remainder of the fetch length. Wave decay is parameterized following the work conducted by Bretschneider (1952) and Mitsuyasu and Kimura (1965) for f_m, the peak frequency (where $f_m = \tilde{f}_m g/U$), while the total energy decay rate follows that described by Jensen (1983b).

19. Wave conditions generated in a given body of water also must include dispersion effects resulting from finite water depth conditions. When the water depths vary from F_i to F_{i+1}, one must consider the conservative transformation mechanisms of shoaling and refraction. Wave shoaling is determined from the evaluation of group speeds governed by linear theory. Wave refraction is neglected under the assumption that: wave conditions found in Atchafalaya Bay appear to be influenced by changes in the wind direction over changes in the direction of wave propagation caused by variations in the bottom topography. This assumption was verified from the prototype results.

20. Finite water depth conditions also lead to bottom dissipation effects on the growing seas. Energy losses associated with bottom friction are empirically modeled using the following sets of equations developed by Bretschneider and Reid (1954):

$$E = E_1 \left(\frac{ff E_1 \phi_f \Delta F_i f_m^4}{K_s} \right)^{-1} \tag{12}$$

where

E = final total energy at F_i

E_1 = original total energy at F_{i-1}

ff = nondimensional friction factor (set at 0.001)

ΔF_i = distance of wave travel within the discrete fetch length

$$K_s = \tanh (k_i h_i) \left[1 + \frac{2k_i h_i}{\sinh (2k_i h_i)} \right]^{-1/2} \tag{13}$$

and

$$\phi_f = \frac{64\pi^3}{3g^2} \left[\frac{K_s}{\sinh (2k_i h_i)} \right]^3 \tag{14}$$

where

k_i = wave number ($k_i = 2\pi/L_i$)

L_i = wavelength evaluated for f_m

h_i = water depth at F_i

21. The most puzzling feature in all the measured results, regardless of the wind and presumed direction of wave propagation, was the lack of high wave conditions. Comparison of this wave-producing environment, based primarily on geographical and bottom topographic constraints (fetch lengths and water depths) and wind intensity, with previous studies (Jensen 1983b, Garcia and Jensen 1983), showed that H_{mo} and T_p results were expected, on the average, to be 2 to 4 ft and 3 to 5 sec, respectively. However, the prototype results showed mean conditions of 0.5 to 0.8 ft and 2.0 to 2.5 sec. There is substantial evidence to attribute part of the energy loss to wave/soft-bottom interactions. If this is true, frictional losses would be minimal, based on the sediment type associated with the two processes. Frictional losses are, in general, related to the sediment size; as the mean grain size increases, so will the shear stress (and thus the work done by the bottom orbital velocities). Thus the friction factor is set one order of magnitude smaller (compared with Bretschneider and Reid 1954, Hasselmann and Collins 1968, or Hsiao 1978) to reduce the energy loss due to bottom friction. For soft-bottom interactions, the rate of energy dissipation will increase (Gade 1958, Dalrymple and Liu

1978, and Forristall and Reece 1984) with a finer grain size. Since Atchafalaya Bay bottom sediments are derived from the riverine environment, one would be led to believe that wave-soft bottom interactions would supersede wave-bottom frictional losses.

22. The second theoretical aspect of SWWM deals primarily with the distribution of the total energy (E_o) in the form of a one-dimensional discrete frequency spectrum ($E(f_j)$). Through the use of similarity principles, Kitaigordskii, Krasitskii, and Zaslavaskii (1975) extended Phillips' deepwater hypothesis (Phillips 1958) of the equilibrium range in the spectrum of wind-generated surface waves to finite depth conditions. The spectral form is defined by

$$E(f_j) = \alpha g^2 (2\pi)^{-4} f_j^{-5} \Phi(\omega_h) \qquad f_j \geq f_m \tag{15}$$

where

$E(f_j)$ = energy density at each discrete frequency band, f_j

$\Phi(\omega_h)$ = nondimensional function dependent on ω_h given by

$$\omega_h = 2\pi f_j \left(\frac{h}{g}\right)^{1/2} \tag{16}$$

The function $\Phi(\omega_h)$ varies from 1.0 in deep water to 0.0 when $h = 0.0$, as shown in Figure 5.

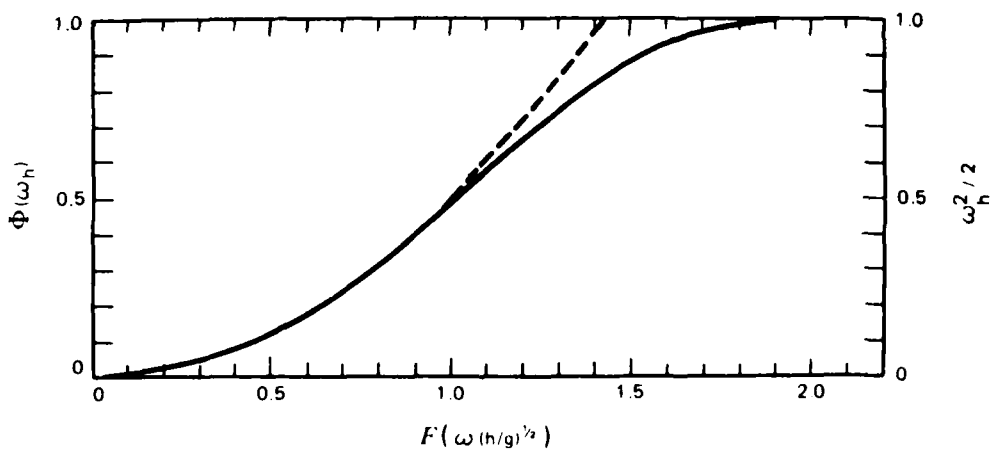

Figure 5. The universal dimensionless function Φ (solid curve) and the function $\omega_h^2/2$ (dashed curve) from Kitaigordskii, Krasitskii, and Zaslavaskii (1975)

When ω_h is less than 1.0, $\Phi(\omega_h)$ can be approximated by:

$$\Phi(\omega_h) \simeq \frac{1}{2} \omega_h^2 \tag{17}$$

and therefore

$$E(f_j) = \frac{1}{2} \alpha g h (2\pi)^{-2} f_j^{-3} \qquad f_j > f_m \tag{18}$$

or the spectral shape changes from an f^{-5} to an f^{-3} in the tail of the energy density spectrum, and more importantly, becomes a function of the water depth.

23. The forward face of the spectrum is assumed to be represented by:

$$E(f_j) = \alpha g^2 (2\pi)^{-4} f_m^{-5} \exp\left(1 - \frac{f_m}{f_j}\right)^4 \Phi'(\omega_h) \qquad f_j < f_m \tag{19}$$

where $\Phi'(\omega_h)$ is evaluated from the ω_h defined at f_m. Field and laboratory data by Goda (1974), Thornton (1977), Ou (1980), Iwata (1980), and Vincent (1981) support the form given by Equation 18. The verification of Equation 19 can be found in Vincent* and is supported in Jensen (1983a).

24. The parametric representation of wave growth assumes a dynamic balance between atmospheric sources and transfers of energy resulting from wave-wave interactions (Figure 3). This parameterization was based on deepwater wave conditions (Hasselmann et al. (1976). During a recent study it was determined that over moderately short fetch lengths (10 to 20 n.m.), this deepwater growth rate expression (Equations 6 and 7) consistently underpredicted the total energy found in the measured data (Garcia and Jensen (1983). The only theoretically consistent location to add the energy would be on the forward face of the spectrum (Figure 6). The function, $E(f,h)_{THEORY}$ is the saturated spectrum based on Equations 15 and 19, and $E(f,h)_{WEIGHTED}$ is the spectrum based on E_o after wave growth. This process also shifts f_m to a lower frequency which has been noticed in field data (Vincent**). As the fetch length increases, the relative amount of added energy decreases, where

---

* Personal communication, C. L. Vincent (1982a), US Army CERC, Fort Belvoir, Va.

** Personal communication, C. L. Vincent (1982b), US Army CERC, Fort Belvoir, Va.

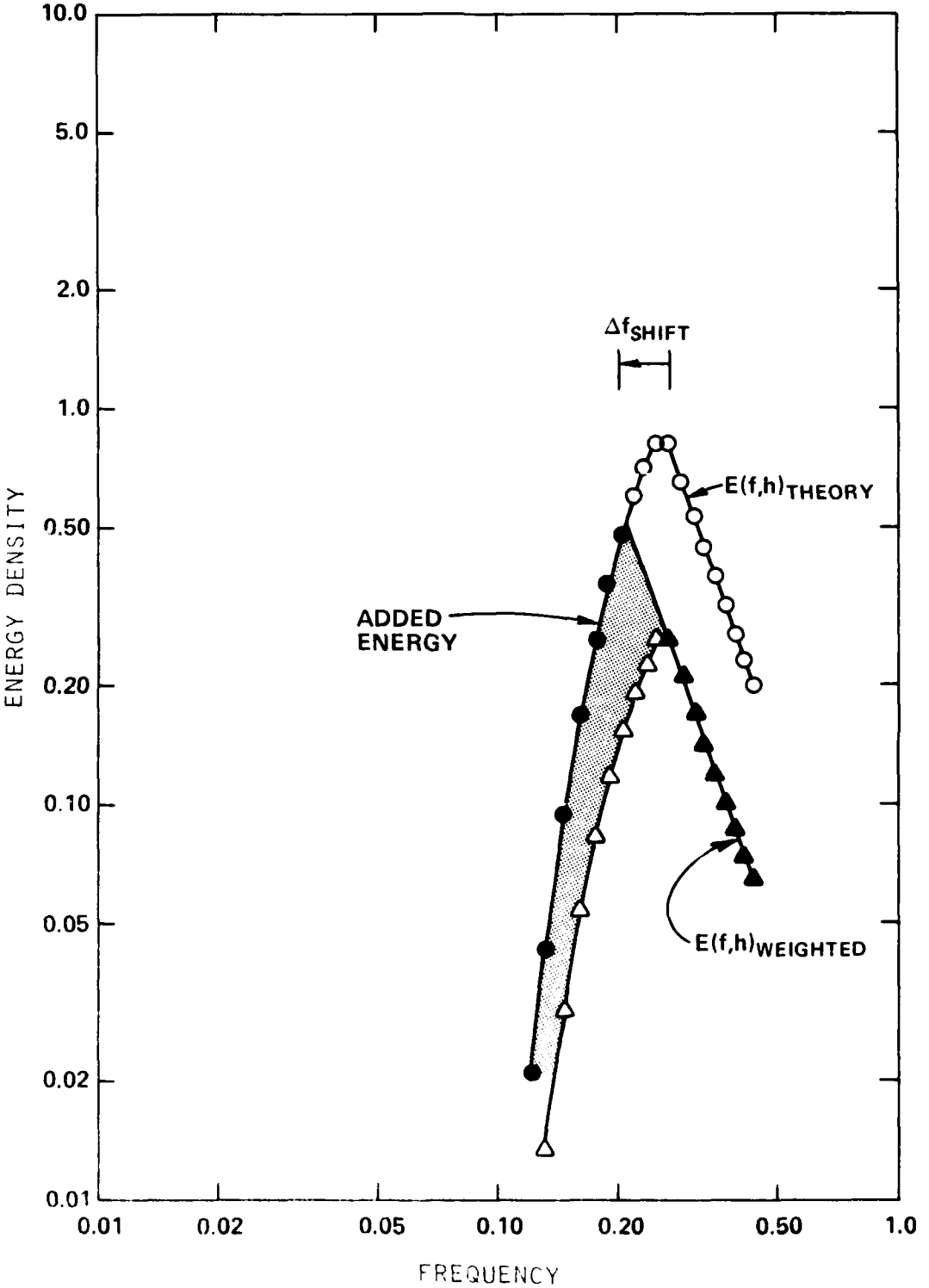

Figure 6. Construction of the final energy density spectrum (solid symbols) caused by shallow-water wave generation

eventually no additional energy is incorporated into the resulting spectrum.

25. It has been shown that the water depth greatly influences the spectral shape and in so doing will influence the maximum wave condition. The parametric formulation follows the work conducted by Vincent (1981). The depth-limiting maximum wave condition is given by

$$H_m = 4\sqrt{\int_{f_c}^{\infty} E(f)\, df} \tag{20}$$

where

H_m = maximum wave condition

f_c = lower frequency bounding the total energy (equal to 0.9 f_m)

$E(f)$ = from Equation 15

Integrating Equation 20, one obtains the absolute limit on the wave condition at a particular water depth where

$$H_m = \frac{(\alpha g h)^{1/2}}{\pi f_c} \tag{21}$$

26. In summary, the physical process governing wave generation and transformations has been theoretically determined using available, "state-of-the-art" techniques. It must be emphasized that not all shallow-water transformation processes have (or can be) measured to determine their relative effect on the total energy, spectral shape, and peak frequency. Therefore the development of the SWWM as employed in this study models the physics of the problem in a general sense while maximizing computational efficiency.

Nondimensional Parameter Comparison

27. Initial comparisons between gage data obtained at WG-25, WG-66, and WG-68 and hindcast results were consistently off both in terms of H_{mo} and T_p. The SWWM overpredicted the measured wave results by a factor of 2, regardless of wind speed or direction, for all three gage locations. Differences in deepwater and shallow-water wave growth are in the ratio between the phase and group speeds of each frequency component of an energy spectrum. Although the same amount of momentum is input to the wave field in shallow water, the amount of energy along a fetch length is only 1/2 of its deepwater value. The wave heights are then $1/\sqrt{2}$ smaller than those predicted

for wave generation in deep water (Resio 1982). This assumes that refraction, shoreline, and energy loss mechanisms are small. Therefore part of the overestimate can be attributed to the deepwater growth rate expressions (Hasselmann et al. 1976) applied to finite water depth conditions. Since the model employs parametric relations for the total energy and peak frequency adapted from deepwater results (Hasselmann et al. 1976), it was anticipated that these relations were inappropriate for Atchafalaya Bay. Figures 3, 4, and 7 display nondimensional frequency ($\tilde{f}_m$), Phillips equilibrium constant (α), and nondimensional energy ($\tilde{E}$) plotted as a function of nondimensional fetch length ($\tilde{X}$), respectively (from Hasselmann et al. 1976).

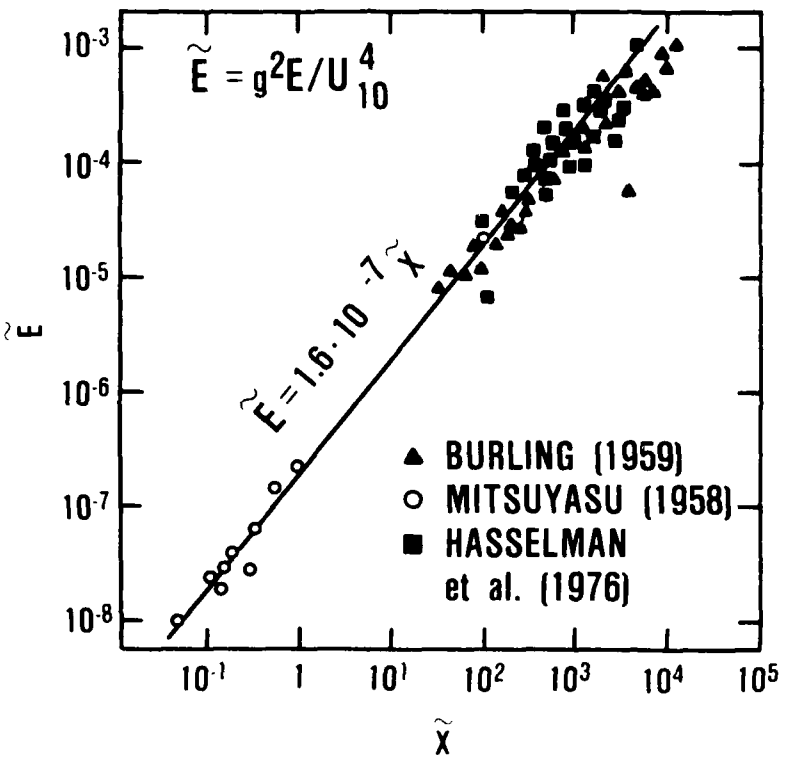

Figure 7. Nondimensional energy versus nondimensional fetch (from Hasselmann et al. 1976)

28. As the nondimensional fetch length increases (in Figures 3, 4, and 7) the data tend to diverge from the fitted curves. This divergence is more dramatically shown in the measured data obtained in Atchafalaya Bay. Taking only wave conditions generated from winds blowing over a finite fetch length (omitting winds from the south), the identical nondimensional parameters were computed and plotted in a similar fashion (Figures 8, 9, and 10). Both Hasselmann's parametric relation (Hasselmann et al. 1976) and a least squares fit on

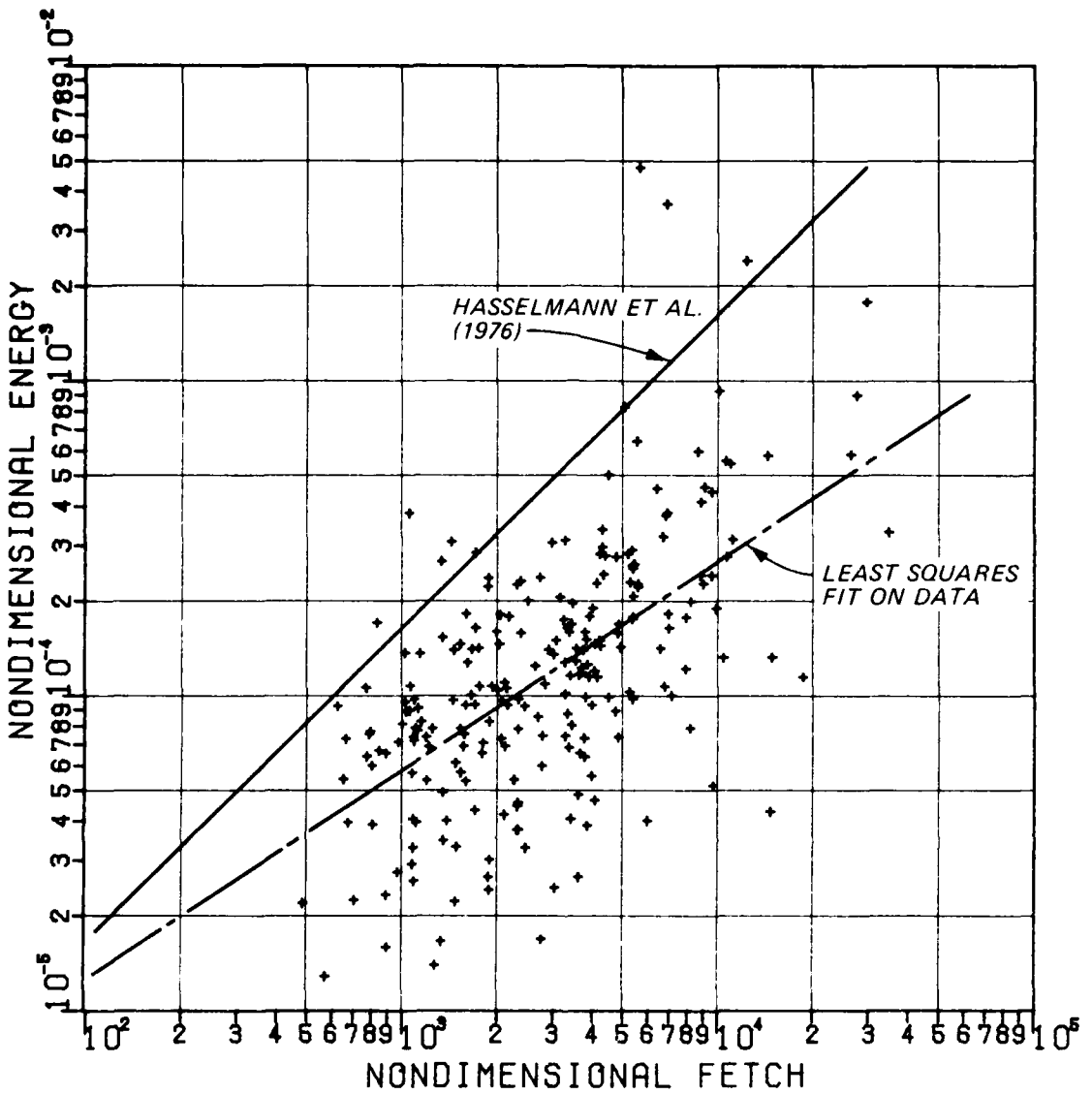

Figure 8. Nondimensional energy versus nondimensional fetch employing Atchafalaya Bay wave data

the Atchafalaya Bay data are plotted. The Atchafalaya Bay data (dimensionless fetches $\tilde{X} > 10^2$) also show the divergent trends evident in Hasselmann's data for $\tilde{E}$ and F_m versus $\tilde{X}$. The scatter found in the plot of α versus $\tilde{X}$ (Figure 10) falls within the range established by Hasselmann et al. 1976 (Figure 4), although the equations for the two lines are slightly different. Assuming the measured data correct (total energy, peak frequency, wind speed, and fetch length), new relations for wave growth over fetch lengths and the dependency of the peak frequency on the fetch length are established. These

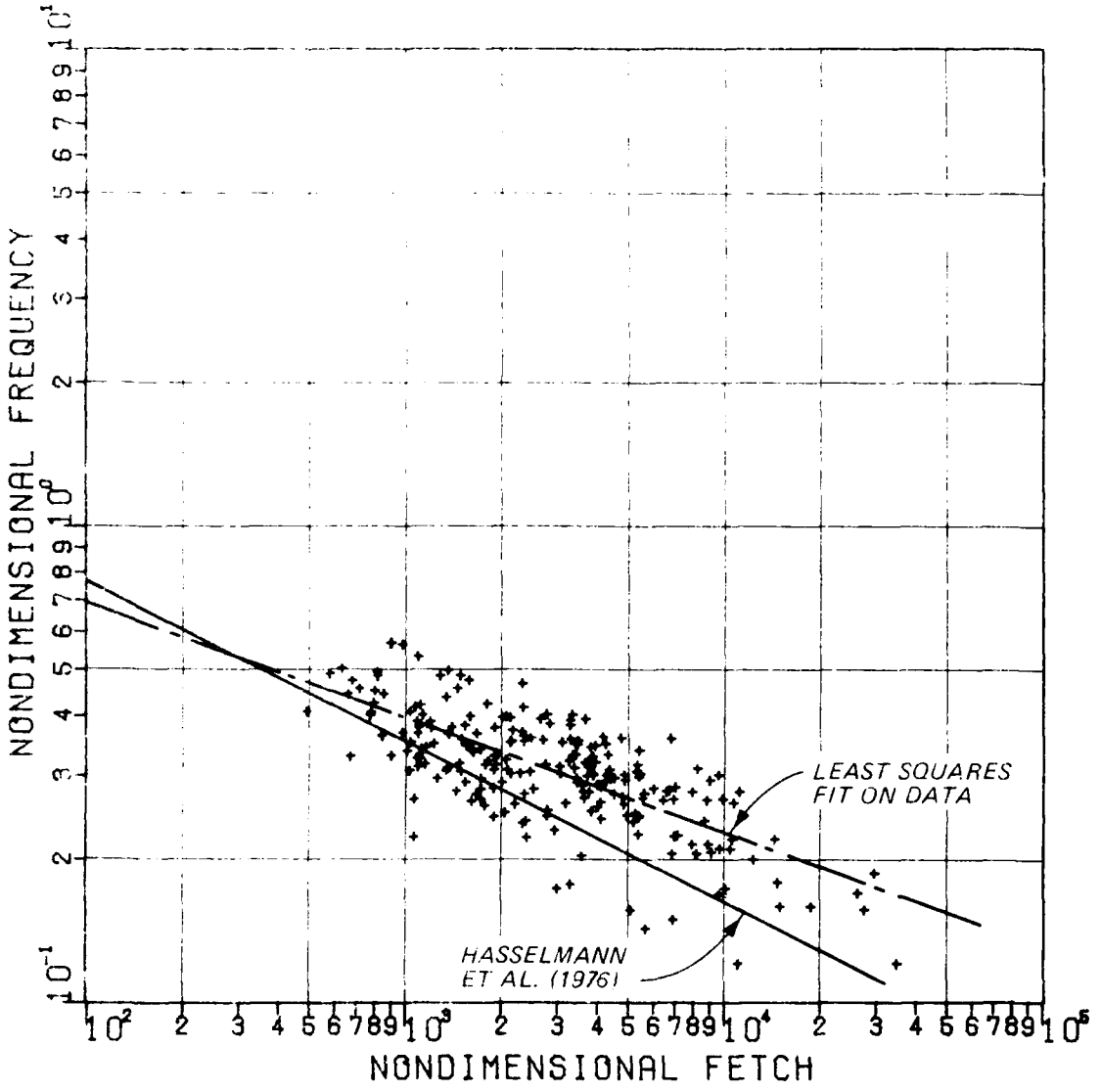

Figure 9. Nondimensional frequency versus nondimensional fetch derived from Atchafalaya Bay wave data

relations are also based on the growth characteristics only over a finite distance rather than over time and infinite fetch. The equations for the nondimensional energy and peak frequency as a function of fetch, employing the Atchafalaya Bay data, are:

$$\hat{E} = 5.51 \times 10^{-7} \hat{X}^{0.672} \tag{22}$$

$$\hat{f}_m = 2.07 \hat{X}^{-0.241} \tag{23}$$

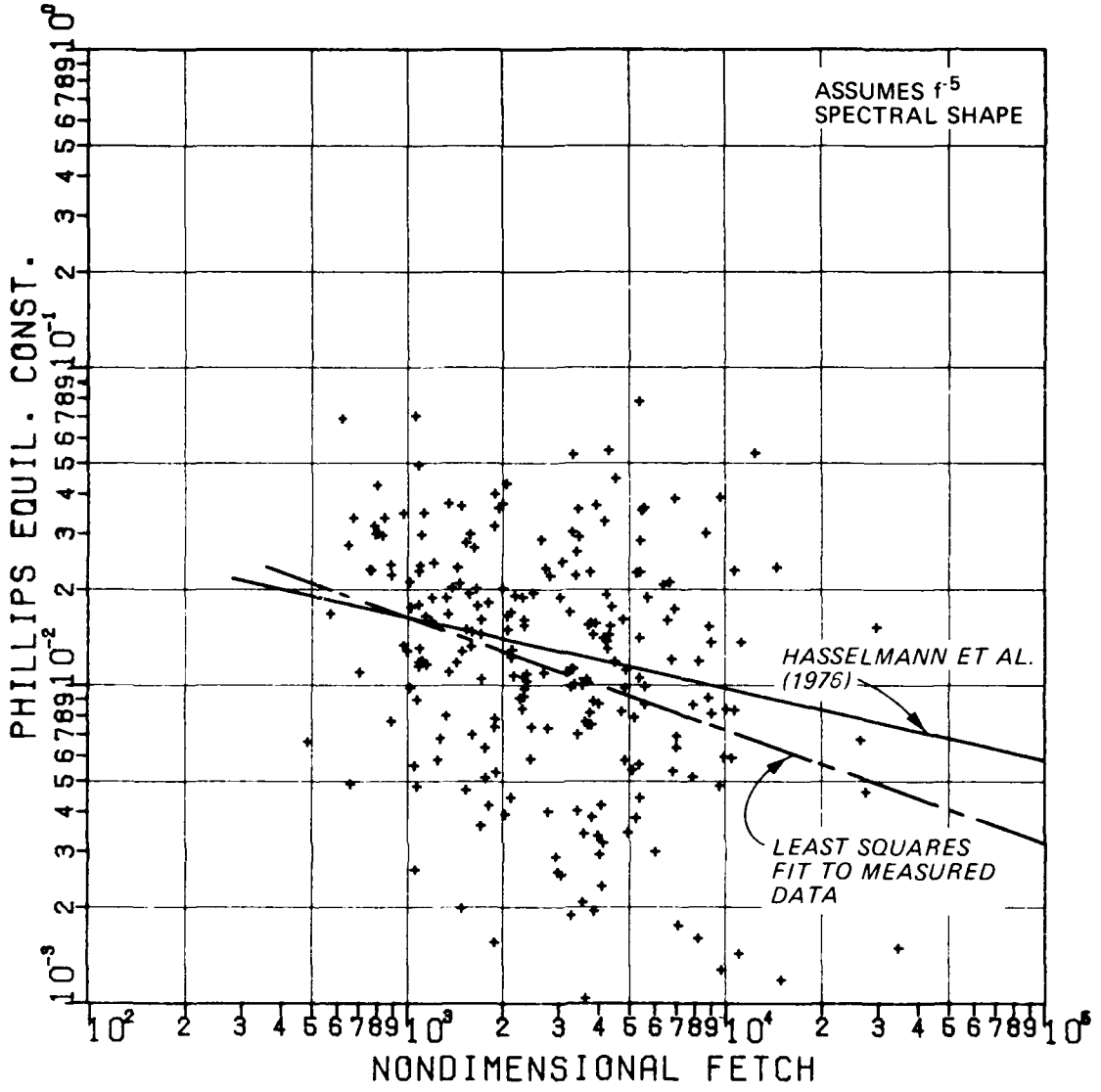

Figure 10. Phillips' equilibrium constant versus nondimensional fetch assuming an f^{-5} spectral shape on the measured Atchafalaya Bay wave information

There is significant scatter in the data above and below the newly defined parametric relations shown in Figures 8 and 9, but in general, the new equation forms, over the average, fit the measured data more consistently than the Hasselmann et al. (1976) forms. These new parametric relations are used in the SWWM; all other mechanisms and solution technique remained the same.

29. From the results given in the above discussion, we find the nondimensional peak frequency $\tilde{f}_m$, nondimensional total energy $\tilde{E}$, and the Phillips equilibrium constant α to be fetch-dependent. The best curve fit

for these variables with respect to the nondimensional fetch $\tilde{X}$ yields:

$$\tilde{f}_m \propto \tilde{X}^{-0.24} \quad , \quad \tilde{E} \propto \tilde{X}^{-0.67} \qquad \alpha \propto \tilde{X}^{-0.35} \tag{24}$$

For a self-similar spectrum $\tilde{E} \propto \alpha f_m^{-4}$, accordingly, the relation between $\tilde{f}_m$, $\tilde{E}$, and α can be constructed and the exponents n_f, n_E, and n_α in the power laws for $\tilde{f}_m$, $\tilde{E}$, and α should satisfy the following relations:

$$4n_f - n_\alpha + n_E = 0 \tag{25}$$

Here, $n_f = -0.24$, $n_\alpha = -0.35$, and $n_E = 0.67$ for the present field data results. Substituting these values into the above relation yields:

$$4(-0.24) - (-0.35) + 0.67 = 0.06 \tag{26}$$

The resulting value of 0.06 lies well within error bands estimated from the individual error band of each curve-fitted exponent. It is reassuring to find that the Atchafalaya Bay wave information and the new fetch-dependent relations retain the notion that the spectrum follows the self-similar trends established in Hasselmann et al. (1976).

30. Equations 22 and 23 can be combined to yield a solution to $\tilde{E}$ as a function of $\tilde{f}_m$. This relation will now be independent of fetch length, and only externally related to the wind speed, given by:

$$\tilde{E} = 4.19 \times 10^{-6} \tilde{f}_m^{-2.79} \tag{27}$$

The measured results are nondimensionalized and plotted in Figure 11. In simplistic terms, Equation 24 fulfills stability requirements on the wave form, since the wave height can be related to $\tilde{E}$, and the wave period can be related to $\tilde{f}_m$. Along with Equation 27, the Hasselmann et al. (1976) and Knowles (1982) equational forms are plotted. The latter study confines its wave measurement program to finite depth conditions (approximately 6 ft) in a restricted-fetch estuary. Although Knowles found that $\tilde{E}$ versus $\tilde{X}$ and $\tilde{f}_m$ versus $\tilde{X}$ would not coincide with Hasselmann's deepwater results, the $\tilde{E}$ versus $\tilde{f}_m$ results compared satisfactorily. From Figure 11, one finds that the Hasselmann et al. (1976) curve appears to be an upper limit to the

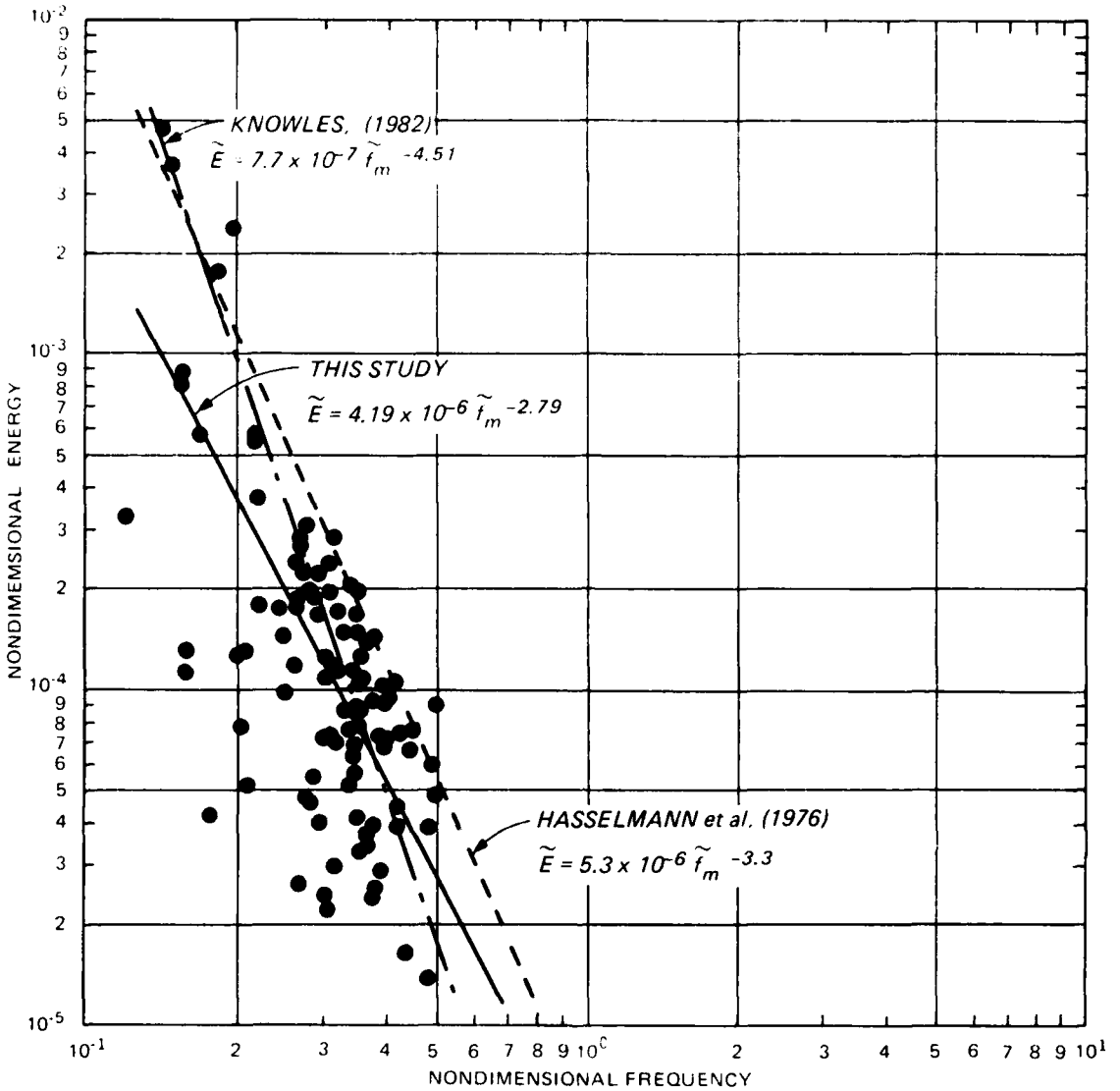

Figure 11. Atchafalaya Bay wave data represented by nondimensional energy versus frequency

Atchafalaya Bay wave results, whereas the Knowles (1982) curve passes more closely through the measured results. As expected, Equation 27 plots through the midrange of the results because $\tilde{f}_m$ and $\tilde{E}$ relations were derived from the method of least squares. The curves show that the Atchafalaya Bay results follow deepwater "steepness" (the ratio of height to wave period squared) conditions, because the slopes are nearly parallel; but the magnitudes in the steepnesses are much smaller. For example, consider a wind speed of 10 knots (17 ft/sec) and a peak frequency of 0.286 Hz (T_p = 3.5 sec), the Atchafalaya

Bay curve will result in a characteristic wave height of 1.03 ft whereas the Hasselmann curve will yield a height of 1.93 ft. This supports the earlier findings that because of the physical constraints to the Atchafalaya Bay wave environment, employing Hasselmann et al. (1976) nondimensional formulations of $\tilde{E}$ and $\tilde{f}_m$ will result in a large error in the computed wave conditions. This is not to say Hasselmann et al. (1976) are incorrect but proves that any variation in the environment will warrant a careful study of the wave mechanisms.

31. One can continue the analysis one step further by relating the nondimensional energy based on measured results ($\tilde{E}_M$) to computed results ($\tilde{E}_C$) derived from the new growth rate relation found in Equation 22. The nondimensional energy based on measured results is given by:

$$\tilde{E}_M = E_M \frac{g^2}{U_{10}^4} \tag{28}$$

where

E_M = total measured energy

g = gravitational acceleration

U_{10} = wind speed measured at a 33 ft (10 m) elevation above the water surface

Figure 12 shows the distribution, based on H_{mo} results greater than 1.0 ft. There is a great deal of scatter above and below the line where $\tilde{E}_M = \tilde{E}_C$, establishing that over an average the new growth rate curve will both over- and underestimate a resulting total energy and not be consistently biased toward one direction.

Test on Assumption of Local Wave Generation Only

32. One major assumption governing the hindcast portion of this study is that wave conditions found within Atchafalaya Bay are primarily generated within the region (i.e., little energy is propagated into the bay from the Gulf of Mexico). Three storm events occurred during the wave measurement program where southerly winds (winds blowing from the south) occurred for at least a 2-day period of time. These wave records were compared to determine the level of energy propagated into Atchafalaya Bay.

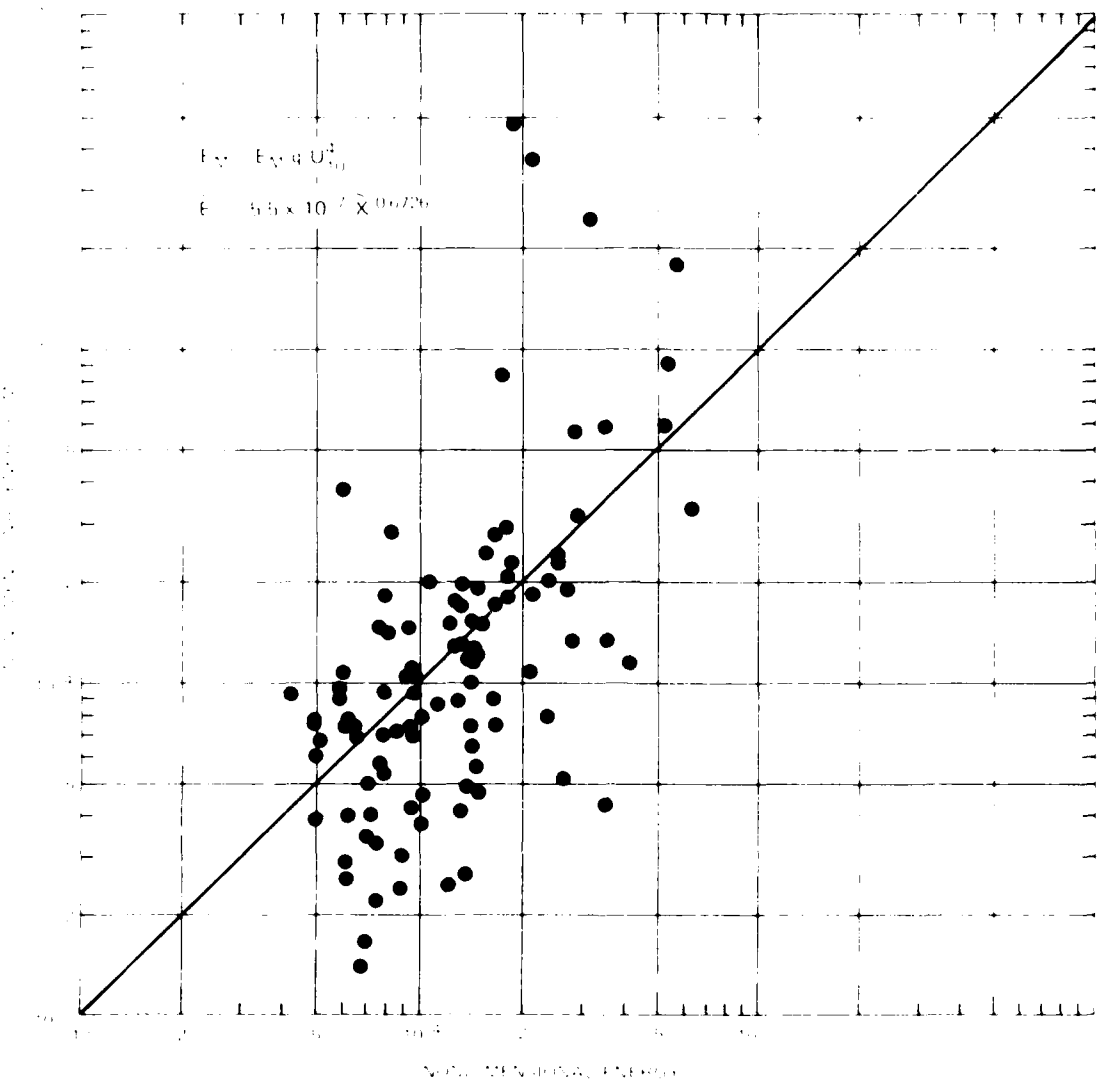

Figure 12. Comparison between measured and computed nondimensional energies

33. Storm A, which occurred from 25-27 November 1981, displayed wind speeds on the average of 8 knots, and the wind direction was predominantly from the southeast (Figure 13). These wind conditions were relatively constant throughout the Gulf of Mexico (the wind speed obtained from a buoy located approximately 200 n.m. south of the bay). Therefore the physical factors (the wind speed, duration, and fetch lengths) were capable of producing large wave conditions as a result of the long fetch length and lengthy duration. The maximum wave conditions observed at WG-68 for this period were on the order of 1.25 ft with a corresponding T_p of 7.0 sec (Figure 14). Assuming that the

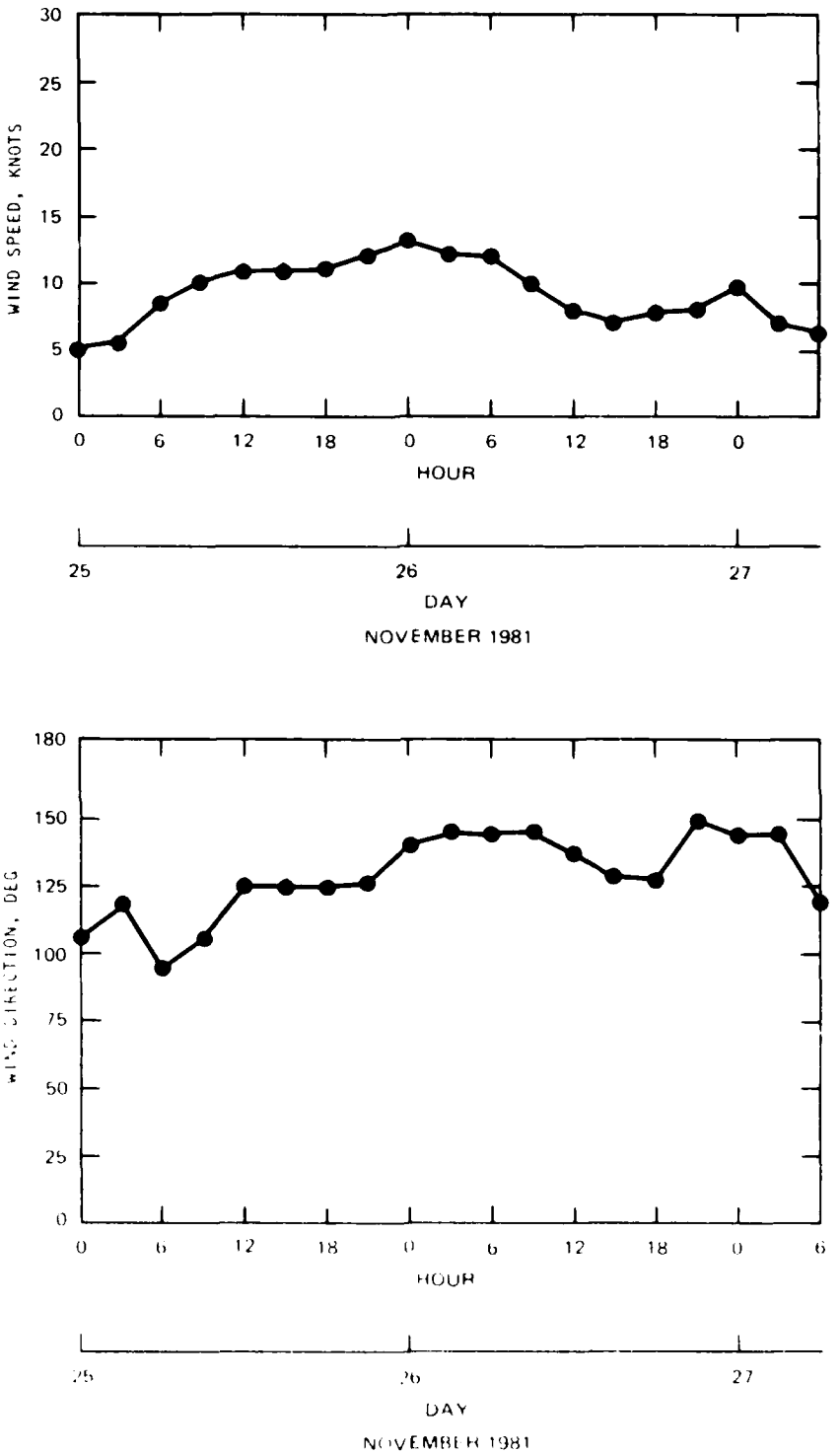

Figure 13. Wind data for Storm A

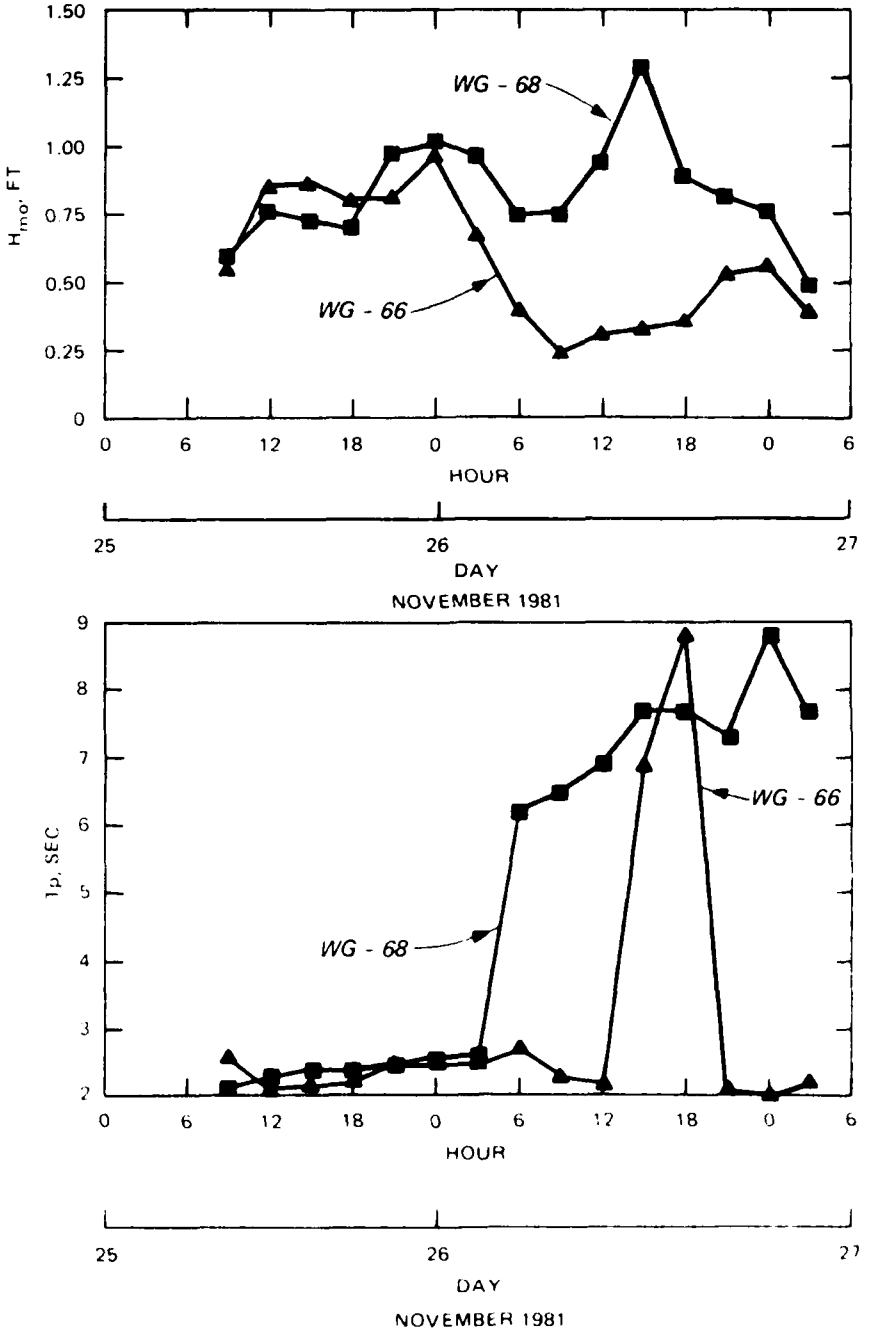

Figure 14. Wave-height and period comparisons for Storm A

waves travel in the direction of the winds, WG-66 should also have "seen" these wave conditions in its wave record which should be of the same order of magnitude as those observed in the WG-68 record because the water depths between the two locations are nearly constant. The initial H_{mo} and T_p results compared within 0.5 ft and 0.2 sec, respectively, and reflect local wave generation.

34. One finds that Gulf-generated waves, characterized by wave periods greater than approximately 6.0 sec, exceed local wave generation, based on the maximum energy found in an energy density spectrum. As the wave period increases over time at WG-68, the period estimates at WG-66 remain at approximately 2.5 sec, except for two occurrences. During this period of time, the energy loss from WG-68 to WG-66 is quite substantial. An energy sink must exist between the two gage locations that reduces long-period wave energy while permitting short period waves to remain unchanged in a near uniform fashion. This comparison suggests that very little long-period wave energy derived from Gulf-generated waves is capable of retaining a significant energy level within Atchafalaya Bay.

35. The second storm (Storm B) in this investigation took place on 21-23 December 1981 where wind speeds and directions remained nearly constant for the duration of the storm. Wind speeds were on the average approximately 12 knots and the direction remained near 180 deg (Figure 15). Comparisons between WG-66 and WG-68 results, in terms of H_{mo} and T_p, are shown in Figure 16. The time-history of H_{mo} data reflects nearly identical wave variation patterns at both gage locations, except that the wave heights at WG-66 are significantly diminished in comparison with WG-68. It is interesting to note that the maximum wave heights observed at WG-68 are between 1.25 to 1.75 ft. With the wind speed of 12 to 25 knots found in the Gulf of Mexico and the fetch length of approximately 200 km, it was expected that maximum H_{mo} conditions would be much larger than those observed. It appears that some local physical constraint south of WG-68 is minimizing the wave climate at that location. Portions of the Old Shell Reef may have migrated south of its previous position or a sandbar system may be present such that all measured data reflect the depth-limited wave climate. The data measured at WG-68 may reflect only postbroken wave energy and re-formation rather than the total energy derived from wave generation in the Gulf of Mexico. An alternate explanation for the differences in wave height and period estimates found at WG-68 and WG-66 is discussed below.

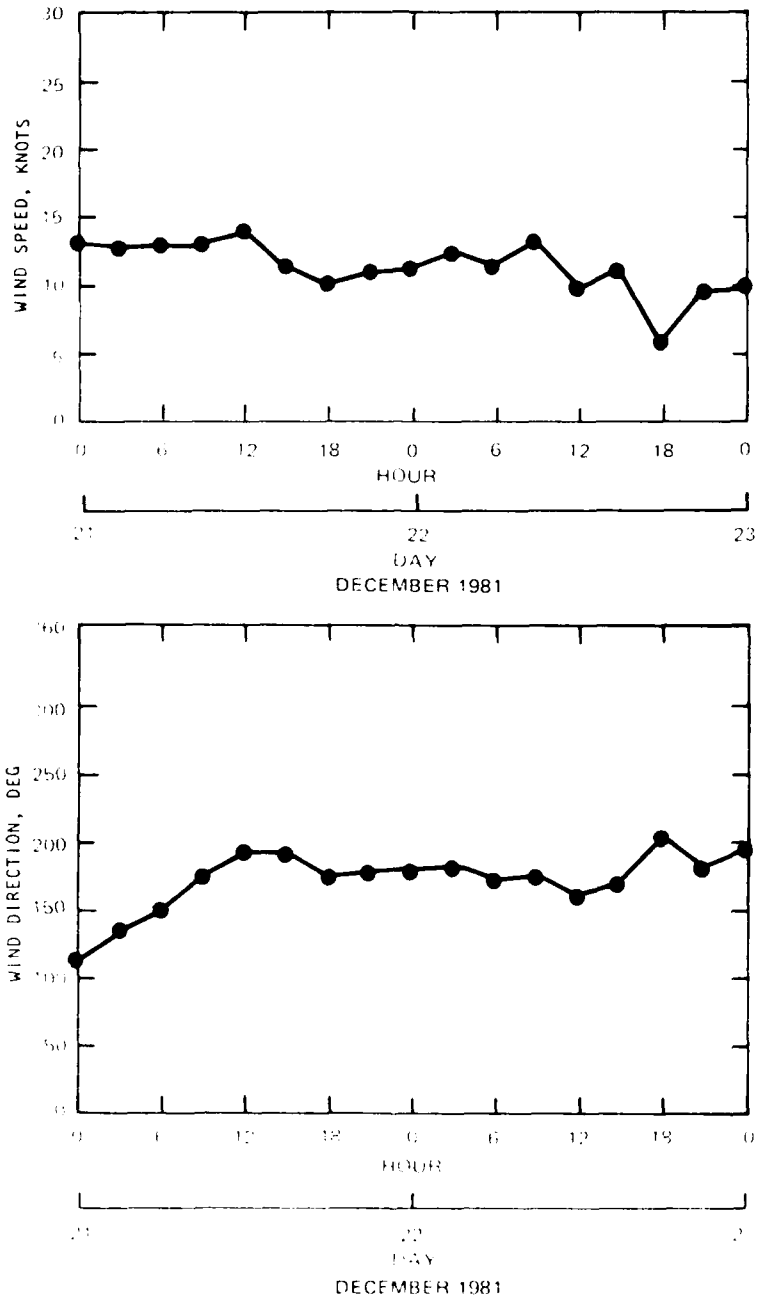

Figure 15. Wind data for Storm B

36. The signature of Gulf-generated waves can be identified as long-period (or low frequency) wave conditions. As these waves propagate into shallow water, they are more susceptible to energy loss mechanisms associated with wave-bottom interactions, in comparison with short-period (2 to 4 sec, locally generated) waves. Forristall and Reece (1984) reported, via a wave

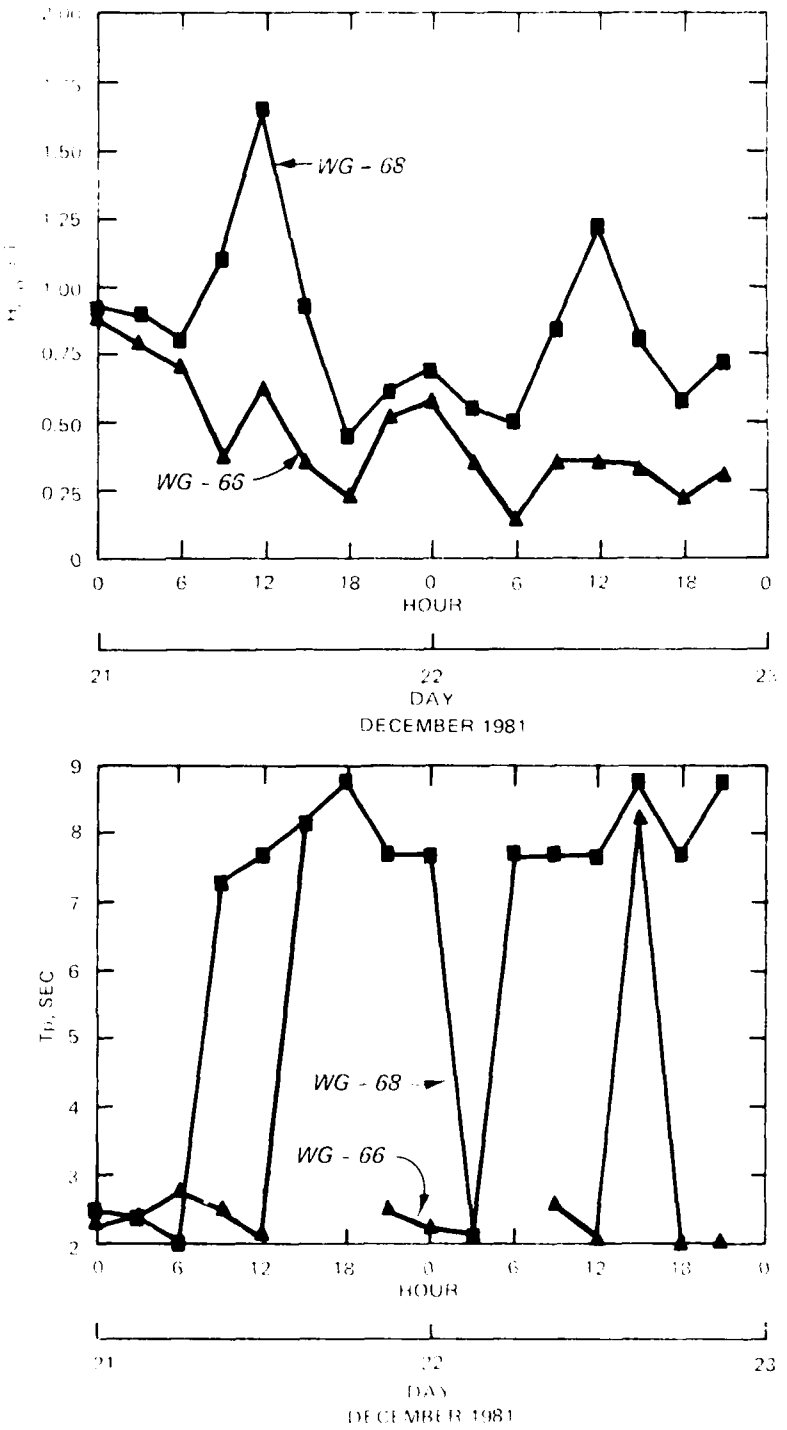

Figure 16. Wave-height and period comparisons for Storm B

measurement program in the Gulf of Mexico, that the wave attenuation can be large. The degree of attenuation was strongly related to a deepwater wave amplitude and the rate of energy loss caused by wave-soft bottom interactions follows a reasonably consistent pattern. Although their wave characteristics and water depths are greater than those found in the Atchafalaya Bay area, the nondimensional wave height and water depth (H/gT^2 and h/gT^2) are both consistent. Therefore the processes causing extreme energy losses in both data sets can be identified. Figure 17 displays the computed spectra for WG-68, WG-25, and WG-66 for a particular time during a southerly wind-producing storm. All three spectra show the peak spectral density occurring near 0.13 Hz. What must be noted is that at the bay entrance (WG-68) the long-period waves dominate the system. As the spectra propagate into the bay, the overall spectral shape remains intact but loses a large amount of energy (80 percent loss at WG-25 and 90 percent loss at WG-66). This loss can only be explained by the absorption of energy from the wave system into the sea floor. Energy losses associated with bottom friction effects are nonlinear (Collins 1972). Because of the nonlinearities, the effect of this mechanism would transform the spectrum into a new shape, shifting the peak frequency to a higher value. As shown in Figure 17, the spectral shape for all three locations remains virtually unchanged, suggesting a mechanism that can be functionally related by an exponential decay (Hsiao 1978).

37. Hence, long-period wave conditions once generated in the Gulf of Mexico will not sustain their energy level in Atchafalaya Bay. One may also conclude that the reasons for a paucity of large wave conditions (3 to 6 ft) within the bay can be caused by this mechanism.

38. The final storm (Storm C) occurred from 2-4 January 1982 (Figure 18) and produced wind speeds of approximately 10 knots. The wind direction slowly changed from 100 deg to approximately 230 deg over the 2-day period. Comparison of the H_{mo} results obtained from WG-66 and WG-68 (Figure 19) again demonstrates that the wave climate is nearly uniform within the bay. The H_{mo} conditions are slightly higher at WG-68, but throughout the storm both gage results show very similar trends.

39. Although the wind direction for Storm C is from the southeast through the south, the effect of Gulf-generated waves found at WG-68 is significantly diminished when compared with the two previous storms. This storm sequence points out that not all southerly winds produce long-period waves at

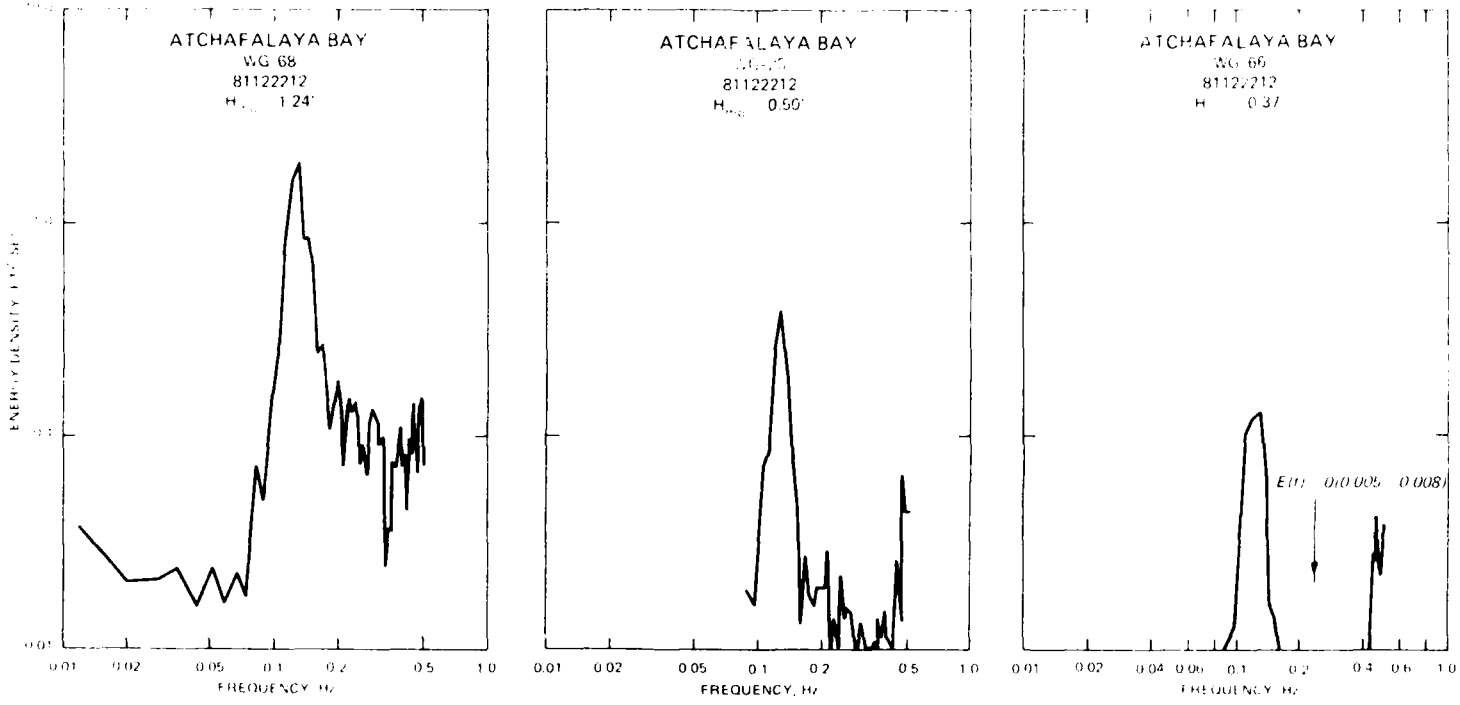

Figure 17. Comparison between spectral estimates for the three gage locations

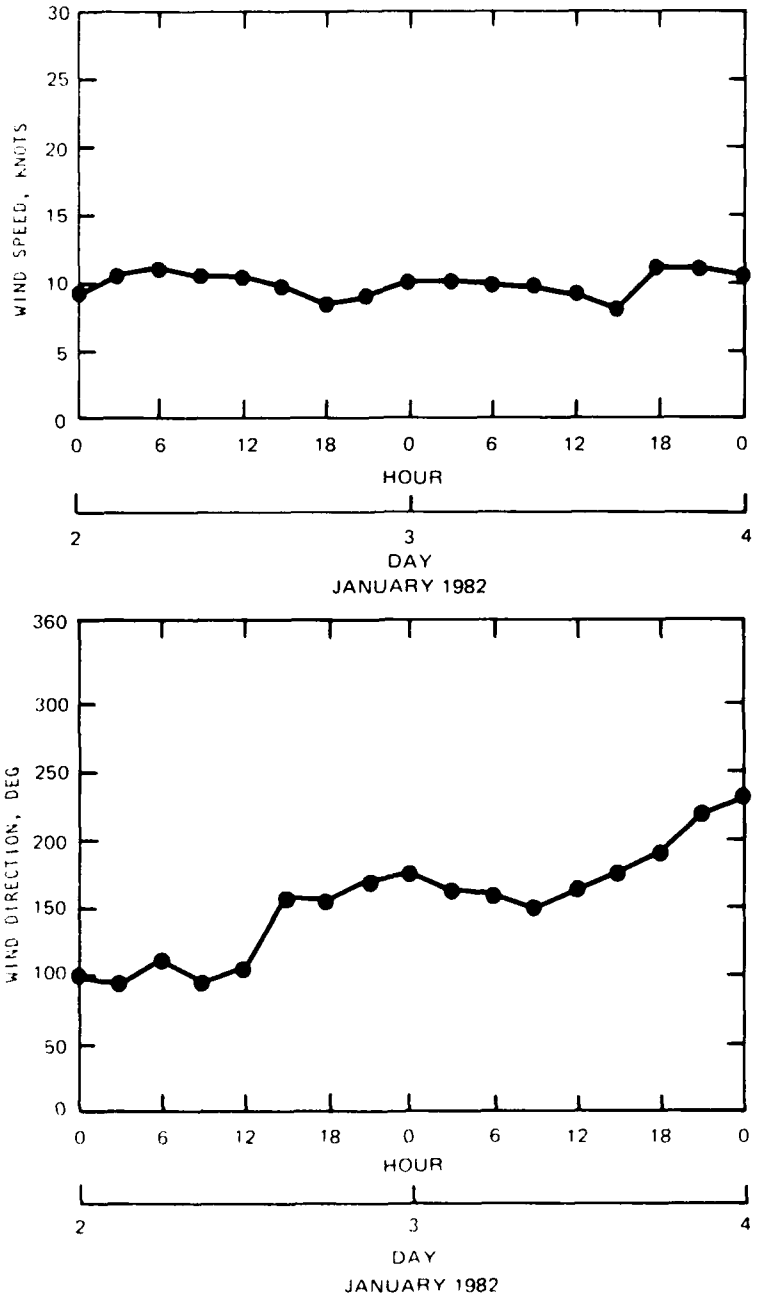

Figure 18. Wind data for Storm C

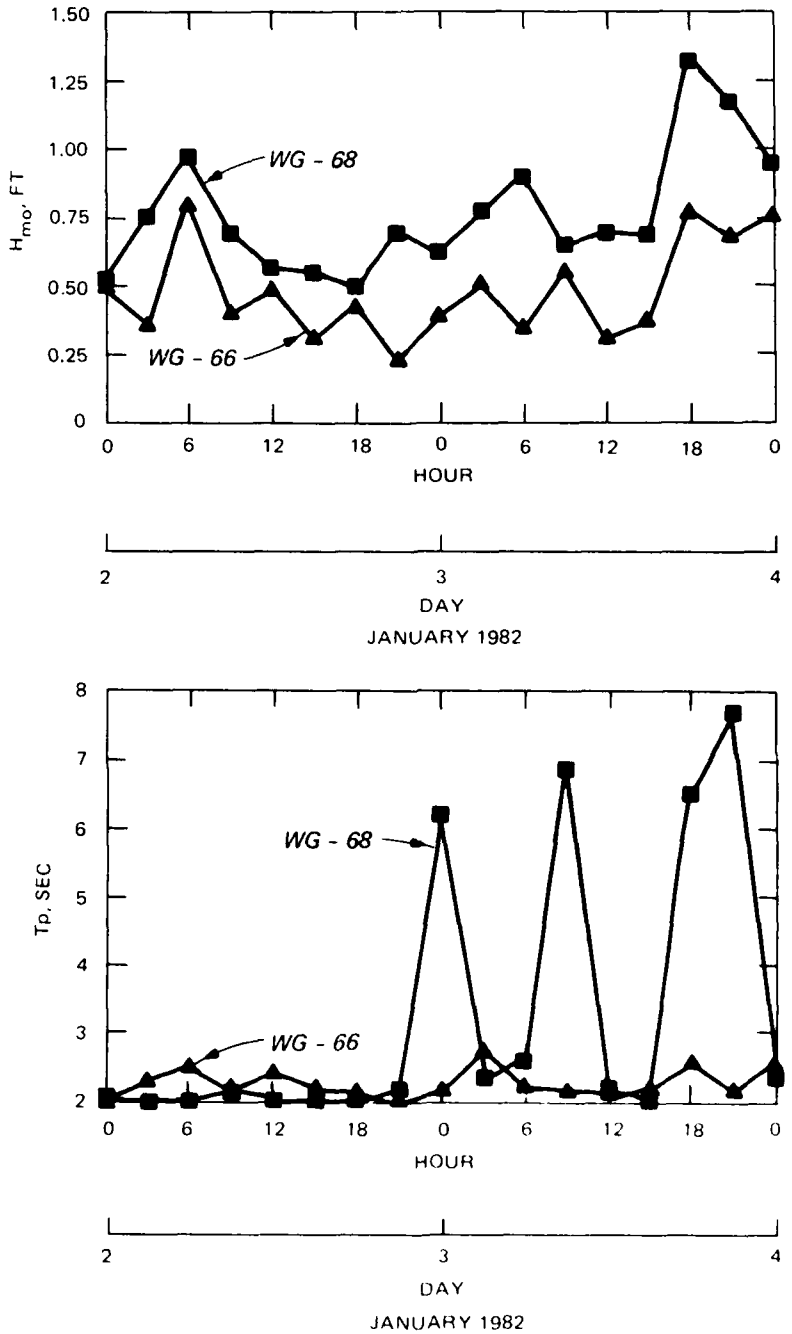

Figure 19. Wave-height and period comparisons for Storm C

the entrance of Atchafalaya Bay. The wave period oscillations found at WG-68 are caused by a two-population wave system that is nearly identical at the respective peak energies. Figure 20 displays the estimate of energy density spectrum at WG-68 on 3 January 1982, 0000 hour. There are two primary peaks (0.16 Hz and 0.41 Hz, signified by the arrows) where the energy densities at these two frequency bands are virtually the same. Only slight changes in the relative amount of energy found in either frequency could shift the T_p value. Since neither the 0.16 Hz nor the 0.41 Hz energy density dominates the wave climate, there will be oscillations in the T_p results. In general, this spectrum characterizes the wave conditions at WG-68, a two-peaked spectrum where

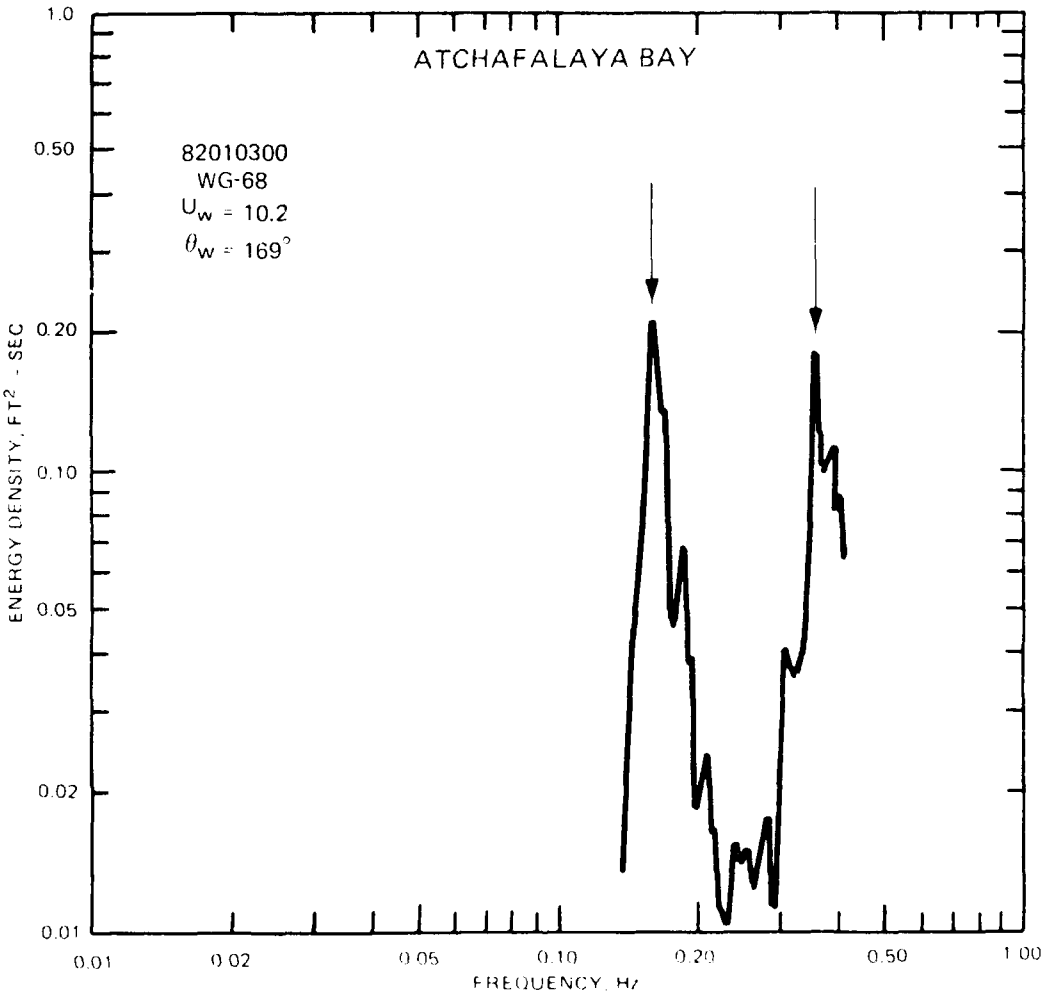

Figure 20. Spectral estimate for WG-68 depicting a two-population wave system, Gulf-generated (0.16 Hz) and locally generated (0.41 Hz)

the two-population wave system is equally weighted in terms of the relative amount of energy.

40. In summary, the data presented show that waves generated in the Gulf of Mexico exist at the entrance to Atchafalaya Bay, but are limited in the number of occurrences and also in the amount of energy they contain. Even if the energy propagates into the bay, the wave characteristics transform into another spectral form where only a small amount of energy is present at the lower frequency and the majority is found at frequencies associated with locally generated conditions. Therefore the assumption that Atchafalaya Bay is cut off from the Gulf of Mexico and wave conditions found in the bay are generated in the local area is verifiable. Rather than cut the bay off at Point Au Fer Shell Feet, the "fetch-limitation-line" is drawn at the 12-ft contour outside the bay (Figure 1) to represent wave conditions from the south more realistically. The fetch limitation within the eastern bay was also assumed due to the complicated delta and dredged material associated with the river channel.

Wave Hindcast Model Verification

41. Verification of the wave hindcast model is an important facet of the hindcast study. As previously discussed, adjustments in the growth rate relations according to Atchafalaya Bay wave conditions were necessary to better approximate the gage results. Those equational forms fulfilled the self-similar spectral trends established by Hasselmann et al. (1976). All the parameters and equational forms were generated on an individual basis (i.e., the total energy as a function of fetch length, the peak spectral frequency as a function of fetch length, and the Phillips equilibrium constant as a function of fetch length). The verification test is to incorporate the newly established growth rate formulations in the wave model and perform comparisons between prototype and hindcast wave estimates. These comparisons then would verify:

a. If the wind direction and speed are uniform over Atchafalaya Bay.

b. If the growth rate expressions and the transformation mechanisms incorporated in the SWWM generate comparable wave estimates for the three gage locations.

c. The overall validity of all subsequent wave hindcast estimates generated by the SWWM in Atchafalaya Bay.

42. The procedures used to verify the model are as follows. For each set of wave gage results, the wind information is used precisely as that in the hindcast portion of this study following the techniques described by Resio and Vincent (1976). The wind data are used to generate a time-varying wind field to drive the wave model. The computed wave characteristics H_{mo} and T_p and spectra $E(f)$ are then plotted against the gage estimates and compared accordingly.

43. The goal of the hindcast model development portion of this study was to incorporate all theoretically sound transformation mechanisms into the SWWM and utilize as much wave gage information to adjust growth rate sequences compatible with the Atchafalaya Bay area. In the end, all coefficients were treated as preestablished constants and were never changed from site to site. The comparisons shown here do not represent attempts at calibrating or adjusting the model but serve as a verification of the wave growth and transformation processes established in the framework of the wave model.

44. Simple yet descriptive techniques are used for the comparisons (i.e., time-history plots, cross plots, and percent occurrence plots). The last of these types of comparisons is probably the most indicative of the ability of the hindcast wave estimates to represent a wave climate accurately. The hindcast wave results are paired according to the gage observation. These paired estimate techniques are used to describe the random error in the hindcast model. However, much of the random error in these computations is attributed to shifts in time between the wave hindcast and observed wave information. Northerly wave condition comparisons

45. Five storm conditions were selected for the verification of the SWWM. The predominant wind directions for all five storms were from the north. The wind conditions were generated by averaging the wind speed and direction information (three 20-min averages every hour) over a 3-hr duration. These data are given in Appendix A, along with all comparisons of measured and hindcast H_{mo} and T_p results.

46. The first storm occurred from 9-12 November 1981. Wind speeds were, on the average, 15 knots (with a maximum of 19.2 knots) and the direction remained ±30 deg from 0 deg, north azimuth. All three gage records exhibited the same trends during the storm period (Figures A1-A3) and maximum H_{mo} conditions, approximately 1.0 to 1.5 ft, occurred on 10 November at 0000 to 0300 hours. A number of data points are missing in the measured H_{mo} and T_p

results. The estimates for these particular times (for example, Figure A1, 10 November 1981 at 1200 hours) are as previously defined (PART II) as "bad data." The hindcast results compare favorably with the measured data for all three locations. There is a slight overprediction of the hindcast H_{mo} when the computed T_p is greater than the measured estimates. The effects of the water depth in which the gages are placed significantly reduce the amount of energy in the high frequency end of the spectrum. This effect is amplified for wave estimates at WG-66. As mentioned in PART II, free-surface spectra were based on the estimate of the variation in the dynamic pressure of the water column measured by each gage. There is a theoretical limit (based on linear wave theory, Shore Protection Manual, (USACERC 1977)) where the gage will no longer "feel" the presence of certain frequency waves because of the water depth. Figure 21 displays that relation, where frequencies greater than 0.46 Hz cannot be resolved at WG-66. The other two wave gages are not constrained; WG-68 is located at 10-ft depth and WG-25 is located at 9.5-ft depth. When the majority of the energy density falls within this range, which is very often for Atchafalaya Bay, the loss in the total energy and thus the H_{mo} results will be significant. Therefore it is expected that the hindcast results should consistently overpredict wave conditions at WG-66. Realizing that the total energy derived from the measured pressure record will not reflect conditions from all frequencies, the differences between the two results (hindcast and measured) are not as great as those shown in the time-history plots.

47. As previously mentioned, when the hindcast peak spectral wave period is greater than the measured results, the hindcast H_{mo} results will also be overpredictive. The overprediction follows from Equation 27 and can be explained simplistically by Figure 22. Since the upper end of an energy density spectrum is limited to 0.5 Hz in the wave model, there are only two choices for f_m when f_m = 0.5 Hz, either 0.5 Hz or something slightly less than 0.5 Hz. If the hindcast f_m is less than the measured results as shown in Figure 22, then the hindcast $E(f)$ will carry slightly more energy as shown by the crosshatched area. The H_{mo} derived from the hindcast information will be greater than the measured results. Limiting the high frequency end of the hindcast spectrum also places a restriction on the H_{mo} results, dependent on the windspeed U_{10} and fetch length through Equation 22. If the limit of 0.5 Hz on f_m did not exist, the hindcast results would follow Equation 23 for f_m and, from Equation 27, the H_{mo} results would be diminished.

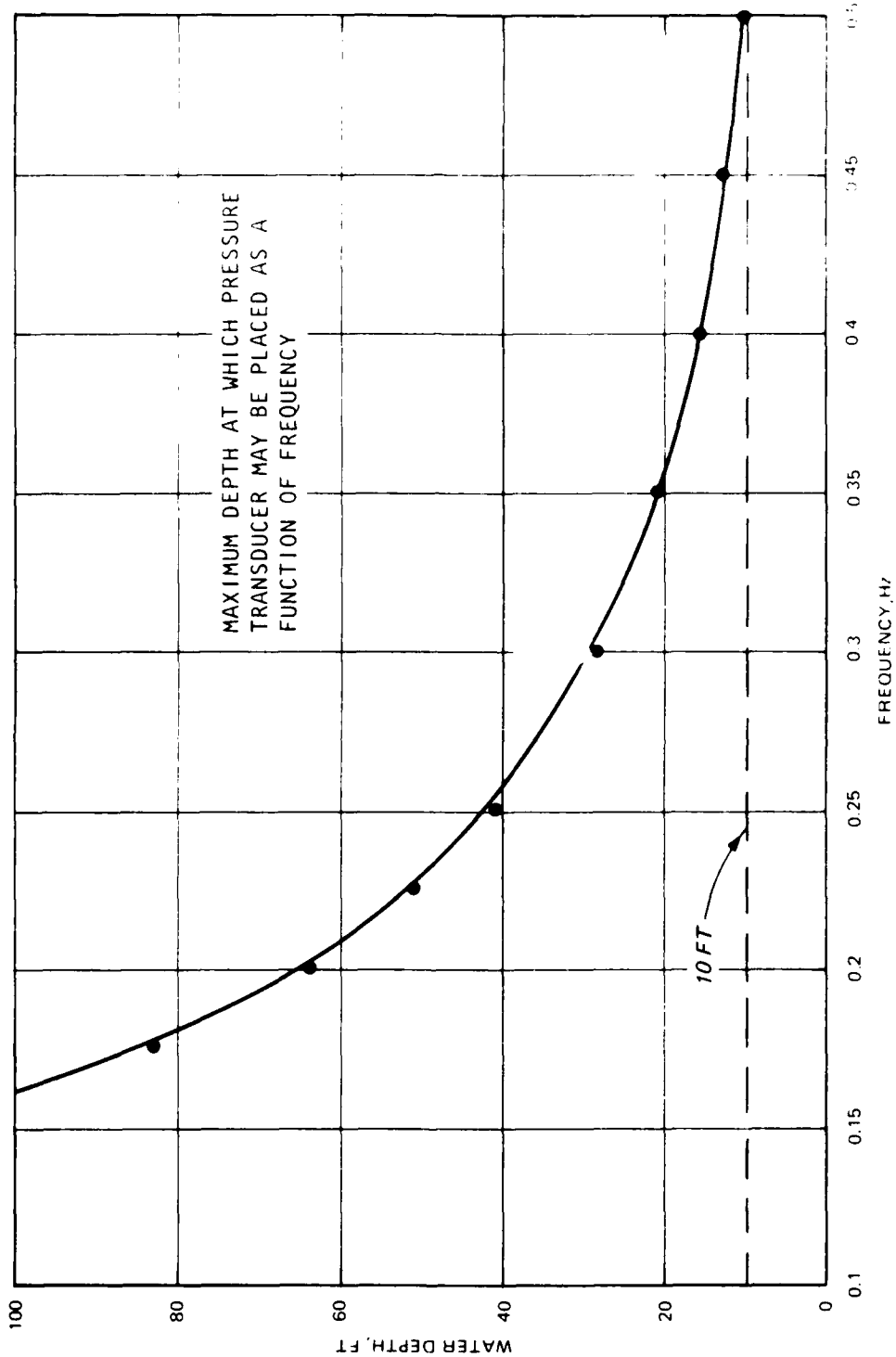

Figure 21. Losses in spectral frequency information caused by various water depths

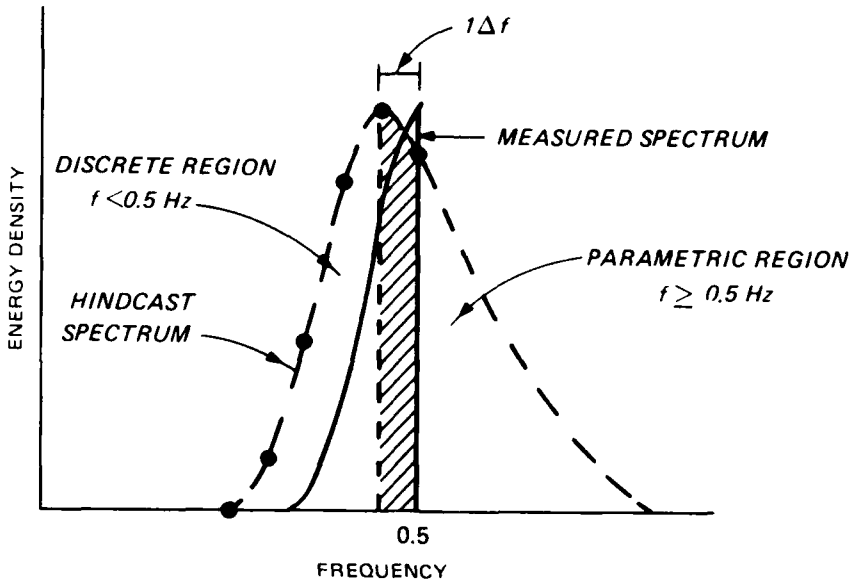

Figure 22. Schematic representation of the potential for increased energy levels in the hindcast wave information

These computations are carried out and presented in Table 1. One must note that the limit to T_p (where $T_p = f_m^{-1}$) is 2.0 sec, and therefore all results for H_{mo} values when $T_p < 2.0$ sec will equal H_{mo} at $T_p = 2.0$ sec. Hence, at low wind speeds, the hindcast results will be greater than the measured data set. Since the gage cannot resolve wave periods less than 2.0 sec, due to the sampling interval and water depth, there would be no way of knowing if the hindcast results were accurate less than 0.5 Hz. It now appears that limiting the hindcast spectral frequencies to 0.5 Hz (consistent with the measured results) will systematically overestimate the H_{mo} results. If an additional parametric region (Figure 22) was established in the hindcast spectrum, independent of the discrete frequency bands and dependent on Equations 23 and 27, the hindcast results would better approximate the wave-height results from the prototype data set.

48. The second storm occurred during 20-22 November 1981 and was characterized by wind speeds of approximately 18 knots and the wind direction which remained nearly constant at 300 deg for the duration of the storm. The measured data reflect the storm's intensity in two of the three gage sites (Figures A4-A6). It appears that the wave climate at WG-25 is governed by localized limiting conditions (for this case), whereas at WG-66 and WG-68, maximum H_{mo} conditions of approximately 2.0 ft existed. The hindcast results are

again in agreement with the trends established by the measured data sets, although at WG-25 the hindcast data tend to overestimate the H_{mo} results by approximately 1.0 ft. The differences may be caused by the new parametric representations of the growth rate and peak frequency changes over fetch lengths defined at WG-25. An alternate cause could be derived from the selection of the fetch length and water depths for the wind direction of 330 deg for WG-25. The water depths used in the model were taken from NOAA bathymetric charts (dated 1977). The depths that now exist within the bay may be significantly different due to the delta growth process in the vicinity at Wax Lake Outlet and the Atchafalaya River mouth.

49. The third storm considered in the verification phase of the study occurred during 23-26 December 1981. The wind speed averaged around 13 knots while the wind direction remained nearly constant at 45 deg. The measured results (Figures A7-A9) at all three gage locations exhibited nearly identical trends (rises and falls of H_{mo}) which would verify the assumption that wind speed and direction remain uniform over the Atchafalaya Bay region. The hindcast estimates for all three gage locations compare favorably with the measured H_{mo} and T_p results. Differences between the two estimates are shown to be no greater than ±0.5 ft for the H_{mo} results and ±0.5 sec for the T_p results. There appears to be a difference between the hindcast and gage results in the time of occurrence of the maximum H_{mo} conditions. This difference is caused by the method employed in the SWWM, i.e., wave propagation is omitted from the model to increase computational efficiency.

50. The largest H_{mo} found in all measured wave records occurred on 31 December 1981 at WG-68. The accompanying energy density spectra for the three gage and hindcast results are compared in Figures 23-25. The abscissa is nondimensionalized with respect to the peak spectral frequency. This allows both spectra to be aligned at the maximum energy and comparisons can be made to explore the frequency related spectral shape. The difference between the gage and hindcast peak frequency is $3\Delta f$ (or 0.0208 Hz) at its maximum. Based on statistical analyses, the 95 percent χ^2 range is shown in these figures, signifying the expected range of the prototype results. The wind conditions for this particular event were approximately 13 knots blowing from the northeast.

51. Local wave generation controls the wave environment for this storm, although a slight amount of Gulf-generated wave energy is visible in the

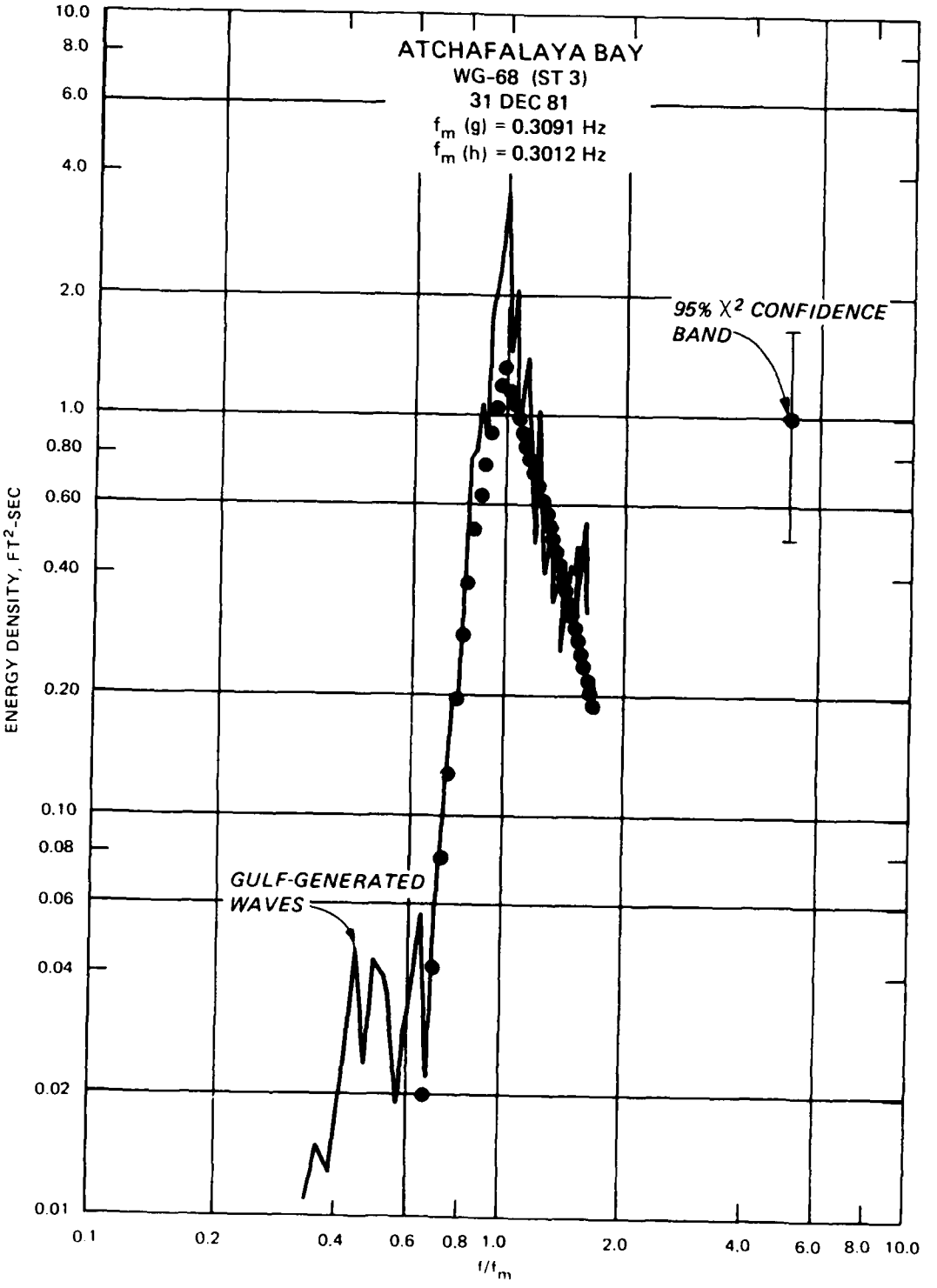

Figure 23. Comparison between hindcast and measured spectral estimates for WC-68

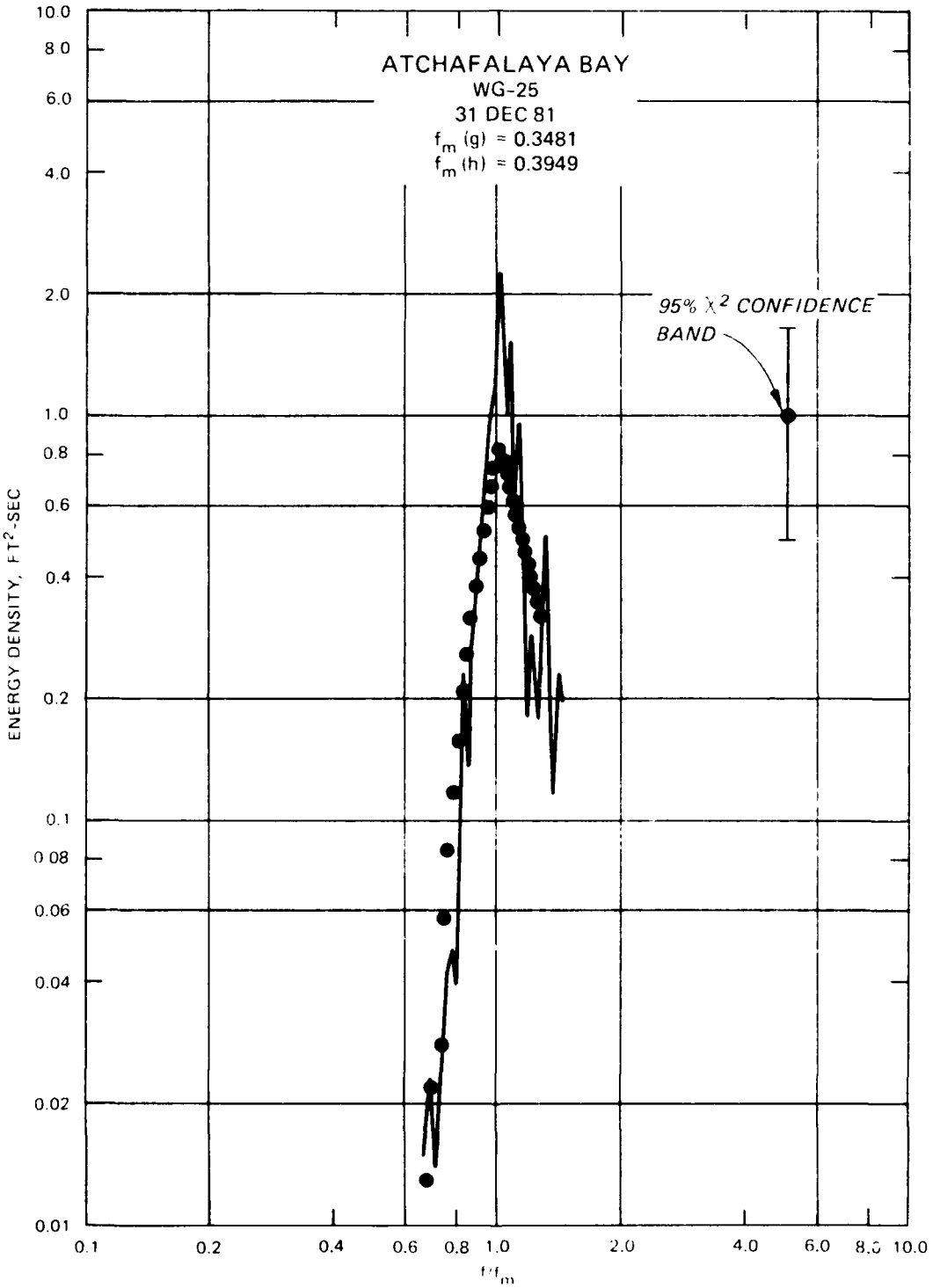

Figure 24. Comparison between hindcast and measured spectral estimates for WG-25

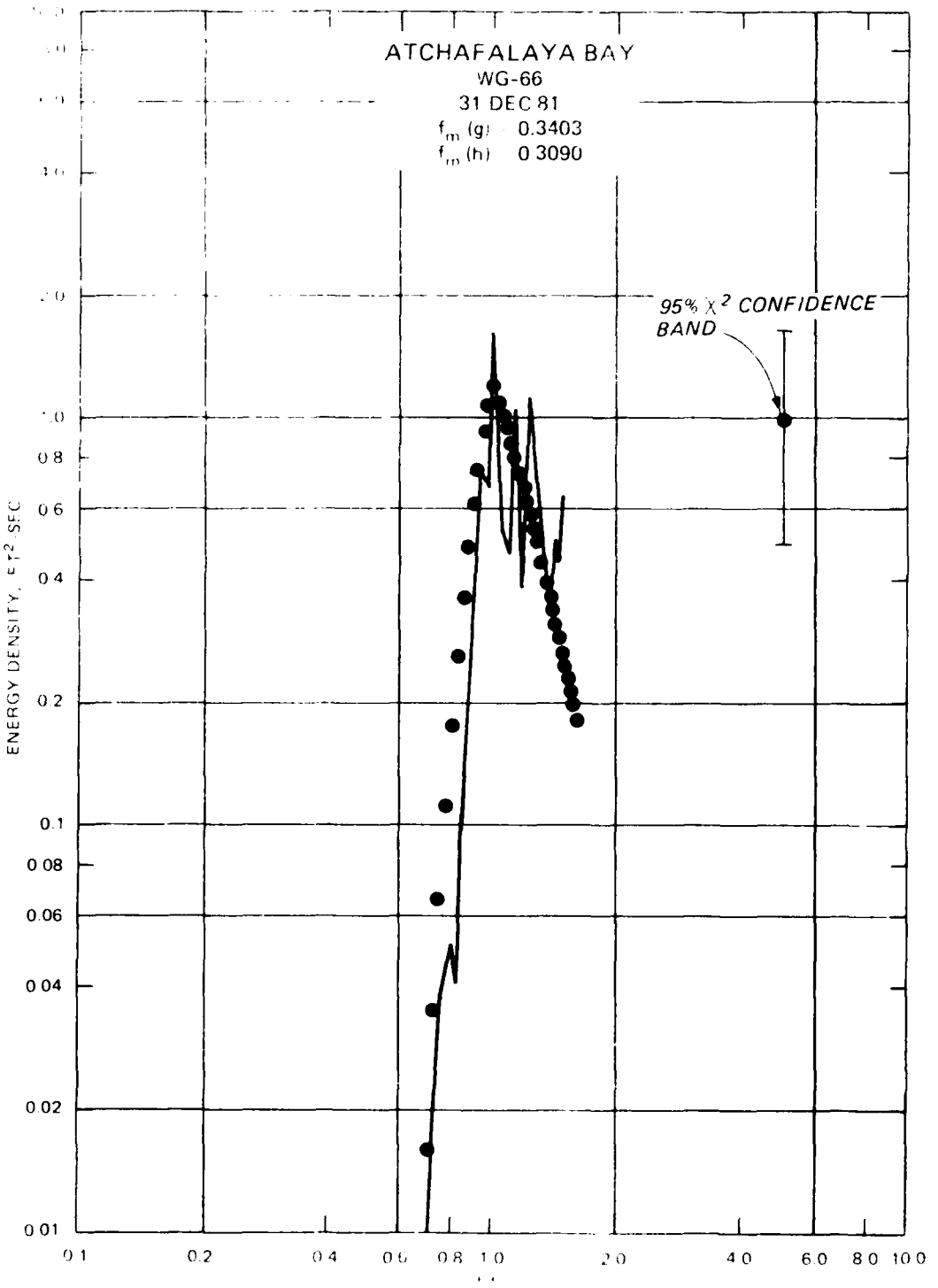

Figure 25. Comparison between hindcast and measured spectral estimates for WG-66

spectrum given for WG-68. The forward face is well approximated by the hindcast spectral shape, and the tail ($f/f_m > 1.0$) appears to be the limiting form compared with the prototype spectra. The hindcast $E(f_m)$ consistently underpredicts the measured results but remains within the 95 percent χ^2 range. As f/f_m approaches 2.0, the measured results tend to fall below the hindcast spectral shape. The water depth above the gages acts like low-pass filters, not allowing the energy in the high frequency wave components to be recorded. Also, the water depth can limit the entire spectral shape (Figure 25). Results for WG-66 (located in deeper water conditions than WG-25 or WG-68) are not as "clean" when compared with the other gage spectra. Even for short-period wave conditions, the theoretical shape functions found in the SWWM accurately depict the measured results.

52. The final two storms in this series occurred during 28-31 December 1981 (Storm 4) and 8-12 January 1982 (Storm 5). The wind speed conditions were on the order of 12 knots with an average wind direction of 50 deg, and 13 knots with an average wind direction of 25 deg for Storms 4 and 5, respectively. For the full duration of the storms, the hindcast results (for all three gage locations) matched the measured H_{mo} and T_p data (Figures A10-A12 for Storm 4 and Figures A13-A15 for Storm 5). Differences between the two data sets for both H_{mo} and T_p were consistently at ±0.25 ft and ±0.5 sec, respectively.

Southerly wave condition comparisons

53. All previous wave comparisons were derived from northerly wind conditions. Land-water boundaries, hence the fetch lengths, were clearly defined for these conditions. The problem of adequately describing a finite fetch length for waves propagating from the south still exists. The assumption that little energy which originates far out into the Gulf can propagate into the bay has been verified; however, the possibility of locally generated waves propagating from the south into the bay must still be accounted for. Therefore, in order to quantify a limiting fetch distance south of Atchafalaya Bay, a series of computations using the wave data were performed to determine where a fetch-limitation-line should be placed.

54. From Equations 22 and 23, the fetch length could be computed from known wind speed and the resulting wave height for all the southerly wind conditions. For each 10-deg wind angle interval, the computed fetch lengths were averaged. The average fetch length then was plotted as a function of wind

speed and distance from each of the gage locations. Although this technique is a crude approximation, it was found that all computed fetch lengths fell within the 12-ft contour defined by the bathymetric chart employed "outside" of Atchafalaya Bay. The fetch-limitation-line was established near the 12-ft contour, which means that wave conditions propagating from the Gulf of Mexico to Atchafalaya Bay would begin wave growth from the 12-ft contour, rather than in the middle of the Gulf. Using this technique, only long-period, low-amplitude wave information would be lost. But from the measured data, the number of occurrences and the intensity (or energy content) of these conditions did not warrant further analysis.

55. Under these assumptions, verification of southerly generated wave conditions was performed. Five storms were selected to verify the fetch-limitation-line assumption. The initial storm (Storm 1A) occurred during 25-27 November 1981; wind speeds averaged around 11 knots and the wind direction remained near 130 deg. The measured wave data for all three gage locations never exceeded 1.25 ft (Figures B1-B3) while the T_p results clearly showed a much stronger trend for longer wave periods. The hindcast H_{mo} results show a strong agreement with the measured results although the results for WG-66 tended to diverge slightly on 26 November 1981 (Figure B2). The largest differences encountered are in the T_p comparisons where the hindcast results tend to be around 2.0 sec, whereas the gage data results increased to 6.0 to 9.0 sec.

56. The influence of Gulf-generated wave conditions propagating into the study area is evident. In general, the energy accompanying these long-period conditions is significantly lower (except for one observation at WG-68) than that during the most intense portion of the storm. For nearly identical wind speeds blowing from the north (Storm 2, Figures A4-A6), the H_{mo} results are approximately a factor of 2 greater than what is observed during this particular storm condition where fetch lengths are on the order of 10 to 100 times as great. Therefore the amount of energy lost employing the SWWM to model southerly wave conditions can be considered negligible in comparison with other equally important storm conditions.

57. The second storm (Storm 2A) for southerly waves occurred during 2-5 December 1981. The wind intensity averaged around 7.5 knots while the direction was predominantly from 235 deg. The measured wave data (Figures B4-B6) showed H_{mo} results much larger than in the previous storm and T_p results

indicated that the waves were locally generated within the area near Atchafalaya Bay rather than derived from the Gulf of Mexico. For the existing measured data set, the hindcast information nearly duplicates the measured results in terms of H_{mo} and T_p.

58. The third storm (Storm 3A) occurred during 21-23 December 1981. The wind speed averaged 11 knots while the direction remained at approximately 180 deg. The measured wave heights displayed in Figures B7-B9 again remain relatively small within the bay (WG-25 and WG-66) while at WG-68 a maximum H_{mo} condition of 1.75 ft was observed. Comparison of the three gage data sets shows that as the wave conditions propagate into Atchafalaya Bay (from WG-68), most long-period information (T_p > 6.0 sec) is lost and the spectra are reformed into the high frequency end. The hindcast H_{mo} estimates tend to overestimate conditions present at both WG-25 and WG-66 (0.5 ft high) but at WG-68, the differences in the two data sets are negligible. The T_p hindcast results compare favorably at all three gage sites except during long-period wave activity.

59. The fourth and fifth storms occurred during 1-4 January 1982 (Storm 4A) and 5-8 January 1982 (Storm 5A). The wind speeds averaged approximately 10 knots and 7.5 knots for Storms 4A and 5A, respectively. The wind directions generally remained constant at 165 deg and 170 deg for the two events. The measured wave data followed the trends established in the three previous storms where the T_p data inside the bay ranged from 2.0 to 3.0 sec, while the wave conditions outside the bay (WG-68) oscillated from predominantly short- to long-period waves (Figures B10-B12). The H_{mo} results indicate that for wind speeds less than approximately 10 knots, there is no appreciable energy in the area (Figures B13-B15). Maximum H_{mo} occurred at WG-68 and for the 5-day period never exceeded 1.5 ft. The hindcast results again compare reasonably well with the measured data. For low wave conditions, the hindcast H_{mo} tends to overpredict the gage results but differences between the two sets seldom exceed 0.25 ft.

Percent occurrence
and extreme comparisons

60. Two additional types of comparisons were made to further verify the SWWM technique--percent occurrence and cross plots. The comparison techniques were used to describe the random error of the hindcast model. For the evaluation of the hindcast wave conditions relative to wave climate representations,

major emphasis must be centered on long-term comparisons of means and probability distributions in which the time factor has been removed. In all subsequent comparisons, the hindcast wave results were paired according to the gage observations. However, much of the presumed random error in these comparisons is attributed to slight shifts between the wave hindcasts and observed wave results.

61. There is a certain degree of uncertainty associated with the statistical representations of the wave climate at a given location. One must be aware that even gage results cannot uniquely describe actual wave conditions during a sampling period. It is assumed that a sample period of 1,024 sec (17.1 min) every 3 hr is a measure of the average conditions existing for that particular interval. Therefore the use of long-term, continuous (defined here as a constant number of observations per day over a prolonged period of time) H_{mo} and T_p results will offset the inconsistency in the actual and measured wave conditions.

62. For each gage site, the percent occurrence for H_{mo} and T_p is compared. The paired results are separated into H_{mo} intervals of 0.25 ft and T_p in intervals of 0.5 sec. These plots are generated for comparison purposes only and should not be construed as the representative wave climate expected for each specified location.

63. Figure 26 displays the percent occurrence of H_{mo} and T_p conditions for WG-68, located south of Atchafalaya Bay. There are large differences in the two results for H_{mo} conditions between 0.25 to 1.0 ft, whereas the results show only slight (less than 1.0 percent) differences in all other categories. The tail of the distribution is well approximated by the hindcast model and zeroes out one category lower than the measured results. The overall mean H_{mo} shows that the hindcast compares identically with the measured results and equals 0.73 ft. The hindcast time-history tended toward overpredicting the gage H_{mo} results. Figure 26 shows that by removing the time dependency the hindcast results look extremely good. In a climatological sense, if the hindcast performs well (i.e., has the same, or nearly the same, probability that a particular wave condition would occur) then the bias in the time-histories is superseded by the results shown in Figure 26.

64. The T_p results show that a large portion (26 percent) of the wave conditions found south of Atchafalaya Bay are produced in the Gulf of Mexico. The relative energy associated with these long-period waves typically amounts

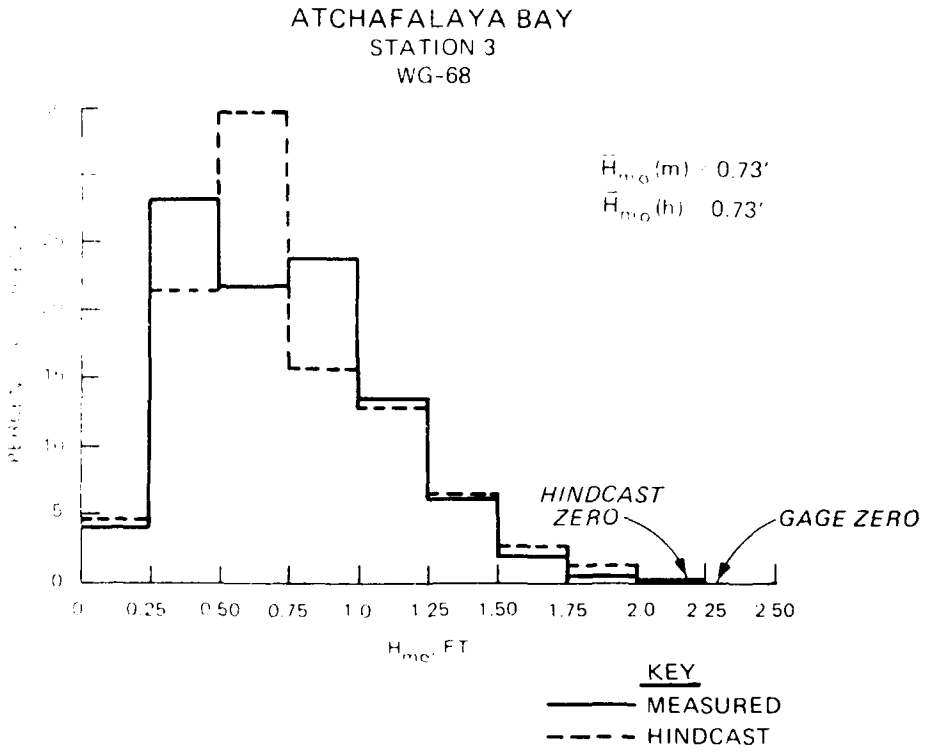

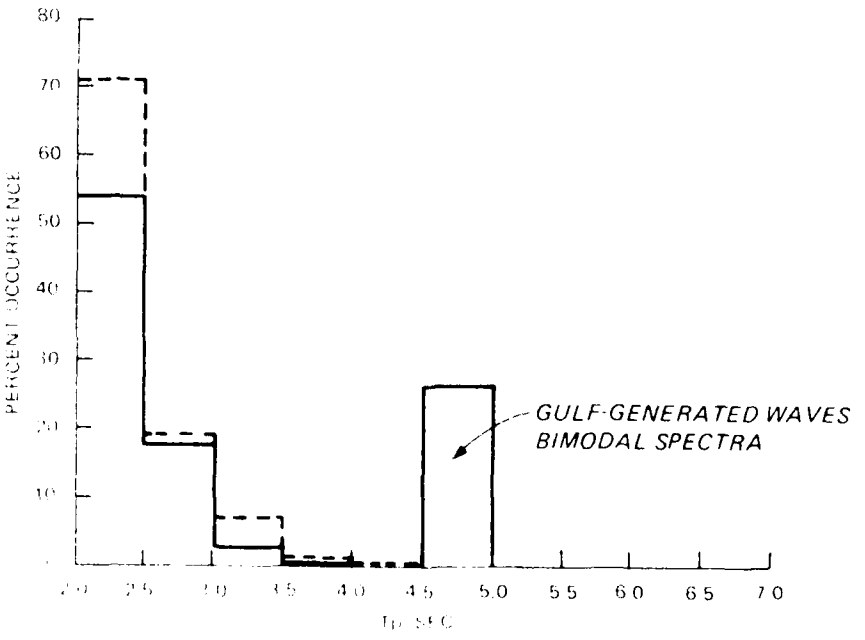

Figure 26. Percent occurrence of H_{mo} and T_p for time-paired measured and hindcast wave information for WG-68

to 25 percent of the total energy found in the spectrum (excluding the extreme case shown in Figure 17). The hindcast results based on the fetch-limitation-line (Figure 1 and Equation 22) spread the underestimate in long-period wave conditions over the entire distribution. Once the long-period waves enter Atchafalaya Bay, the energy is absorbed by the bottom, as will be seen in subsequent figures (and shown in PART II).

65. The percent occurrence of H_{mo} and T_p for WG-25 is displayed in Figure 27. Once inside Atchafalaya Bay, the percent occurrence of Gulf-generated waves substantially decreases (from 26 percent at WG-68 to 7 percent at WG-25). The hindcast H_{mo} distribution represents the measured conditions for results greater than 0.75 ft and zeroes out at the identical H_{mo} category. For wave heights less than 0.75 ft, the hindcast information oscillates above and below the measured values; but over the average, the hindcast H_{mo} falls slightly greater (0.04 ft or 7.1 percent) than the measured condition. The T_p distribution generated by the SWWM displays nearly identical results established in the measured data set, with exception of the long-period, Gulf-generated wave conditions. At this station location, approximately 90 percent of the measured T_p information lies within the range between 2.0 to 2.5 sec, whereas in the other two locations (WG-68 and WG-66) this percentage decreases significantly. Geographical and bottom topographical constraints at WG-25 limit significant wave growth and are adequately represented by the hindcast model.

66. The remaining statistical distributions based on measured and hindcast wave information for WG-66 are displayed in Figure 28. The broad trends in the H_{mo} gage results appear very similar to that found in Figure 26 for WG-68. There is a specific reason for a diverse population of wave conditions to exist at this particular location, especially very small (0.0 to 0.25 ft) H_{mo} conditions. The large number of small waves tends to depress the overall gage mean H_{mo} to 0.58 ft, or within the range established at WG-25. One reason for this could be attributed to the local water depth near the gage location. As discussed in PART III, a water depth of 11 ft tends to "clip off" the high frequency end of the energy density spectrum. In so doing, a slight amount of energy would not be resolved (although it would exist within the free surface) and the wave heights would be lower. If the lost energy could be accounted for, the entire distribution shown in Figure 28 would significantly change. The most dramatic change would be at the lower end of the H_{mo}

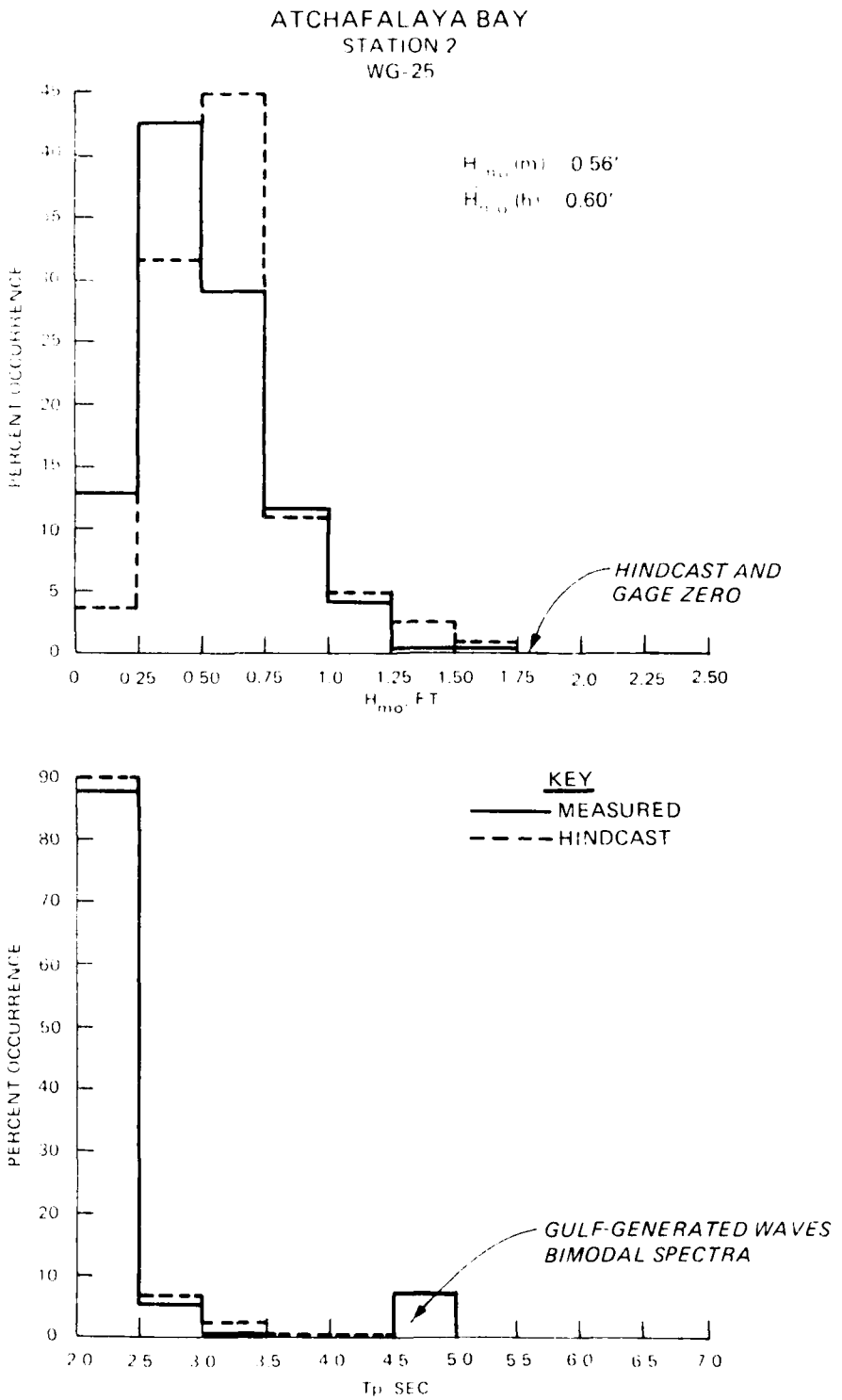

Figure 27. Percent occurrence of H_{mo} and T_p for time-paired measured and hindcast wave information for WG-25

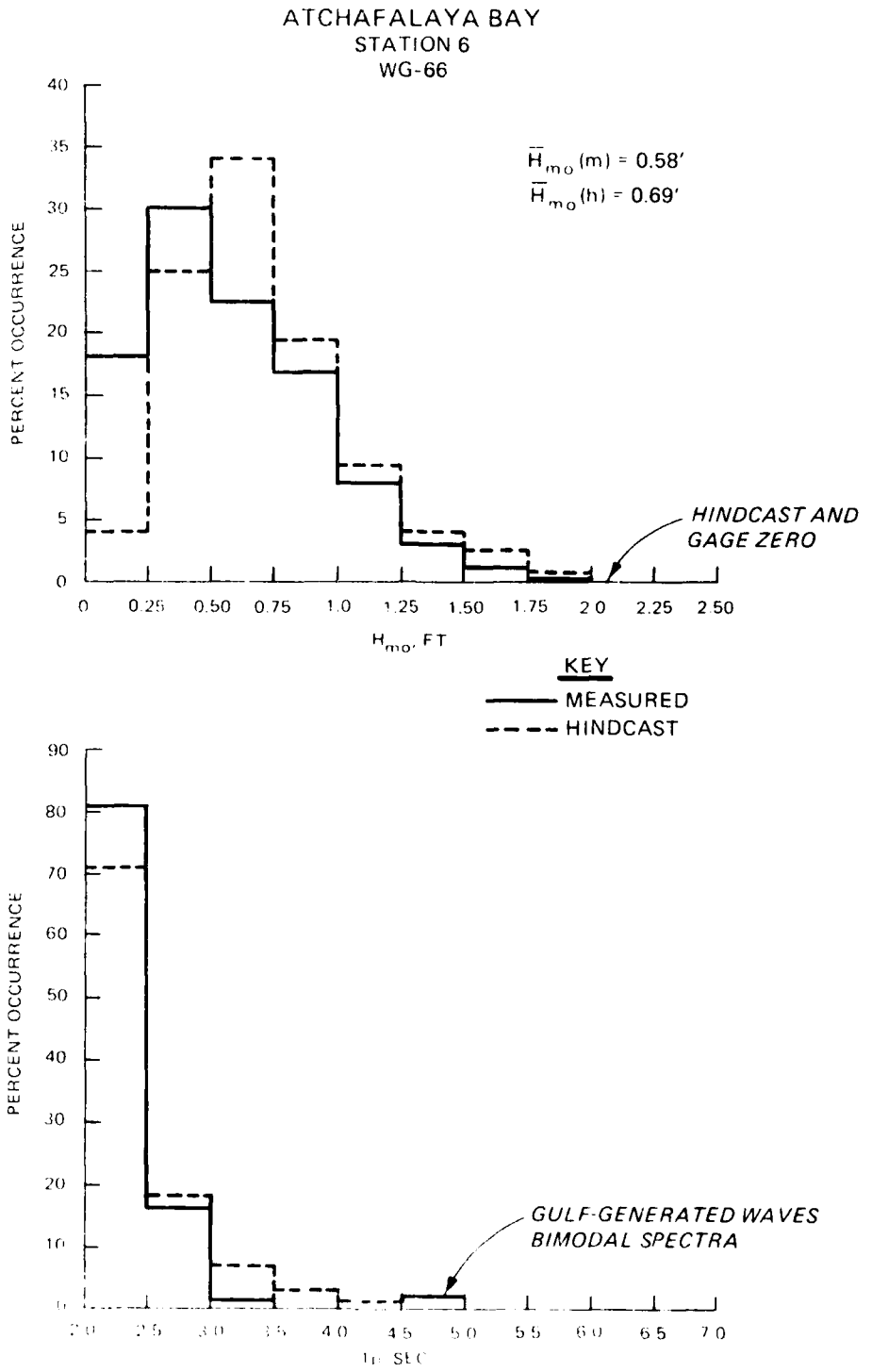

Figure 28. Percent occurrence of H_{mo} and T_p for time-paired measured and hindcast wave information for WG-66

distribution, where the energy level is already low. Excluding H_{mo} results less than 0.75 ft, the hindcast model adequately represents the measured conditions although uniformly overpredicting the percent distribution by approximately 4 percent. The hindcast mean wave height is 19 percent larger than that found in the measured results; but considering the loss of the high frequency information in the gage data, the difference between the two results is not unexpected.

67. The T_p distribution generated from the gage results clearly shows (Figure 28) that as Gulf-generated waves propagate farther into Atchafalaya Bay, their influence diminishes. Only 2 percent of the measured conditions had T_p conditions greater than 4.5 sec, whereas outside the bay (WG-68), 26 percent of the wave climate was under the influence of long-period waves. This shows that local wave generation characterized by extremely short-period waves controls the wave environment in Atchafalaya Bay. Although the hindcast model overpredicts the percentages in T_p categories from 2.5 to 4.5 sec, the greatest difference is only 6.0 percent.

68. A final comparison is made between extreme storm wave conditions. The H_{mo} results were derived by selecting the largest 10 to 20 storm events within the gage sampling period. The maximum H_{mo} from a particular event was recovered. The dates for these events were then used to scan the hindcast results to select the maximum H_{mo} from the same storm. The maximum H_{mo} conditions are not identically paired in time (lag time caused by nonpropagation of wave conditions in the hindcast model) but are representative of the event. The comparisons are shown in graphical form (Figure 29) and are also found in Table 2. Figure 29 shows that the hindcast results under extreme storm wave conditions do not clearly show a bias toward overestimating or underestimating the measured information. The trends shown in Figure 29 follow the results found in both the time-history and percent occurrence comparisons. The hindcast model underpredicts the results at WG-68 caused by neglecting Gulf-generated waves and primarily overestimates the measured conditions at WG-66, where high frequency energy is lost in the gage data because of the water depth. The mean H_{mo} values for the data sets are plotted and the resulting difference shows that the hindcast model is 2.0 percent (or 0.03 ft) larger than the measured results.

69. In summary, wave information derived from the SWWM compares favorably with the gage data for nearly all wind angles (from 0 to 360 deg); thus

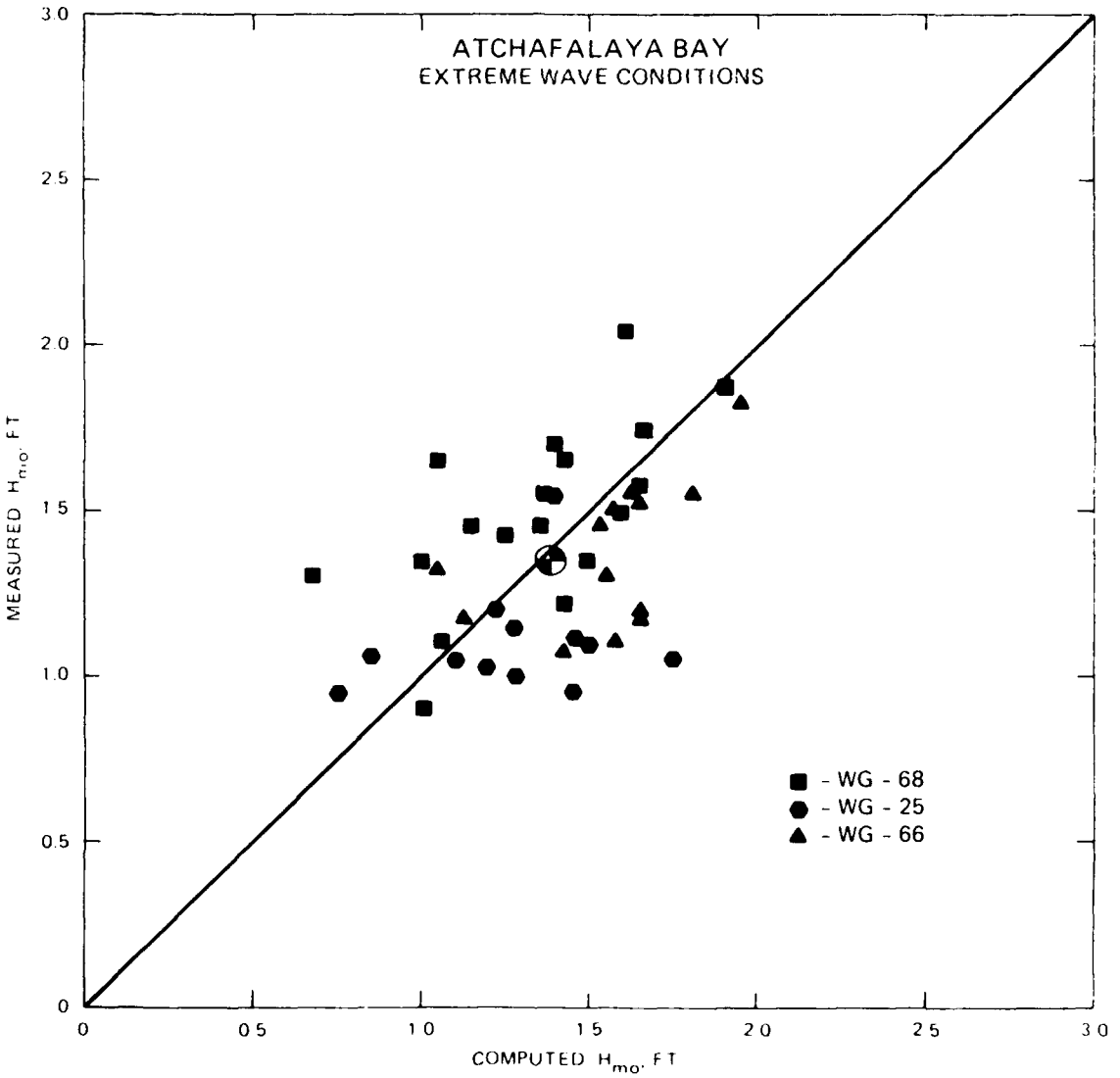

Figure 29. Cross plot of measured and hindcast extreme H_{mo} conditions existing in a specific event for the three gage locations

the assumptions governing the methodology of the SWWM are verified. Wind speeds and directions can be considered as uniform over Atchafalaya Bay. The growth of wave energy is assumed to be dependent on fetch lengths (and wind speeds) rather than duration. Although long-period wave energy exists in the area, it is limited in intensity. When the predominant spectral energy is situated in the low frequency end of the spectrum for locations outside Atchafalaya Bay, the inside locations retain nearly the same amount of energy but distribute it in the higher frequency range (suggesting that wave breaking and reformation processes occur between outside and inside the bay). Although the

fetch-limitation-line located south of Atchafalaya Bay (near the 12-ft contour) was a rough estimate of maximum growth rates for southerly waves, comparisons with measured data verified that the estimate was correct.

PART IV: ONE-YEAR WAVE HINDCAST

Introduction

70. The verified SWWM is designed to compute wave conditions at arbitrarily selected locations in Atchafalaya Bay. All wave conditions generated assume constant water depths over time, therefore neglecting changes in the water elevation caused by tides, surges, and freshwater discharges. In order to improve computational efficiency, a polar coordinate system is selected wherein the origin is placed at each of the 10 selected station locations (Table 3 and Figure 1). Fetch-length rays are projected outward from the origin at 10-deg intervals. A total of 36 rays exist for each station. The selection of the 36 rays assures that the variability of the shoreline boundaries is accurately described. Fetch length and water depths are discretized into 10 subsections along the total length of each ray. The water depth selected for each subsection is averaged from available NOAA bathymetric charts (dated 1977). The parameters h_i (discrete water depth), F_i (discrete fetch length), and F_t $\left(\text{total fetch length, where } F_t = \sum_{i=1}^{10} F_i\right)$ then become direct functions of a given wind direction. In many instances, the wind direction will not correspond identically to a given fetch-length ray. When this occurs, a new $F_t(\theta_w^*)$ and $h_i(F_i, \theta_w)$ are computed via linear interpolation between two discrete fetch-length rays.

71. The input conditions to the SWWM are the wind speed (adjusted to 10-m elevation) and the wind direction. The proper fetch length, F_t, and water depths, h_i, are then selected for each station for the given wind direction. This procedure is followed for every 3-hr interval using the approximately 1-year period of wind data recorded (Ebersole 1985).

One-Year Wave Hindcast Products

72. This section of the report is intended only to serve as a general description of simple wave characteristics such as height, period, and

* The parameter θ_w is the predominant wind angle measured in degrees azimuth, "from which they came."

direction of wave propagation. More detailed analysis of one-dimensional spectral properties and interrelations between various wave parameters related to storm characteristics are beyond the scope of this report.*

73. The 1-year hindcast only considers a single population of wave conditions defined as sea (although during periods of time, the nondimensional peak frequency is less than 0.13, defined as swell by Hasselmann et al. (1976)). Also all waves travel in the direction of the wind, and the wind speed and direction are assumed to be uniform over Atchafalaya Bay.

74. The wave parameters H_{mo} (Equation 2), T_p (Equation 3), and ψ given at each station every 3 hr for approximately 1 year are used as a basis to construct the joint percent occurrence tables found in Appendix C. When measured wind data were not available, the wave conditions (H_{mo}, T_p, ψ, and $E(f)$) were all set to zero and not used in the analysis. The wave directions are assumed to be those from which the waves are coming (Figure 30) and are measured clockwise in degrees from the north (0.0 deg).

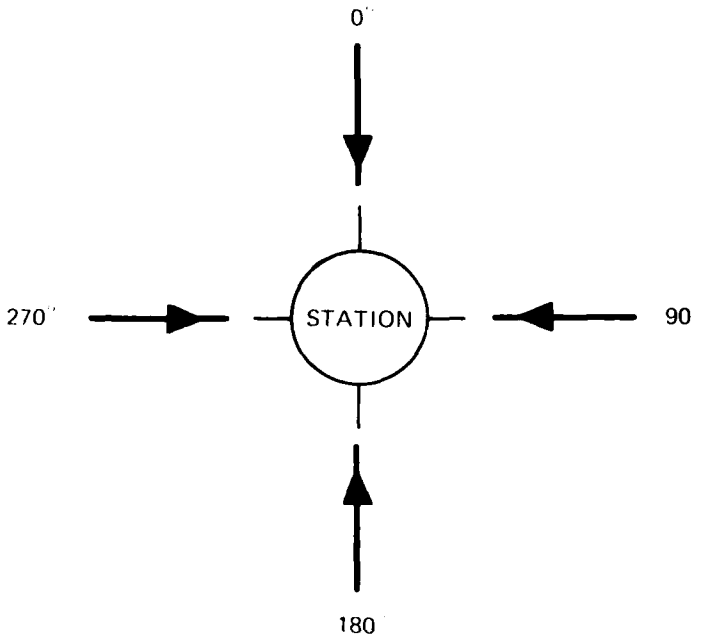

Figure 30. Direction of wave propagation

75. Two products are presented:

a. Seasonal Percent Occurrence Tables.

b. One-Year Percent Occurrence Tables.

A brief description of each product is given and instructions on their use, including examples, are provided.

* One-dimensional frequency spectra and H_{mo}, T_p, and ψ (direction of wave propagation) are stored at 3-hr intervals for 1 year for each station.

Seasonal and 1-year
percent occurrence tables

76. Two types of tables are printed for each of the two products: azimuth tables and all-directions tables. At each location, for both the seasonal and yearly products, 16 azimuth tables and 1 all-direction table are printed. The azimuth tables (Figure 31) give the percent occurrence of characteristic waves in terms of height and period ranges for a specified station, season,* and direction. The title of each table identifies the station, season, angle class, and water depth. The angle class specification for each table represents waves coming from directions approximately 11.25 deg to either side of the labeled direction. For example, 0 deg represents directions $\geq$348.75 deg and $<$11.25 deg. The wave period ranges are in 0.5-sec intervals and the height ranges are in 0.25-ft increments. Values in the azimuth tables represent the percent of the season that waves occur from the specified angle class for the indicated height and period range combinations. The values have been multiplied by 1,000 to allow more accuracy with less printing space. Summations of period and height ranges are provided in the last column and row of each table. The summations are also multiplied by 1,000. The last line in each azimuth table contains the following information for the specified angle class, season, and location:

a. The average H_{mo} .

b. The largest H_{mo} .

c. Percent of waves occurring in the specified season from the indicated angle class.

77. The all-directions table for each season (Figure 32) is printed after the 337.5-deg angle class table for the specified season. These tables give the percent occurrence of significant waves within the same specified height and period ranges coming from all directions for the indicated season and station. Percent values in the all-directions tables are multiplied by 100. The parameters listed in the last line of this table are derived from all directions for the specified season. The total number of cases represents the number of 3-hr average wave conditions that were hindcast during the indicated season. This number reflects how much wind data were available to

* Season 1 is December through February, Season 2 is March through May, Season 3 is June through August, and Season 4 is September through November.

STATION 1 SEASON 1 ANGLE CLASS (DEG AZIMUTH)= 0.
WATER DEPTH = [illegible] FEET
PERCENT OCCURRENCE(X1000) OF HEIGHT AND PERIOD BY DIRECTION

HEIGHT(FEET)	PERIOD(SECONDS)										TOTAL
	0.0-0.4	0.5-0.9	1.0-1.4	1.5-1.9	2.0-2.4	2.5-2.9	3.0-3.4	3.5-3.9	4.0-4.4	4.5-LONGER	
0. - 0.24	.	.	.	.	.	.	.	.	.	.	
0.25 - 0.49	.	.	.	.	286	.	.	.	.	.	[illegible]
0.50 - 0.74	.	.	.	.	.	.	.	.	.	.	
0.75 - 0.99	.	.	.	.	.	143	.	.	.	.	1.4
1.00 - 1.24	.	.	.	.	.	.	.	.	.	.	
1.25 - 1.49	.	.	.	.	.	.	.	.	.	.	
1.50 - 1.74	.	.	.	.	.	.	.	.	.	.	
1.75 - 1.99	.	.	.	.	.	.	.	.	.	.	
2.00 - 2.24	.	.	.	.	.	.	.	.	.	.	
2.25 - 2.49	.	.	.	.	.	.	.	.	.	.	
2.50 - GREATER	.	.	.	.	.	.	.	.	.	.	
TOTAL	0	0	0	0	286	143	0	0	0	0	[illegible]

AVERAGE HS(FT) = 0.59 LARGEST HS(FT) = 0.88 ANGLE CLASS % = 0.4

STATION 1 SEASON 1 ANGLE CLASS (DEG AZIMUTH)= 22.5
WATER DEPTH = 6.50 FEET
PERCENT OCCURRENCE(X1000) OF HEIGHT AND PERIOD BY DIRECTION

HEIGHT(FEET)	PERIOD(SECONDS)										TOTAL
	0.0-0.4	0.5-0.9	1.0-1.4	1.5-1.9	2.0-2.4	2.5-2.9	3.0-3.4	3.5-3.9	4.0-4.4	4.5-LONGER	
0. - 0.24	.	.	.	.	.	.	.	.	.	.	0
0.25 - 0.49	.	.	.	.	[illegible]	.	.	.	.	.	[illegible]
0.50 - 0.74	.	.	.	.	[illegible]	.	.	.	.	.	[illegible]
0.75 - 0.99	.	.	.	.	[illegible]	[illegible]	.	.	.	.	[illegible]
1.00 - 1.24	.	.	.	.	.	[illegible]	1575	.	.	.	[illegible]
1.25 - 1.49	.	.	.	.	.	.	143	.	.	.	1.3
1.50 - 1.74	.	.	.	.	.	.	.	.	.	.	0
1.75 - 1.99	.	.	.	.	.	.	.	.	.	.	0
2.00 - 2.24	.	.	.	.	.	.	.	.	.	.	0
2.25 - 2.49	.	.	.	.	.	.	.	.	.	.	0
2.50 - GREATER	.	.	.	.	.	.	.	.	.	.	0
TOTAL	0	0	0	0	[illegible]	2721	1718	0	0	0	[illegible]

AVERAGE HS(FT) = 0.77 LARGEST HS(FT) = 1.29 ANGLE CLASS % = 10.0

STATION 1 SEASON 1 ANGLE CLASS (DEG AZIMUTH)= 45.0
WATER DEPTH = 6.50 FEET
PERCENT OCCURRENCE(X1000) OF HEIGHT AND PERIOD BY DIRECTION

HEIGHT(FEET)	PERIOD(SECONDS)										TOTAL
	0.0-0.4	0.5-0.9	1.0-1.4	1.5-1.9	2.0-2.4	2.5-2.9	3.0-3.4	3.5-3.9	4.0-4.4	4.5-LONGER	
0. - 0.24	.	.	.	.	143	.	.	.	.	.	[illegible]
0.25 - 0.49	.	.	.	.	[illegible]	.	.	.	.	.	[illegible]
0.50 - 0.74	.	.	.	.	[illegible]	.	.	.	.	.	[illegible]
0.75 - 0.99	.	.	.	.	[illegible]	.	.	.	.	.	[illegible]
1.00 - 1.24	.	.	.	.	.	286	.	.	.	.	[illegible]
1.25 - 1.49	.	.	.	.	.	.	.	.	.	.	0
1.50 - 1.74	.	.	.	.	.	.	.	.	.	.	0
1.75 - 1.99	.	.	.	.	.	.	.	.	.	.	0
2.00 - 2.24	.	.	.	.	.	.	.	.	.	.	0
2.25 - 2.49	.	.	.	.	.	.	.	.	.	.	0
2.50 - GREATER	.	.	.	.	.	.	.	.	.	.	0
TOTAL	0	0	0	0	11459	286	0	0	0	0	[illegible]

AVERAGE HS(FT) = 0.53 LARGEST HS(FT) = 1.08 ANGLE CLASS % = 11.7

STATION 1 SEASON 1 ANGLE CLASS (DEG AZIMUTH)= 67.5
WATER DEPTH = 6.50 FEET
PERCENT OCCURRENCE(X1000) OF HEIGHT AND PERIOD BY DIRECTION

HEIGHT(FEET)	PERIOD(SECONDS)										TOTAL
	0.0-0.4	0.5-0.9	1.0-1.4	1.5-1.9	2.0-2.4	2.5-2.9	3.0-3.4	3.5-3.9	4.0-4.4	4.5-LONGER	
0. - 0.24	.	.	.	.	[illegible]	.	.	.	.	.	[illegible]
0.25 - 0.49	.	.	.	.	[illegible]	.	.	.	.	.	[illegible]
0.50 - 0.74	.	.	.	.	[illegible]	.	.	.	.	.	[illegible]
0.75 - 0.99	.	.	.	.	.	.	.	.	.	.	[illegible]
1.00 - 1.24	.	.	.	.	.	.	.	.	.	.	[illegible]
1.25 - 1.49	.	.	.	.	.	.	.	.	.	.	[illegible]
1.50 - 1.74	.	.	.	.	.	.	.	.	.	.	[illegible]
1.75 - 1.99	.	.	.	.	.	.	.	.	.	.	[illegible]
2.00 - 2.24	.	.	.	.	.	.	.	.	.	.	[illegible]
2.25 - 2.49	.	.	.	.	.	.	.	.	.	.	[illegible]
2.50 - GREATER	.	.	.	.	.	.	.	.	.	.	[illegible]
TOTAL	0	0	0	0	[illegible]	0	0	0	0	0	[illegible]

AVERAGE HS(FT) = 0.47 LARGEST HS(FT) = 0.60 ANGLE CLASS % = 8.5

Figure 31. Example of the seasonal statistical table for various angle classes

STATION 1 SEASON 1 FOR ALL DIRECTIONS
WATER DEPTH = 0.50 FEET
PERCENT OCCURRENCE(X100) OF HEIGHT AND PERIOD FOR ALL DIRECTIONS

HEIGHT(FEET)	PERIOD(SECONDS)										TOTAL
	0.0-0.4	0.5-0.9	1.0-1.4	1.5-1.9	2.0-2.4	2.5-2.9	3.0-3.4	3.5-3.9	4.0-4.4	4.5-LONGER	
0. - 0.24	.	.	.	.	401	14	.	.	.	.	415
0.25 - 0.49	.	.	.	.	4434			.	.	.	4[illegible]
0.50 - 0.74	.	.	.	.	3137	71	14	.	.	.	3[illegible]
0.75 - 0.99	.	.	.	.	469	501	57	14	.	.	1[illegible]
1.00 - 1.24	.	.	.	.	.	272	285	42	42	.	[illegible]
1.25 - 1.49	.	.	.	.	.	.	57	57		.	1[illegible]
1.50 - 1.74	.	.	.	.	.	.	14	28	14	.	[illegible]
1.75 - 1.99	.	.	.	.	.	.	.	14		.	1[illegible]
2.00 - 2.24	.	.	.	.	.	.	.	.	.	.	[illegible]
2.25 - 2.49	.	.	.	.	.	.	.	.	.	.	[illegible]
2.50 - GREATER	.	.	.	.	.	.	.	.	.	.	[illegible]
TOTAL	0	0	0	0	8451	858	428	155	56	0	[illegible]

AVE HS(FT) = 0.56 LARGEST HS(FT) = 1.77 TOTAL CASES = 698.

Figure 32. Example of the all-directions seasonal statistical table

perform the hindcast during that particular season. All calm wave conditions (H_{mo} less than 0.01 ft) are removed from these tables because of the method employed in the SWWM. This constraint will not alter the data since: (a) we are dealing with a very small number of occurrences within a given period of time in Atchafalaya Bay and (b) the magnitude of H_{mo} is so small that whether one considers a wave height of 0.01 ft or 0.0 ft is of no real consequence.

78. The 1-year tables (examples are shown in Figures 33 and 34) are of the same format described above. These tables (angle class tables and all-directions tables) are based on the full 1-year data set (or the cumulative total of the four sets of seasonal tables).

Use of the tables

79. The following examples illustrate how to use these percent occurrence tables. In order to find the number of hours that waves with heights greater than 0.75 ft and less than 0.99 ft and periods between 2.5 and 2.9 sec are expected to occur from 0 deg at Station 1 during Season 1 (December, January, February), the value read in the table for the specified station, season angle class, height, and period should first be divided by 1,000 (yields 0.143 percent, Figure 31). Then 0.143 is divided by 100 to give the probability and multiplied by the total number of hours in Season 1 to yield the number of hours that the specified wave is expected to occur. The simple conversion process is:

$$\frac{\text{value read in table}}{1{,}000} \div 100 \times \text{number of hours in time interval} = \text{number of hours specified wave is expected to occur} \qquad (29)$$

STATION 1 1 YEAR ANGLE CLASS (DEG AZIMUTH) = 0.
WATER DEPTH = 5.50 FEET
PERCENT OCCURRENCE(X1000) OF HEIGHT AND PERIOD BY DIRECTION

HEIGHT(FEET)	PERIOD(SECONDS)										TOTAL
	0.0-0.4	0.5-0.9	1.0-1.4	1.5-1.9	2.0-2.4	2.5-2.9	3.0-3.4	3.5-3.9	4.0-4.4	4.5-LONGER	
0. - 0.24	.	.	.	.	86	.	.	.	.	.	86
0.25 - 0.49	.	.	.	.	340	.	.	.	.	.	340
0.50 - 0.74	.	.	.	.	6	.	.	.	.	.	6
0.75 - 0.99	.	.	.	.	.	46	.	.	.	.	46
1.00 - 1.24	.	.	.	.	.	.	.	.	.	.	.
1.25 - 1.49	.	.	.	.	.	.	.	.	.	.	.
1.50 - 1.74	.	.	.	.	.	.	.	.	.	.	.
1.75 - 1.99	.	.	.	.	.	.	.	.	.	.	.
2.00 - 2.24	.	.	.	.	.	.	.	.	.	.	.
2.25 - GREATER	.	.	.	.	.	.	.	.	.	.	.
TOTAL	0	0	0	0	432	46	0	0	0	0	478

AVERAGE HS(FT) = 0.42 LARGEST HS(FT) = 0.88 ANGLE CLASS % = 0.5

STATION 1 1 YEAR ANGLE CLASS (DEG AZIMUTH) = 22.5
WATER DEPTH = 5.50 FEET
PERCENT OCCURRENCE(X1000) OF HEIGHT AND PERIOD BY DIRECTION

HEIGHT(FEET)	PERIOD(SECONDS)										TOTAL
	0.0-0.4	0.5-0.9	1.0-1.4	1.5-1.9	2.0-2.4	2.5-2.9	3.0-3.4	3.5-3.9	4.0-4.4	4.5-LONGER	
0. - 0.24	.	.	.	.	3	.	.	.	.	.	3
0.25 - 0.49	.	.	.	.	2715	.	.	.	.	.	2715
0.50 - 0.74	.	.	.	.	1382	.	.	.	.	.	1382
0.75 - 0.99	.	.	.	.	1507	1395	.	.	.	.	2902
1.00 - 1.24	.	.	.	.	.	722	914	.	.	.	1636
1.25 - 1.49	.	.	.	.	.	.	96	.	.	.	96
1.50 - 1.74	.	.	.	.	.	.	.	.	.	.	.
1.75 - 1.99	.	.	.	.	.	.	.	.	.	.	.
2.00 - 2.24	.	.	.	.	.	.	.	.	.	.	.
2.25 - GREATER	.	.	.	.	.	.	.	.	.	.	.
TOTAL	0	0	0	0	5246	2118	1010	0	0	0	8374

AVERAGE HS(FT) = 0.72 LARGEST HS(FT) = 1.29 ANGLE CLASS % = 8.4

STATION 1 1 YEAR ANGLE CLASS (DEG AZIMUTH) = 45.0
WATER DEPTH = 5.50 FEET
PERCENT OCCURRENCE(X1000) OF HEIGHT AND PERIOD BY DIRECTION

HEIGHT(FEET)	PERIOD(SECONDS)										TOTAL
	0.0-0.4	0.5-0.9	1.0-1.4	1.5-1.9	2.0-2.4	2.5-2.9	3.0-3.4	3.5-3.9	4.0-4.4	4.5-LONGER	
0. - 0.24	.	.	.	.	132	.	.	.	.	.	132
0.25 - 0.49	.	.	.	.	4[illegible]	.	.	.	.	.	[illegible]
0.50 - 0.74	.	.	.	.	3[illegible]	192	.	.	.	.	[illegible]
0.75 - 0.99	.	.	.	.	[illegible]	.	.	.	.	.	[illegible]
1.00 - 1.24	.	.	.	.	.	337	.	.	.	.	337
1.25 - 1.49	.	.	.	.	.	.	.	.	.	.	.
1.50 - 1.74	.	.	.	.	.	.	.	.	.	.	.
1.75 - 1.99	.	.	.	.	.	.	.	.	.	.	.
2.00 - 2.24	.	.	.	.	.	.	.	.	.	.	.
2.25 - GREATER	.	.	.	.	.	.	.	.	.	.	.
TOTAL	0	0	0	0	9290	529	0	0	0	0	9819

AVERAGE HS(FT) = 0.52 LARGEST HS(FT) = 1.15 ANGLE CLASS % = 9.8

STATION 1 1 YEAR ANGLE CLASS (DEG AZIMUTH) = 67.5
WATER DEPTH = 5.50 FEET
PERCENT OCCURRENCE(X1000) OF HEIGHT AND PERIOD BY DIRECTION

HEIGHT(FEET)	PERIOD(SECONDS)										TOTAL
	0.0-0.4	0.5-0.9	1.0-1.4	1.5-1.9	2.0-2.4	2.5-2.9	3.0-3.4	3.5-3.9	4.0-4.4	4.5-LONGER	
0. - 0.24	.	.	.	.	[illegible]	.	.	.	.	.	[illegible]
0.25 - 0.49	.	.	.	.	[illegible]	.	.	.	.	.	[illegible]
0.50 - 0.74	.	.	.	.	[illegible]	[illegible]	.	.	.	.	[illegible]
0.75 - 0.99	.	.	.	.	.	[illegible]	.	.	.	.	[illegible]
1.00 - 1.24	.	.	.	.	.	.	.	.	.	.	.
1.25 - 1.49	.	.	.	.	.	.	.	.	.	.	.
1.50 - 1.74	.	.	.	.	.	.	.	.	.	.	.
1.75 - 1.99	.	.	.	.	.	.	.	.	.	.	.
2.00 - 2.24	.	.	.	.	.	.	.	.	.	.	.
2.25 - GREATER	.	.	.	.	.	.	.	.	.	.	.
TOTAL	0	0	0	0	10110	96	0	0	0	0	10206

AVERAGE HS(FT) = 0.46 LARGEST HS(FT) = 0.75 ANGLE CLASS % = 10.2

Figure 33. Example of the 1-year statistical table for various angle classes

STATION 1 1 YEAR FOR ALL DIRECTIONS
WATER DEPTH = [illegible] FEET
PERCENT OCCURRENCE (X100) OF HEIGHT AND PERIOD FOR ALL DIRECTIONS

HEIGHT(FEET)	PERIOD(SECONDS)										TOTAL
	0.0-0.4	0.5-0.9	1.0-1.4	1.5-1.9	2.0-2.4	2.5-2.9	3.0-3.4	3.5-3.9	4.0-4.4	4.5-LARGER	
0. - 0.24	.	.	.	.	670	9	.	.	.	.	[illegible]
0.25 - 0.49	.	.	.	.	4656	[illegible]	.	.	.	.	[illegible]
0.50 - 0.74	.	.	.	.	2035	[illegible]	[illegible]	.	.	.	[illegible]
0.75 - 0.99	.	.	.	.	414	[illegible]	[illegible]	[illegible]	.	.	[illegible]
1.00 - 1.24	.	.	.	.	9	[illegible]	[illegible]	[illegible]	[illegible]	.	[illegible]
1.25 - 1.49	.	.	.	.	.	[illegible]	[illegible]	[illegible]	[illegible]	.	[illegible]
1.50 - 1.74	.	.	.	.	.	[illegible]	[illegible]	[illegible]	[illegible]	.	[illegible]
1.75 - 1.99	.	.	.	.	.	[illegible]	[illegible]	[illegible]	[illegible]	.	[illegible]
2.00 - 2.24	.	.	.	.	.	.	.	.	.	.	[illegible]
2.25 - 2.49	.	.	.	.	.	.	.	.	.	.	[illegible]
2.50 - GREATER	.	.	.	.	.	.	.	.	.	.	[illegible]
TOTAL	0	0	0	0	8755	744	277	127	77	4	[illegible]

AVE HS(FT) = 0.52 LARGEST HS(FT) = 1.77 TOTAL CASES = 2077

Figure 34. Example of the all-directions 1-year statistical table

For this example:

$$\frac{143}{1{,}000} \div 100 \times 2{,}160 \approx 3 \text{ hr}$$

The following tabulation lists the approximate number of hours in each season for 1 year:

Season	Number of Hours in Season for 1 Year
1 (D, J, F)	~2,160
2 (M, A, M)	~2,208
3 (J, J, A)	~2,208
4 (S, O, N)	~2,184

80. The all-directions tables can be used in a similar fashion. To find the number of hours waves >1.75 ft and <1.99 ft are expected to occur within a typical year for Station 1 during Season 1 for all directions and periods, divide the value in the "total" column for the specified H_{mo} range by 100, which yields a percent of 0.14 (Figure 32). Divide 0.14 by 100 to get the probability, then multiply by the number of hours in Season 1 for 1 year. That is:

$$\frac{14}{100} \div 100 \times 2{,}160 \approx 3 \text{ hr}$$

81. This procedure may also be used when dealing with the wave estimates in the 1-year tables. The number of hours in the time interval found in Equation 29 would now be the sum for all four seasons or 8,760 hr/year.

PART V: DISCUSSION OF HINDCAST RESULTS

82. The Shallow-water Wave Model (SWWM) was developed to adequately describe the physical processes involved in wave growth and finite depth wave transformations. Detailed comparisons of the SWWM results with measured wave data in Atchafalaya Bay were performed. Adjustments to the parameterization given by Hasselmann et al. (1976), for wave energy growth and peak frequency changes over fetch lengths, were needed to improve the reliability of the SWWM's results within the bay. The changes were based on prototype results where nondimensionally the Atchafalaya Bay wave information reflected trends established in previous studies. Although the nondimensional relations varied from Hasselmann et al. (1976) and Knowles (1982), the parameters supported a self-similar spectral shape. Also, the assumption that southerly generated wave conditions have a minimal effect on the Atchafalaya Bay wave climate was verified. That particular verification was based on comparisons between wave gage results and spectral estimates. The reason for the loss in long-period wave information was assumed to be caused by wave/soft-bottom interactions, and trends found in the Atchafalaya Bay measured wave conditions were similar to previous studies where in-depth analyses were performed.

83. After implementation of the new growth rate expressions, the SWWM wave estimates were compared with existing wave gage information. Time-history, percent occurrence, and extreme wave-height comparisons were performed. In general, the hindcast accurately described time sequences in the wave estimates at all three gage locations for a large number of variable wind conditions. Statistically, the hindcast results compared favorably with the distribution of H_{mo} and T_p found in the wave gage data. The maximum H_{mo} estimated from the top 10 to 20 storm events determined from the measured results were compared with similar hindcast conditions. The hindcast results did not show strong trends toward over- or underestimating the maximum measured H_{mo} conditions. Accurately estimating wave information via the SWWM in a time-history, percent occurrence, and extreme sense at three locations provides the basis to generate the wave climate in other areas in Atchafalaya Bay.

84. Approximately 1 year of hindcast wave information was produced for 10 locations in the Atchafalaya Bay region. For this period of time, characteristic wave height, peak period, mean direction of wave propagation, and

1-dimensional frequency spectral wave estimates are available every 3 hr for each station.

85. As a final point, it should be emphasized that the information presented in this report constitutes only a small portion of that available from the complete hindcast wave information set stored on magnetic tape. For many purposes, the present occurrence tables may not suffice. However, the basic hindcast information can be reprocessed into many alternate forms more compatible with the type of problem given. This information should provide an excellent data base to determine the influence of wave conditions on sediment motion or other coastal engineering problems in Atchafalaya Bay.

REFERENCES

Bretschneider, C. L. 1952. "The Generation and Decay of Wind Waves in Deep Water," Transactions, American Geophysical Union, Vol 33, No. 3, pp 381-389.

Bretschneider, C.L., and Reid, R. O. 1954. "Changes in Wave Height due to Bottom Friction, Percolation and Refraction," Technical Memorandum No. 45, Beach Erosion Board, CE.

Collins, J. I. 1972. "Prediction of Shallow-Water Spectra," Journal of Geophysical Research, Vol 77, No. 15, pp 2693-2707.

Dalrymple, R. A., and Liu, P. L.-F. 1978. "Waves over Soft Muds: A Two-Layer Fluid Model," Journal of Physical Oceanography, Vol 8, pp 1121-1131.

Ebersole, B. A. 1985 (Feb). "The Atchafalaya River Delta; Wind Climatology," Technical Report HL-82-15, Report 8, US Army Engineer Waterways Experiment Station, Vicksburg, Miss.

Forristall, G. Z., and Reece, A. M. 1984. "Measurements of Wave Attenuation due to a Soft Bottom: The Swamp Experiment," Symposium on the Practice of Physical Oceanography in Honor of R. O. Reid, Texas A&M University.

Gade, H. G. 1958. "Effects of a Nonrigid Impermeable Bottom on Plane Surface Waves in Shallow Water," Journal of Marine Research, Vol 16, pp 61-82.

Garcia, A. W., and Jensen, R. E. 1983 (Jun). "Wave Data Acquisition and Hindcast for Saginaw Bay, Michigan," Technical Report HL-83-14, US Army Engineer Waterways Experiment Station, Vicksburg, Miss.

Goda, Y. 1974. "Estimation of Wave Statistics from Spectral Information," Proceedings, International Symposium on Ocean Wave Measurement and Analysis, American Society of Civil Engineers, Vol 1, pp 320-337.

Hasselmann, K. 1962. "On the Non-Linear Energy Transfer in a Gravity Wave Spectrum-General Theory," Journal of Fluid Mechanics, Vol 12, Part 1, pp 481-500.

Hasselmann K., and Collins, J. I. 1968. "Spectral Dissipation of Finite-Depth Gravity Waves due to Turbulent Bottom Friction," Journal of Marine Research, Vol 26, pp 1-12.

Hasselmann, K., et al. 1973. "Measurements of Wind-Wave Growth and Swell Decay During the Joint North Sea Wave Project JONSWAP," Dtsch, Hydrogr. Z., Vol 8, Supplement A8, No. 12

Hasselmann, K., et al. 1976. "A Parametric Wave Prediction Model," Journal of Physical Oceanography, Vol 6, pp 200-228.

Hsiao, Shu-Chi, Vincent. 1978. "On the Transformation Mechanisms and the Prediction of Finite-Depth Water Waves, Ph. D. Dissertation, University of Florida, Gainesville, Fla.

Iwata, Kenchiro. 1980. "Wave Spectrum Changes due to Shoaling and Breaking. I - Minus - Three - Power - Law on Frequency Spectrum," Osaka University, Technical Report, Vol 30, No. 1517-1550, pp 269-278.

Jensen, R. E. 1983a (Apr). "Mississippi Sound Wave Hindcast Study," Technical Report HL-83-5, US Army Engineer Waterways Experiment Station, Vicksburg, Miss.

Jensen, R. E. 1983b (Sep). "Methodology for the Calculation of a Shallow-Water Wave Climate," Wave Information Study 8, US Army Engineer Waterways Experiment Station, Vicksburg, Miss.

Kitaigordskii, S. A. 1962. "Application of the Theory of Similarity to the Analysis of Wind-Generated Wave [illegible] a Stochastic Process," Bull. Acad. Sci. USSR Ser. Geophys., No. 1, [illegible], pp 105-117.

Kitaigordskii, S. A., Krasitskii, [illegible], and Lastovskii, M. M. 1975 (Jul). "On Phillips' Theory of Equilibrium Range in the Spectra of Wind-Generated Gravity Waves," Journal of Physical Oceanography, Vol 5, No. 3, pp 410-420.

Knowles, C. E. 1982. "On the Effects of Finite Depth on Wind-Wave Spectra: I. A Comparison with Deep-Water Equilibrium-Range Slope and other Spectral Parameters," Journal of Physical Oceanography, Vol 12, pp 556-568.

Mitsuyasu, Hisashi. 1968. "On the Growth of the Spectrum of Wind Generation Waves (II)," Reports of Research Institute for Applied Mechanics, Kysusha University, Vol 17, No. 59, pp 235-248.

. 1969. "On the Growth of the Spectrum of Wind-Generated Waves (II)," Reports of Research Institute for Applied Mechanics, Kysusha University, Vol 17, No. 59, pp 235-248.

Mitsuyasu, Hisashi, and Kimura, Hisao. 1965. "Wind Wave in Decay Area," Coastal Engineering in Japan, Vol 8, pp 21-35.

National Oceanic and Atmospheric Administration (NOAA), National Ocean Survey. 1977. Chart No. 11349 and 11351, US Department of Commerce, Washington, DC.

On, Shan-Hwei. 1980. "The Equilibrium Range in the Frequency Spectra of the Wind Generated Gravity Waves," Proceedings, 4th Conference on Ocean Engineering in the Republic of China.

Phillips, O. M. 1957. "On the Generation of Waves by Turbulent Wind," Journal of Fluid Mechanics, Vol 2, pp 417-445.

. 1958. "The Equilibrium Range in the Spectrum of Wind Generated Waves," Journal of Fluid Mechanics, Vol 4, pp 426-434.

Resio, D. T. 1981. "The Estimation of Wind-Wave Generation in a Discrete Spectral Model," Journal of Physical Oceanography, Vol 11, No. 4, pp 510-525.

. 1982. "Wave Prediction in Shallow Water," 14th Offshore Technology Conference, Houston, Tex., OTC 4247, pp 147-160.

[illegible]sio, D. T., and Vincent, C. L. 1976. "Estimation of Winds over the Great Lakes," Miscellaneous Paper H-76-12, US Army Engineer Waterways Experiment Station, Vicksburg, Miss.

Thornton, E. B. 1977. "Rederivation of the Saturation Range in a Frequency Spectrum of Wind-Generated Gravity Waves," Journal of Physical Oceanography, Vol 7, pp 137-140.

US Army Coastal Engineering Research Center. 1977. "Shore Protection Manual," 3rd ed. (Vols I, II, and III), Stock No. 008-022-00113-1, US Government Printing Office, Washington, DC.

Vincent, C. L. 1981. "A Method for Estimating Depth-Limited Wave Energy," Rep. CETA 81-16, US Army Coastal Engineering Research Center, Fort Belvoir, Va.

. 1982 (May). "Shallow Water Wave Modeling," 1st International Conference on Meteorology and Air-Sea Interaction in the Coastal Zone, The Hague.

Table 1

Parametric Growth Rate Estimates

Fetch Length n.m.	Parameter	Wind Speed, knots 2.0	4.0	6.0	8.0	10.0	12.0	14.0	16.0	18.0	20.0
2	H_{mo}, ft	0.04	0.09	0.15	0.22	0.30	0.38	0.47	0.56	0.65	0.75
	T_p, sec	0.6*	0.9	1.1	1.3	1.4	1.6	1.7	1.8	2.0	2.1
6	H_{mo}, ft	0.5	0.13	0.22	0.32	0.43	0.55	0.68	0.81	0.94	1.08
	T_p, sec	0.8	1.2	1.4	1.7	1.9	2.1	2.2	2.4	2.6	2.7
10	H_{mo}, ft	0.06	0.15	0.26	0.38	0.51	0.65	0.80	0.96	1.12	1.29
	T_p, sec	0.9	1.3	1.6	1.9	2.1	2.3	2.5	2.7	2.9	3.0
14	H_{mo}, ft	0.07	0.17	0.29	0.43	0.57	0.73	0.90	1.07	1.25	1.44
	T_p, sec	1.0	1.4	1.8	2.1	2.3	2.5	2.7	2.9	3.1	3.3
18	H_{mo}, ft	0.07	0.19	0.32	0.46	0.63	0.80	0.98	1.17	1.36	1.57
	T_p, sec	1.1	1.5	1.9	2.2	2.4	2.7	2.9	3.1	3.3	3.5
22	H_{mo}, ft	0.08	0.20	0.34	0.50	0.67	0.85	1.05	1.25	1.46	1.68
	T_p, sec	1.1	1.6	2.0	2.3	2.6	2.8	3.1	3.3	3.5	3.7
26	H_{mo}, ft	0.08	0.21	0.36	0.53	0.71	0.90	1.11	1.32	1.54	1.78
	T_p, sec	1.2	1.7	2.1	2.4	2.7	2.9	3.2	3.4	3.6	3.8
30	H_{mo}, ft	0.09	0.22	0.38	0.55	0.74	0.95	1.16	1.39	1.62	1.86
	T_p, sec	1.2	1.7	2.1	2.5	2.8	3.0	3.3	3.5	3.8	4.0

* All wave periods less than 1.0 sec would be considered as ultragravity waves and are not meaningful in the overall hindcast.

Table 2

Maximum Wave-Height Conditions

Station Number	Date Year, Month Day, Hour	H_{mo}, ft		T_p, sec	
		Measured	Hindcast	Measured	Hindcast
WG-68	81103018	1.45	1.14	2.75	2.75
	81110221	1.10	1.06	2.58	2.64
	81110900	1.56	1.38	3.93	3.16
	81111003	1.58	1.65	2.87	4.06
	81112000	1.87	1.90	3.08	4.19
	81112615	1.30	0.68	7.73	2.35
	81113021	1.66	1.42	7.73	3.24
	81120121	1.69	1.64	2.05	3.81
	81120421	1.44	1.35	2.87	2.94
	81121103	1.23	1.42	2.30	3.16
	81121500	1.75	1.66	3.50	3.50
	81121803	1.50	1.58	3.00	3.16
	81122009	1.42	1.25	2.87	2.87
	81122112	1.65	1.04	7.73	2.44
	81122909	1.34	1.49	2.39	3.16
	81123100	2.04	1.61	3.24	3.32
	82010318	1.34	1.00	6.54	2.69
	82010509	1.01	0.93	2.08	2.48
WG-25	81103018	0.94	0.75	2.44	2.11
	81111003	0.91	1.45	2.01	2.87
	81111921	1.05	1.74	2.80	3.08
	81113021	1.14	1.28	2.75	3.41
	81120121	1.22	1.46	3.00	2.81
	81121406	1.06	0.85	2.35	2.30
	81121500	1.10	1.49	2.35	2.94
	81121800	1.03	1.19	2.30	2.48
	81123100	1.46	1.23	2.87	2.58
	82010800	1.00	1.28	2.19	2.58
	82011021	1.54	1.39	2.22	2.58
	82011209	1.05	1.10	2.26	2.22
WG-66	81110206	1.33	1.05	2.94	2.64
	81111000	1.17	1.65	2.58	3.24
	81112000	1.82	1.95	2.64	3.50
	81113018	1.08	1.43	2.48	3.50
	81120200	1.20	1.65	2.53	3.24
	81121500	1.52	1.64	2.64	3.24
	81121721	1.30	1.54	2.58	3.01
	81122909	1.17	1.12	2.35	2.35
	81123100	1.46	1.52	2.94	3.24
	82010721	1.55	1.63	2.75	3.08
	82011021	1.55	1.81	2.81	3.32
	82011209	1.21	1.57	2.53	3.16
	82011406	1.51	1.57	2.87	3.16

Table 3

Station Locations and Water Depths

Station No.	Water Depth ft	Longitude, W deg	Latitude, N deg
1	5.5	91.41	29.35
2*	9.5	91.41	29.45
3***	10.0	91.54	29.39
4	6.0	91.69	29.45
5	3.0	91.60	29.51
6†	11.0	91.68	29.60
7	7.0	91.74	29.69
8	6.0	91.87	29.67
9	8.0	92.03	29.68
10	8.0	91.93	29.77

* WG-25.
*** WG-68.
† WG-66.

APPENDIX A: NORTHERLY WIND AND WAVE DATA FOR VERIFICATION OF THE SHALLOW-WATER WAVE MODEL

1. Results presented in this appendix (Table A1 and Figures A1-A15) are derived from measured wind and wave data obtained during the monitoring program in Atchafalaya Bay. Under each storm number identifier are lines of data. They are the date (year, month, day, hour), wind speed (in knots measured at a 10-m overwater elevation), and wind direction (measured in degrees azimuth, "from which they came").

2. All comparisons of hindcast and measured H_{mo} and T_p are presented graphically and are clearly identified.

Table A1

Northerly Storm Wind Conditions

Storm Number	Date Year, Month Day, Hour	Wind Speed knots	Wind Direction deg azimuth
1	81110909	7.9	331.0
	81110912	15.4	322.3
	81110915	14.4	329.4
	81110918	12.6	328.2
	81110921	12.1	322.4
	81111000	15.8	312.0
	81111003	19.1	325.5
	81111006	19.2	332.3
	81111009	17.6	342.1
	81111012	13.7	330.8
	81111015	14.7	321.4
	81111018	14.1	333.8
	81111021	15.7	333.3
	81111100	14.5	20.6
	81111103	13.9	18.8
	81111106	14.5	16.9
	81111109	13.5	14.0
	81111112	8.7	33.6
	81111115	6.4	301.6
	81111118	6.5	320.2
	81111121	8.7	315.0
	81111200	12.1	13.1
	81111203	11.8	27.6
	81111206	10.8	38.7
2	81111921	16.9	321.7
	81112000	22.9	332.6
	81112003	22.5	336.9
	81112006	22.0	331.9
	81112009	20.4	337.4
	81112012	14.2	323.9
	81112015	11.7	310.1
	81112018	12.4	333.7
3	81122306	14.8	340.1
	81122309	12.4	27.8
	81122312	11.8	19.1
	81122315	7.1	67.7
	81122318	8.7	41.9
	81122321	12.2	36.5
	81122400	14.8	48.6
	81122403	14.3	48.0
	81122406	15.9	35.8

(Continued)

(Sheet 1 of 3)

Table A1 (Continued)

Storm Number	Date Year, Month Day, Hour	Wind Speed knots	Wind Direction deg azimuth
3	81122409	19.1	52.4
	81122412	14.7	55.7
	81122415	13.7	30.7
	81122418	17.2	30.1
	81122421	14.5	37.5
	81122500	13.3	17.5
	81122503	13.0	14.0
	81122506	11.6	17.3
	81122509	10.6	25.8
4	81122903	10.0	48.9
	81122906	13.0	41.9
	81122909	17.9	52.4
	81122912	17.5	49.2
	81122915	15.6	49.2
	81122918	18.9	79.5
	81122921	10.2	60.6
	81123000	9.4	55.7
	81123003	13.2	58.4
	81123006	12.3	56.0
	81123009	12.7	72.8
	81123012	12.7	75.3
	81123015	12.1	68.1
	81123018	10.1	71.0
5	82010721	19.2	22.2
	82010800	18.5	19.9
	82010803	19.5	25.2
	82010806	16.7	25.7
	82010809	16.3	35.0
	82010812	13.5	32.8
	82010815	8.7	26.6
	82010818	11.1	25.5
	82010821	13.2	13.1
	82010900	13.5	17.5
	82010903	11.6	17.0
	82010906	8.3	15.6
	82010909	8.2	21.6
	82010912	7.3	321.3
	82010915	9.1	325.9
	82010918	8.0	316.4
	82010921	4.7	330.6
	82011000	4.4	23.4
	82011003	4.1	17.3
	82011006	4.9	13.4

(Continued)

(Sheet 2 of 3)

Table A1 (Concluded)

Storm Number	Date Year, Month Day, Hour	Wind Speed knots	Wind Direction deg azimuth
5	82011009	6.5	50.0
	82011012	14.9	43.9
	82011015	11.6	37.3
	82011018	13.7	30.5
	82011021	21.3	16.3
	82011100	19.1	19.8
	82011103	17.2	23.7
	82011106	16.5	19.9
	82011109	13.4	38.6
	82011112	10.0	31.1
	82011115	5.8	60.1
	82011118	6.2	74.4

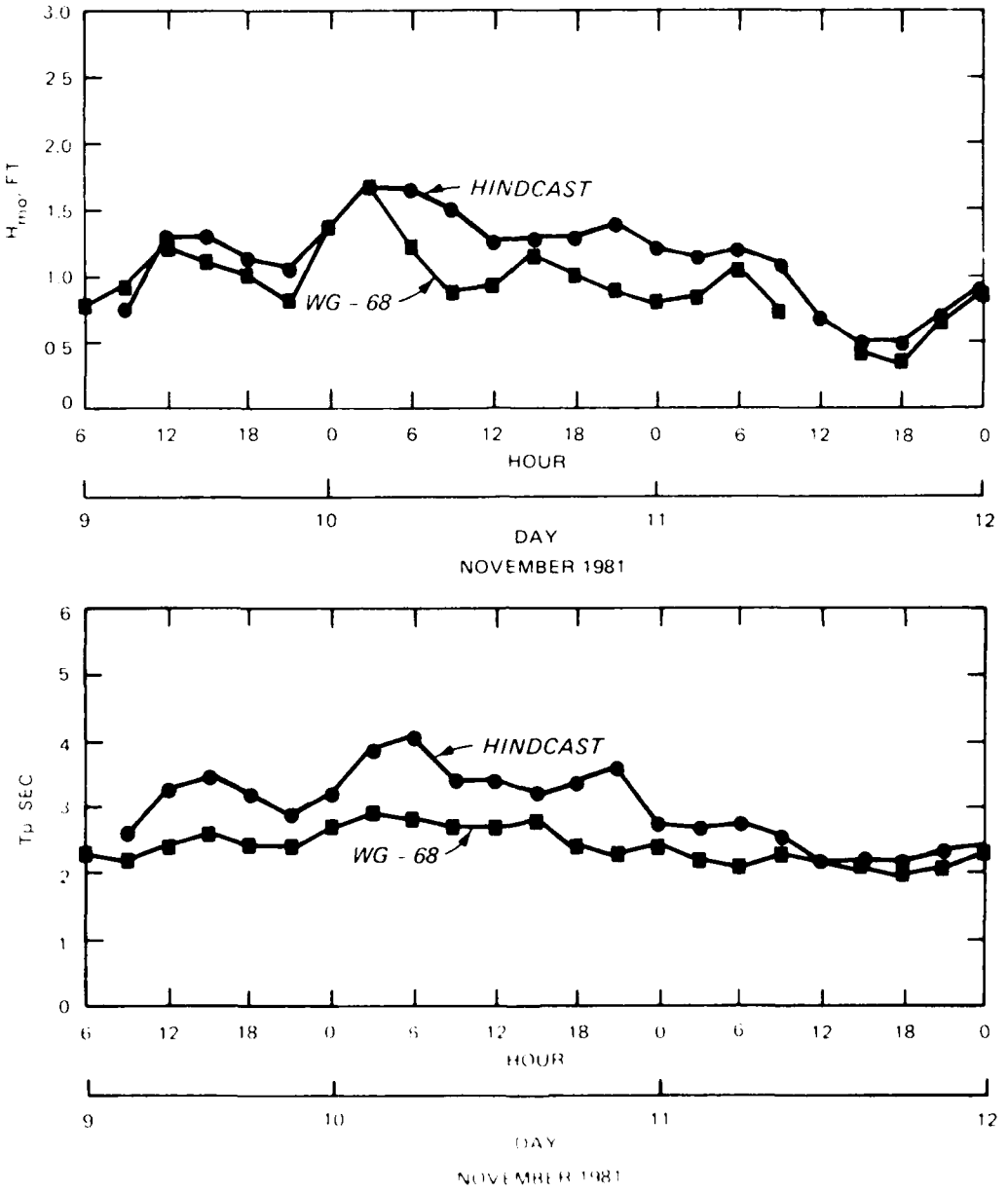

Figure A1. Wave comparisons for Storm 1 at WG-68

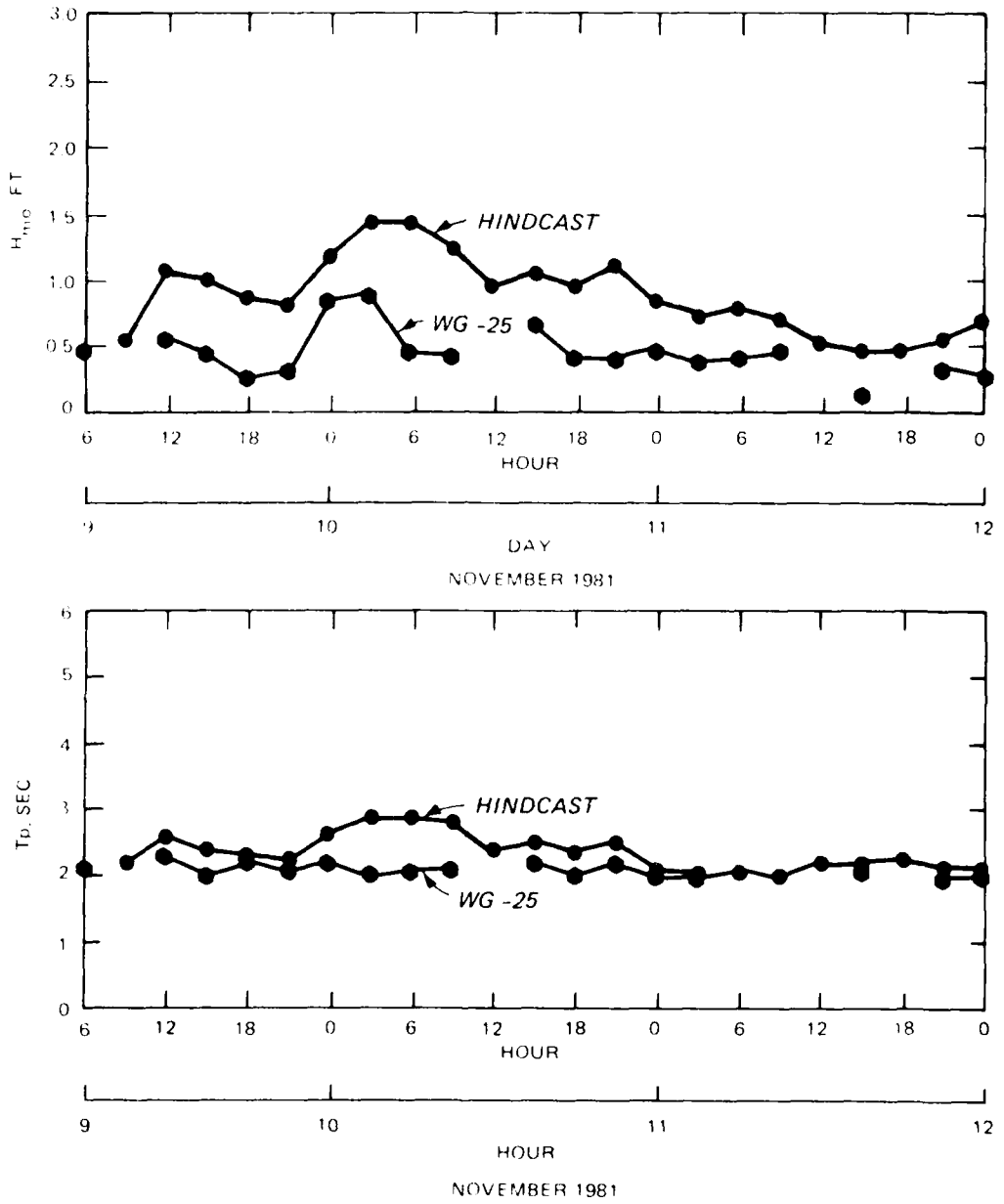

Figure A2. Wave comparisons for Storm 1 at WG-25

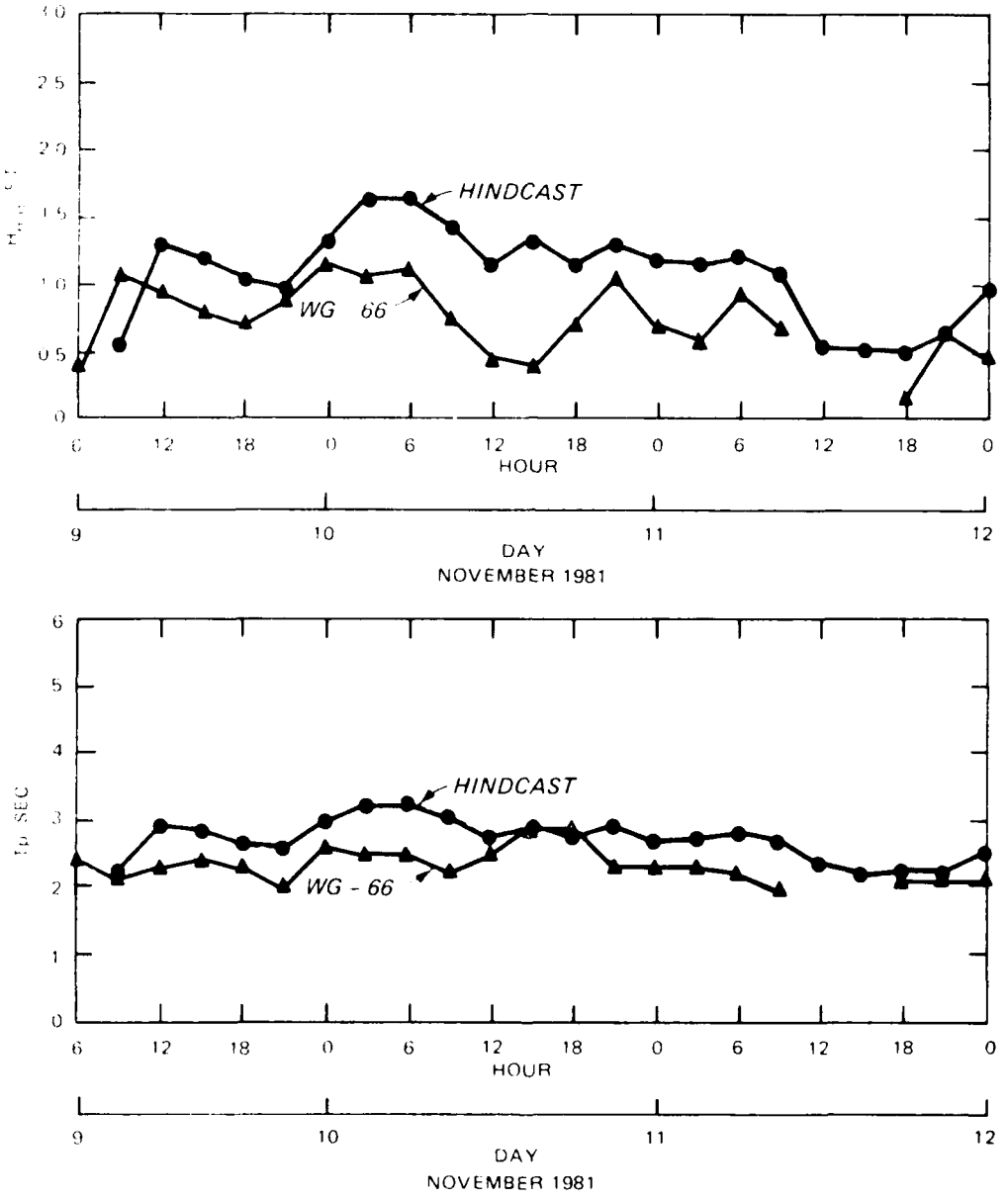

Figure A3. Wave comparisons for Storm 1 at WG-66

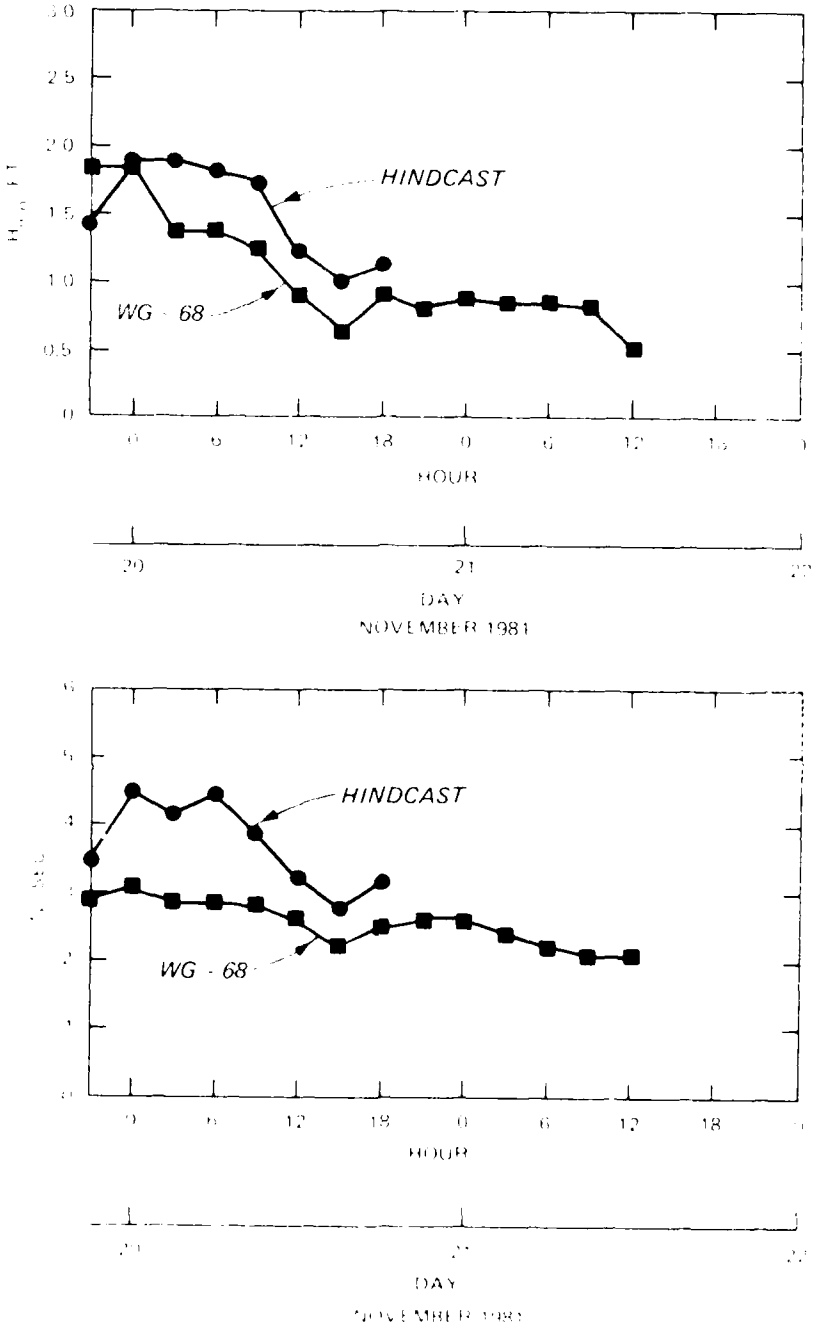

Figure A6. Wave comparisons for Storm 2 at WG-68

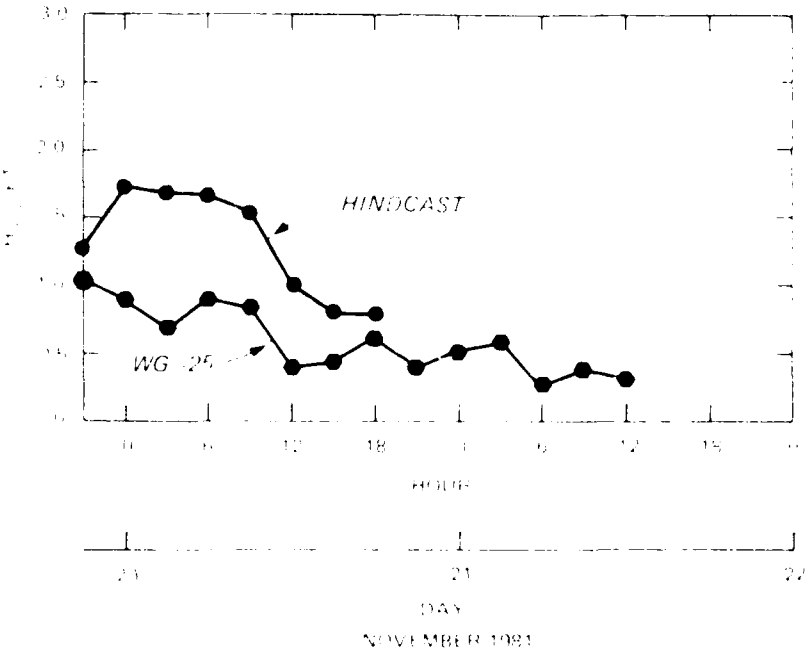

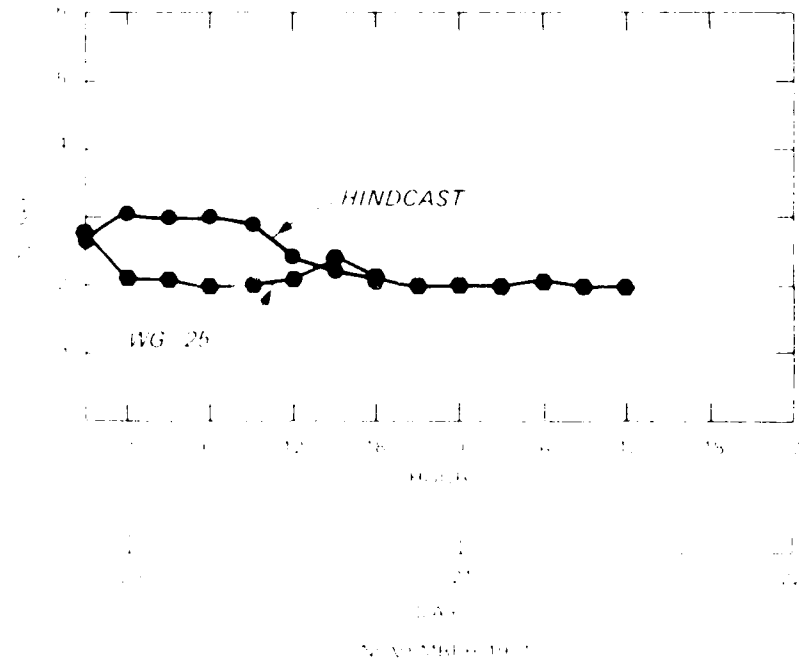

Figure V-

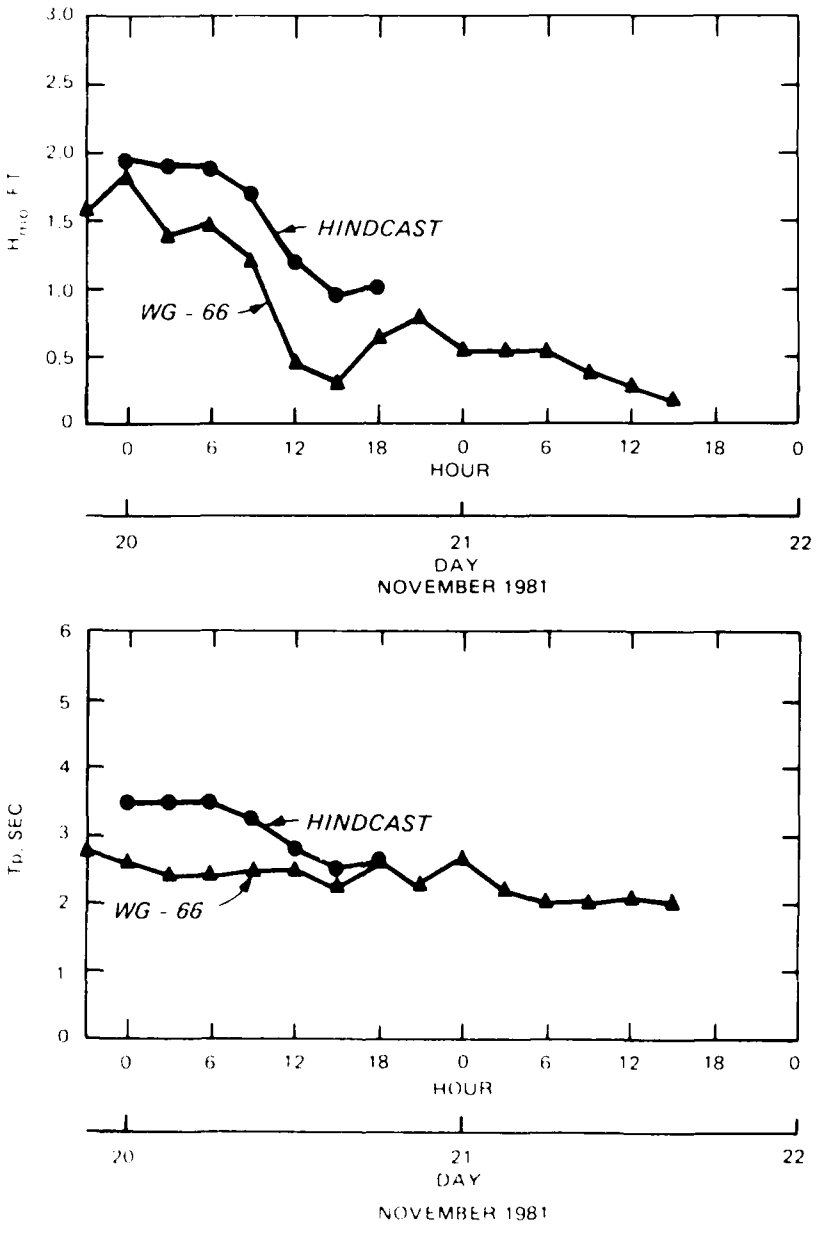

Figure A6. Wave comparisons for Storm 2 at WG-66

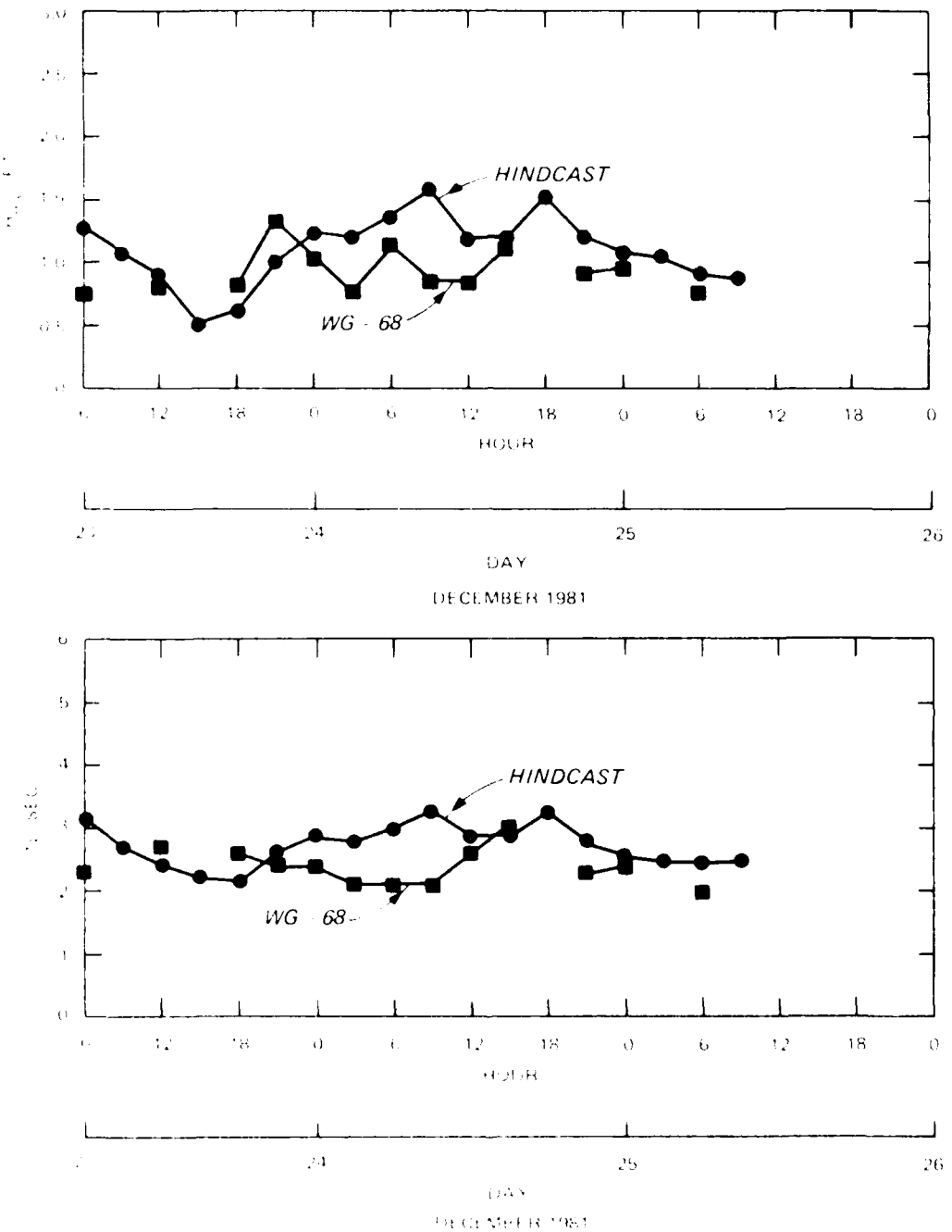

Figure A7. Wave comparisons for Storm 3 at WG-68

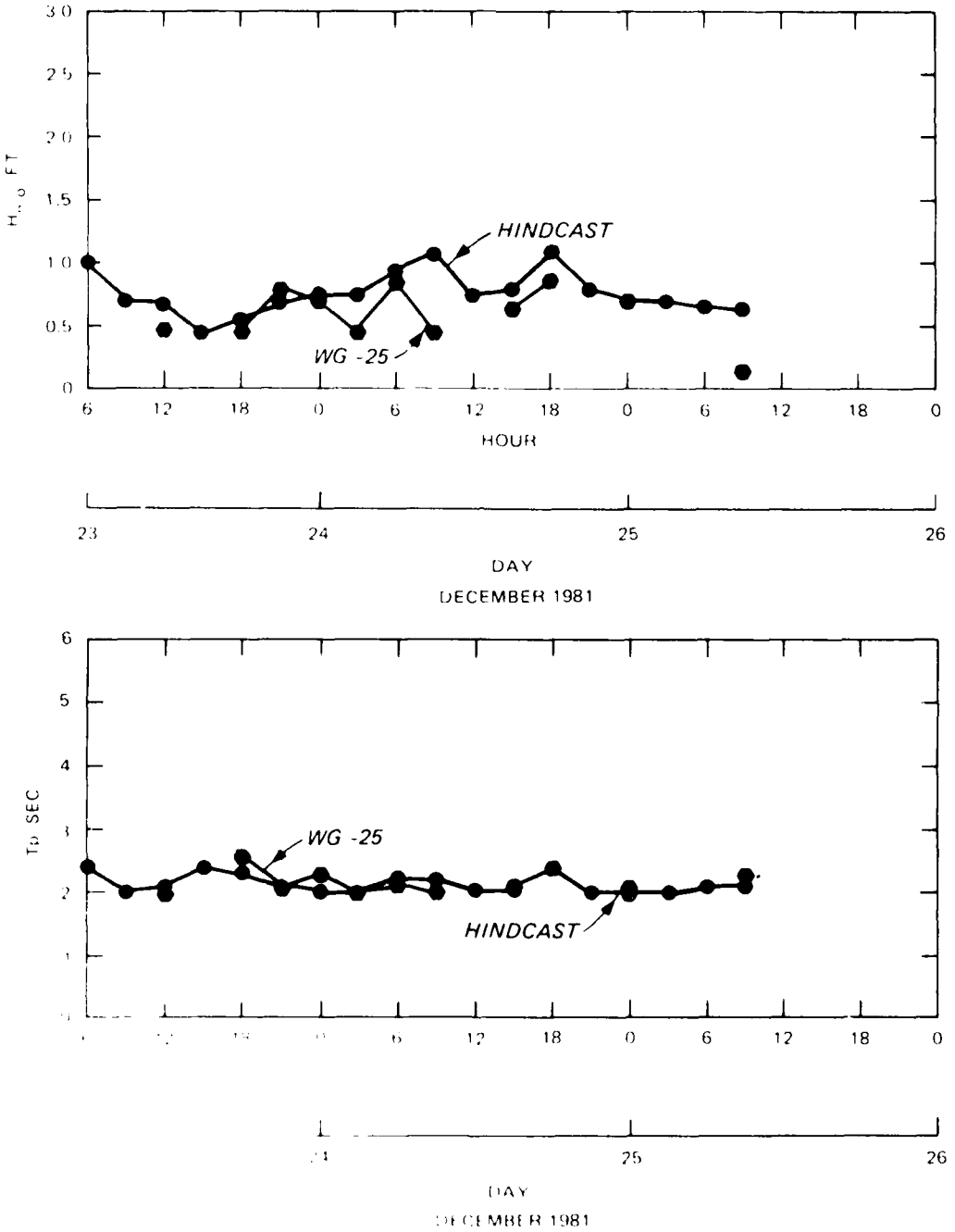

[illegible] Comparisons for Storm 3 at WG-25

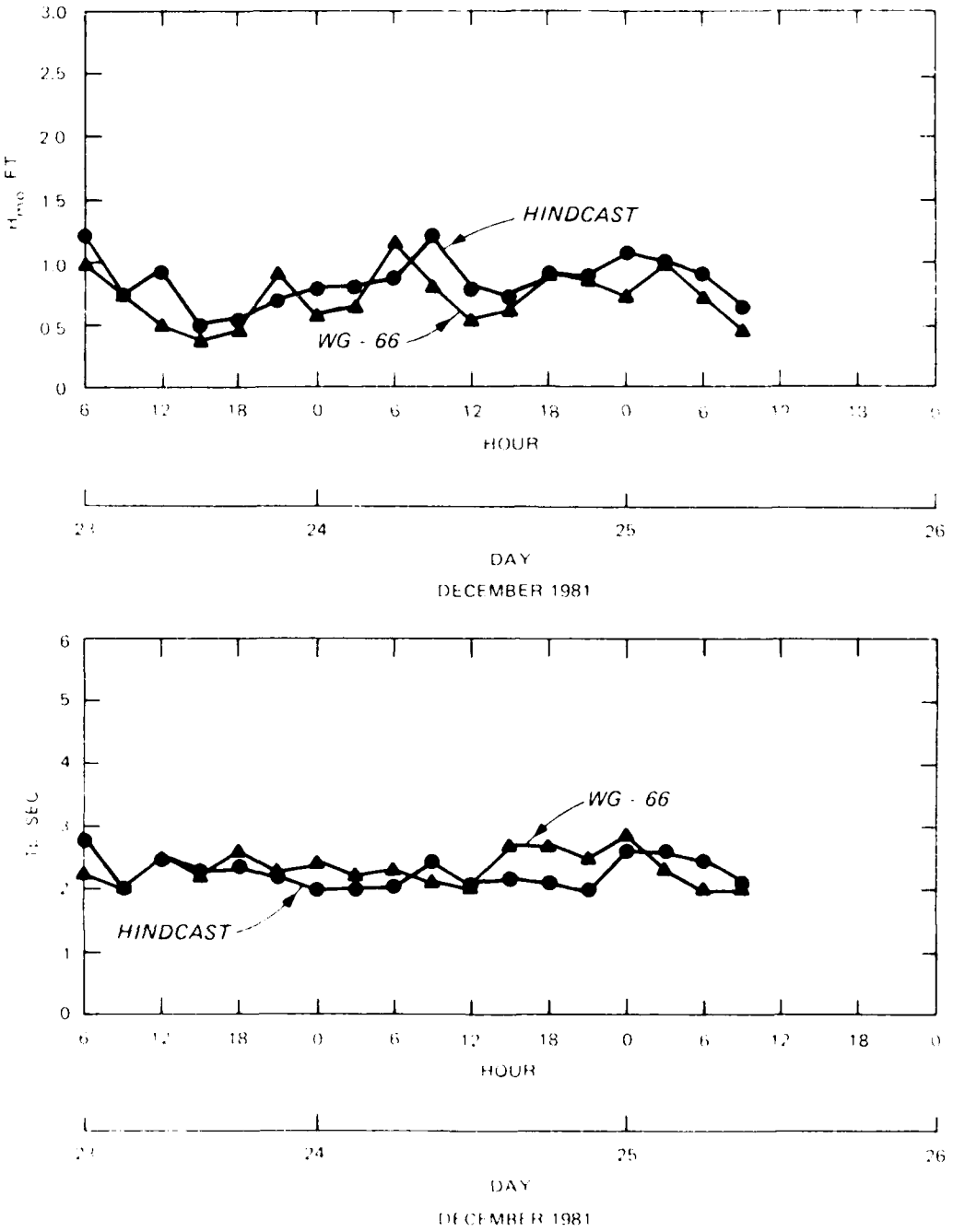

Figure A9. Wave comparisons for Storm 3 at WG-66

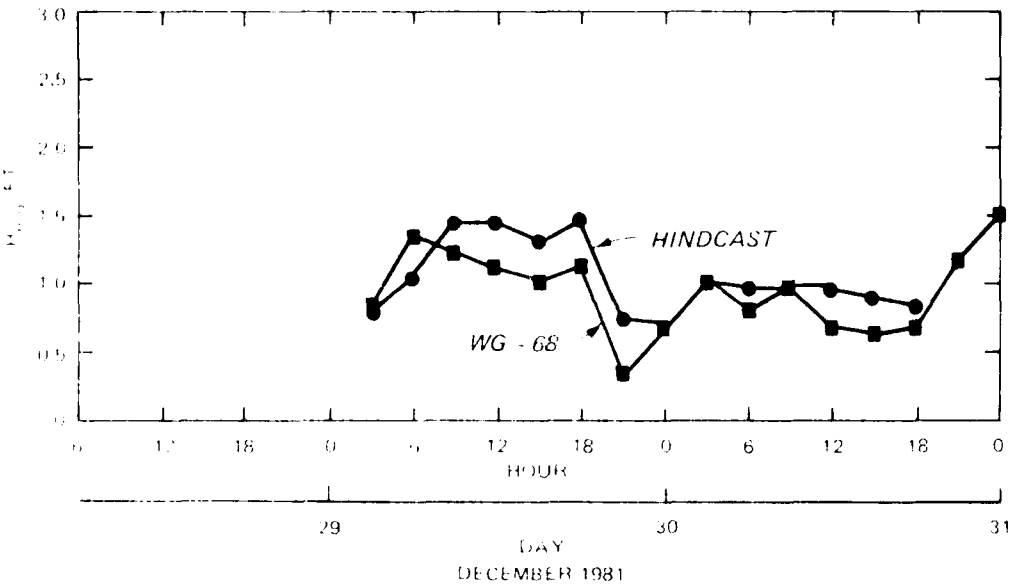

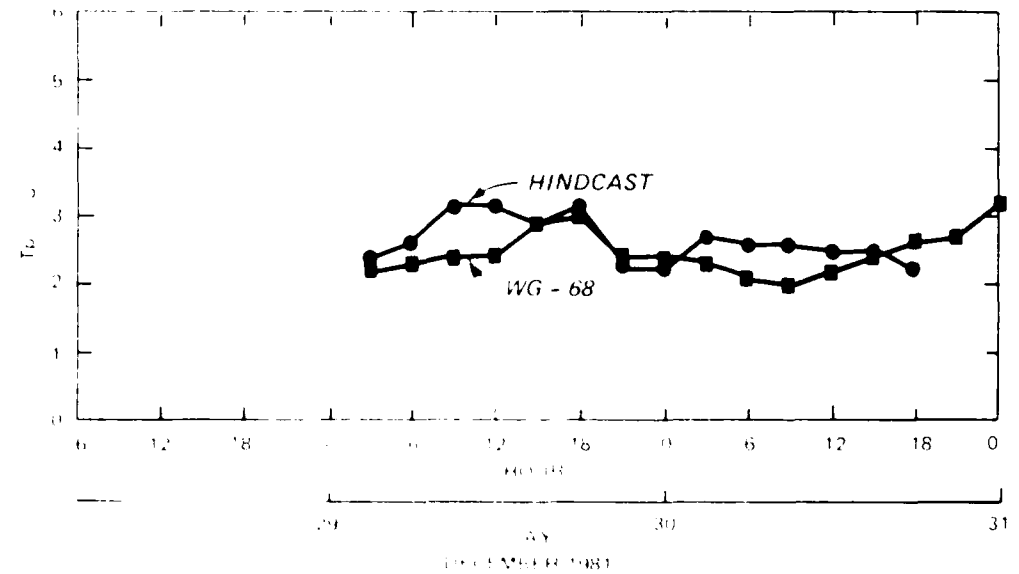

Figure A14. Wave temperature for Storm 4 at WG-68

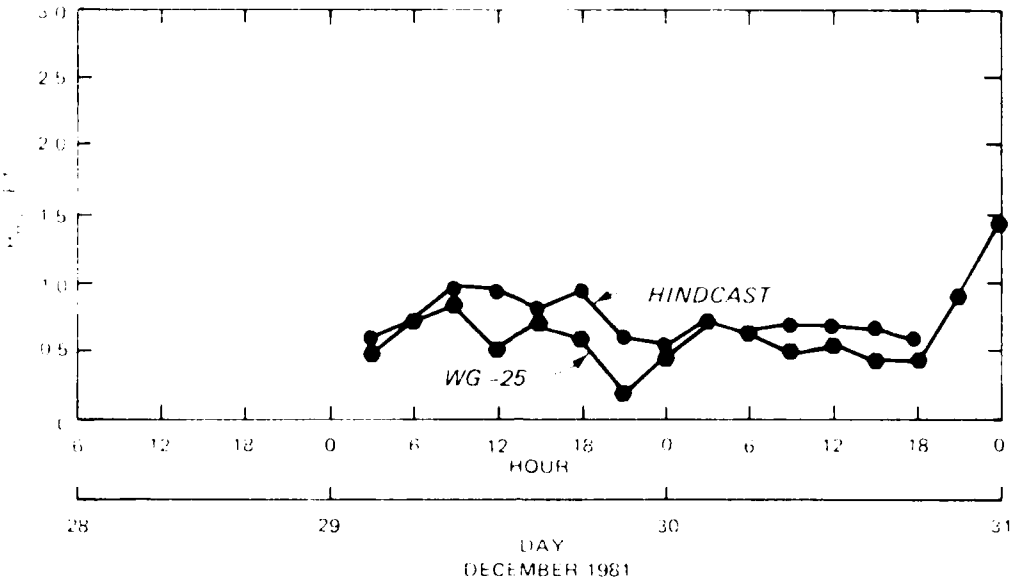

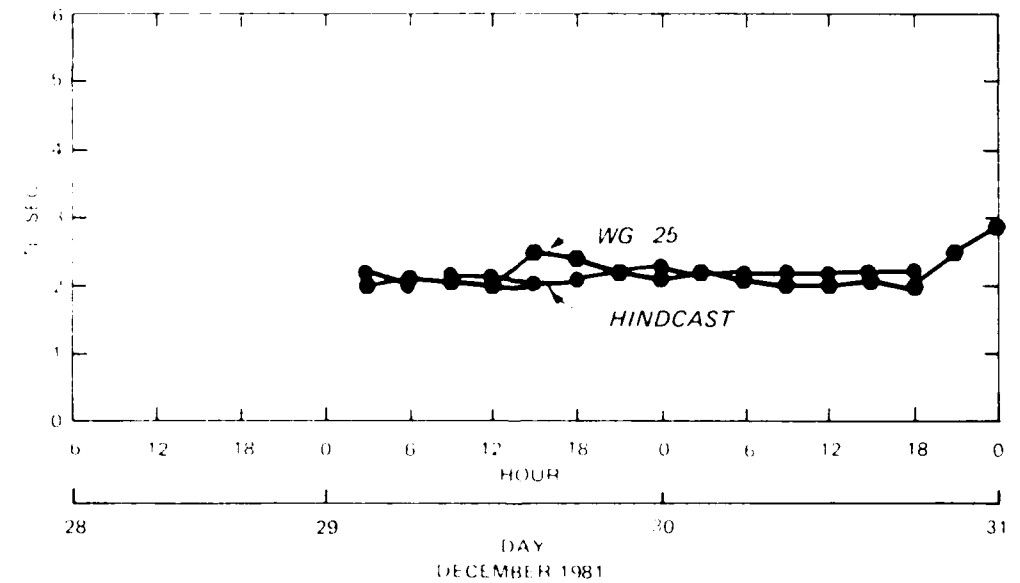

Figure A11. Wave comparisons for Storm 4 at WG-25

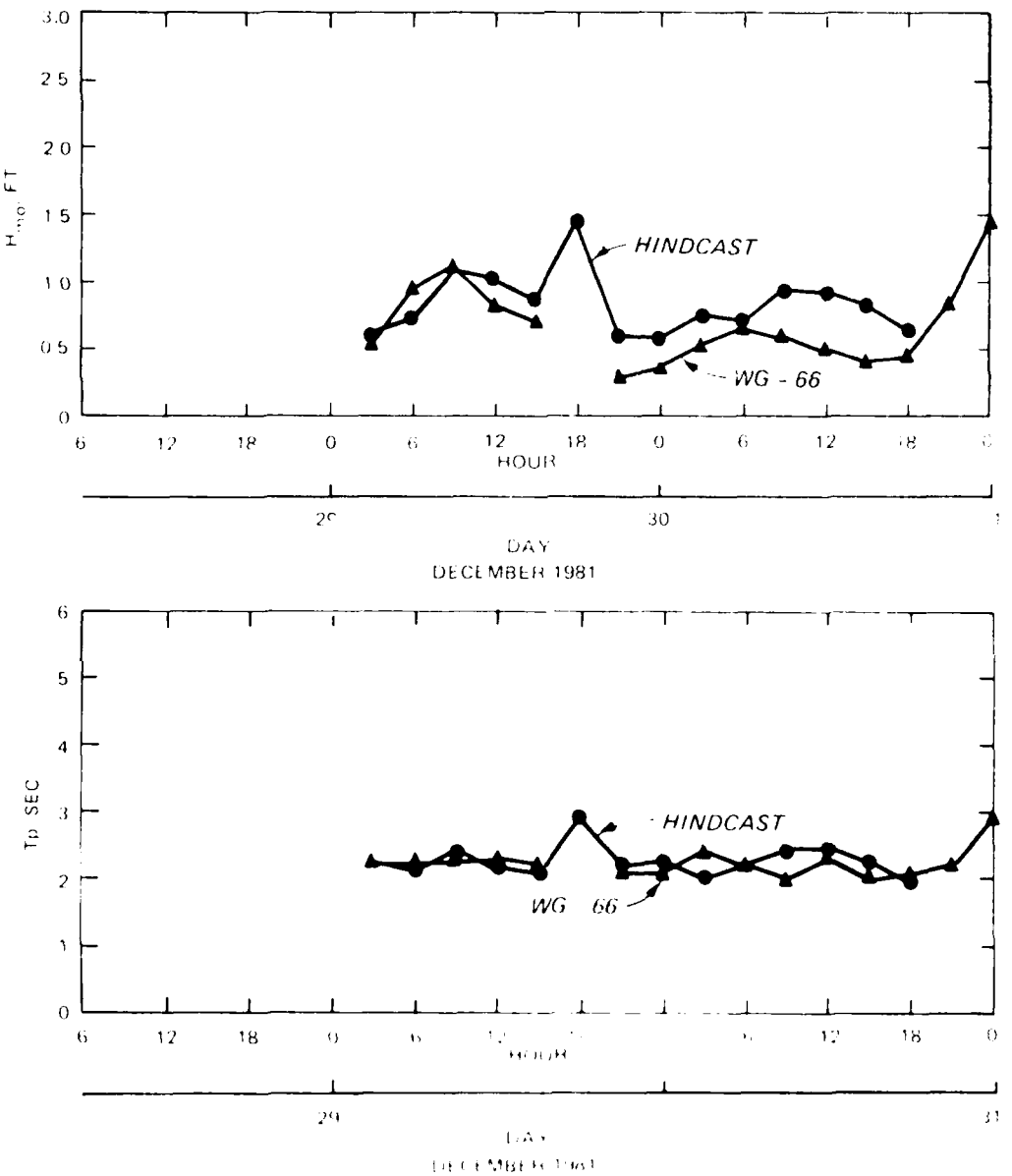

Figure A12. Wave comparisons for Storm 4 at WG-66

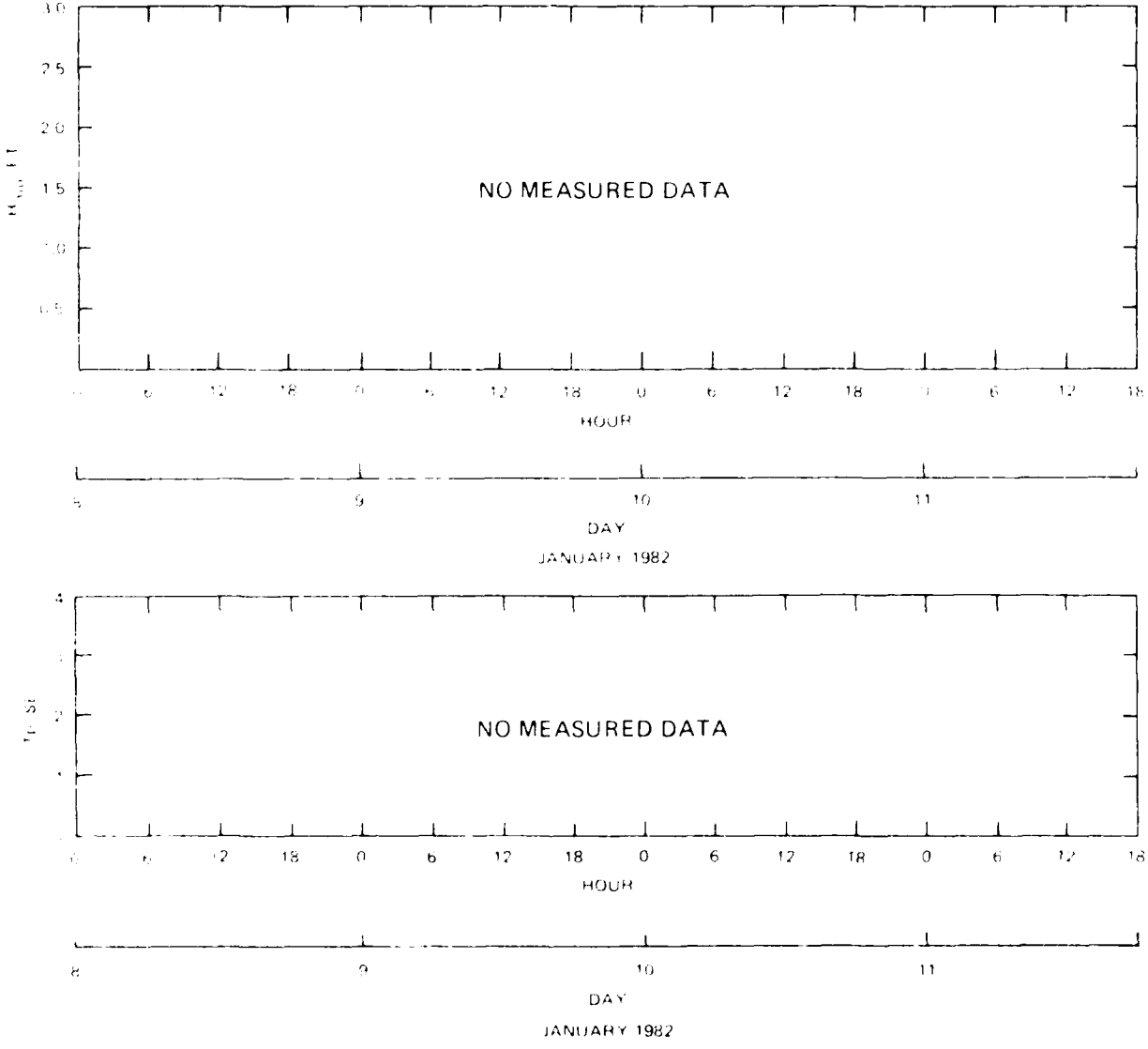

Figure A13. Wave comparisons for Storm 1 at WG-08

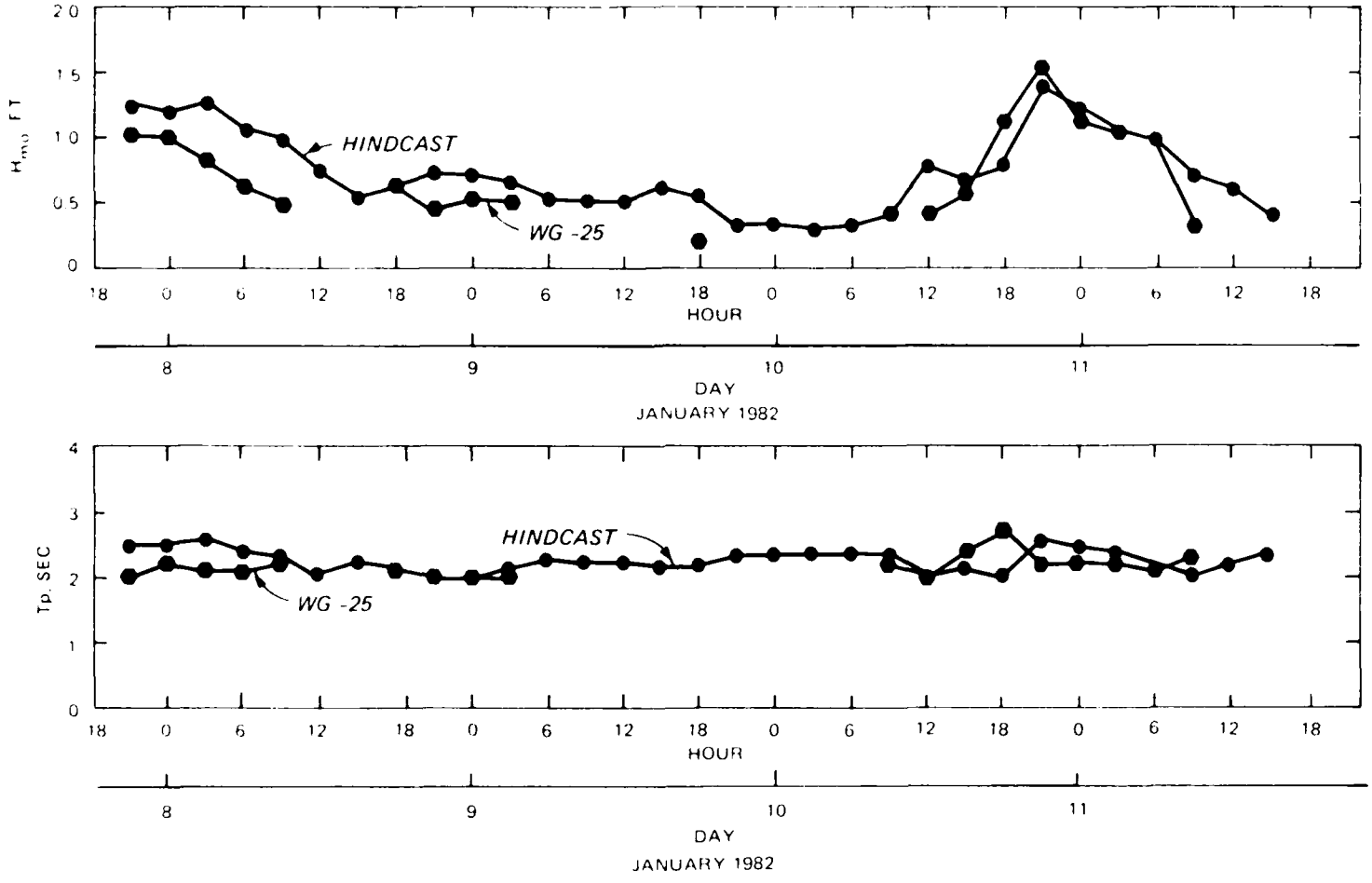

Figure A14. Wave comparisons for Storm 5 at WG-25

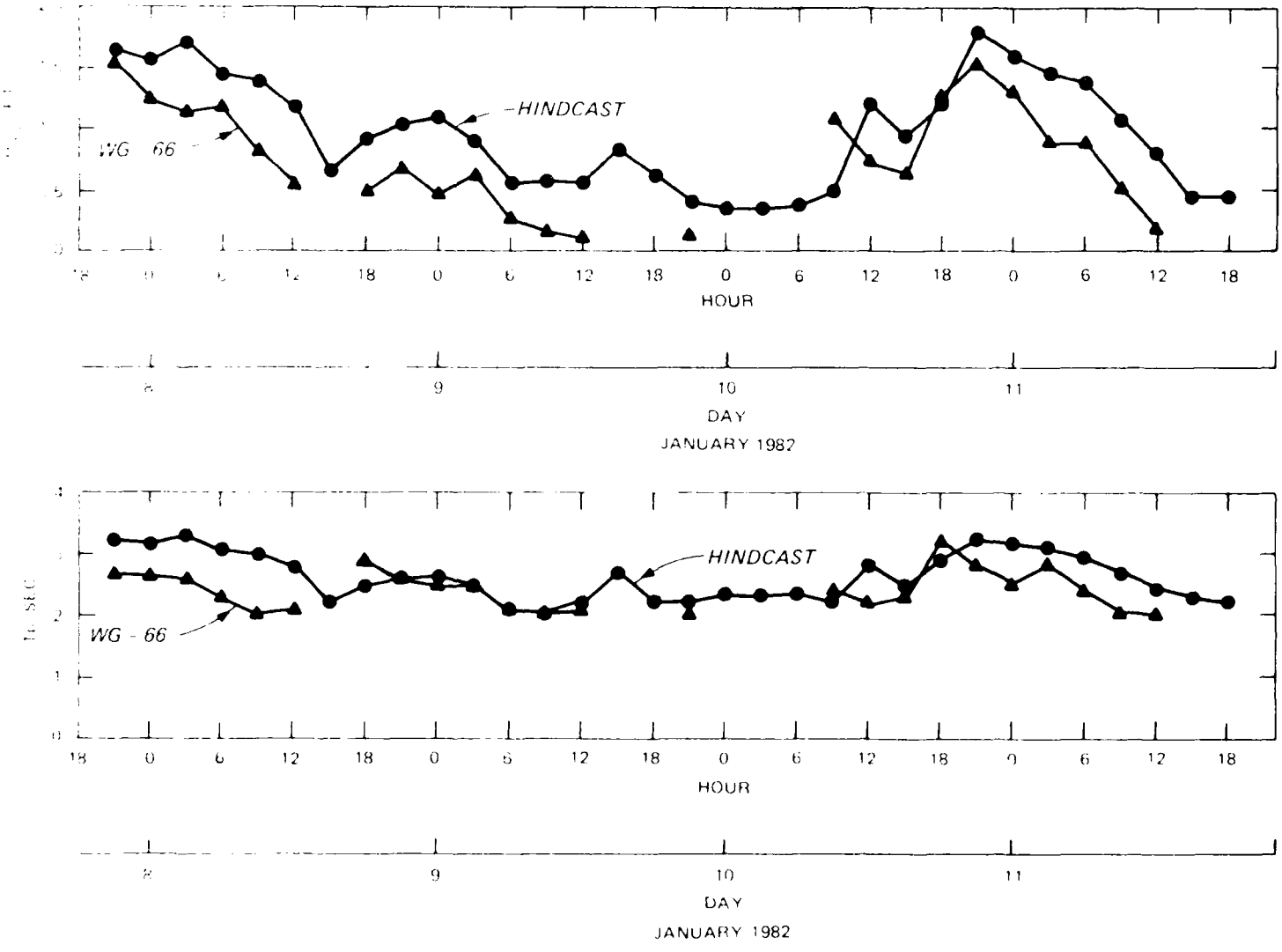

Figure A16. Wave comparisons for Storm 3 at WG-66

APPENDIX B: SOUTHERLY WIND AND WAVE DATA FOR VERIFICATION OF THE SHALLOW-WATER WAVE MODEL

1. Results presented in this appendix (Table B1 and Figures B1-B10) are derived from measured wind and wave data obtained during the monitoring program in Atchafalaya Bay. Under each storm number identifier are lines of data; they are the date (year, month, day, hours), wind speed (in knots, measured at a 10-m overwater elevation), and wind direction (measured in degrees azimuth, "from which they came").

2. All comparisons of hindcast and measured H_{mo} and T_p are presented graphically and are clearly identified.

Table E-1

Southerly Storm Wind Conditions

Storm Number	Date Year, Month Day, Hour	Wind Speed knots	Wind Direction deg azimuth
1A	81112509	10.1	106.7
	81112512	10.8	125.6
	81112515	10.8	123.9
	81112518	11.0	123.9
	81112521	12.2	125.9
	81112600	12.1	141.0
	81112603	12.1	145.5
	81112606	12.6	144.0
	81112609	9.7	145.4
	81112612	8.0	132.6
	81112615	7.1	128.5
	81112618	7.8	126.9
	81112621	8.0	148.5
	81112700	9.3	138.6
	81112703	7.1	138.7
2	81120215	5.8	312.1
	81120218	5.2	265.3
	81120221	7.6	259.0
	81120300	8.1	247.9
	81120303	8.0	244.2
	81120306	8.4	244.0
	81120309	9.4	238.7
	81120312	8.8	181.2
	81120315	6.8	196.3
	81120318	7.5	207.0
	81120321	6.8	217.3
	81120400	6.3	230.3
	81120403	7.1	272.2
	81120406	10.8	146.0
3A	81122109	8.4	109.3
	81122103	12.8	128.5
	81122106	13.8	143.7
	81122109	13.0	164.0
	81122112	14.3	18[illegible]
	81122115	11.[illegible]	194.6
	81122118	10.[illegible]	18[illegible]
	81122[illegible]	11.[illegible]	1[illegible]
	81122[illegible]	11.[illegible]	17[illegible]
	81122[illegible]	12.[illegible]	181.[illegible]
	81122[illegible]	13.[illegible]	17[illegible]
	81122[illegible]	[illegible]	17[illegible]
	81122[illegible]	[illegible]	1[illegible]

AD-A156 693 THE ATCHAFALAYA RIVER DELTA REPORT 10 WAVE HINDCASTS 2/2
MAIN TEXT AND APPEND..(U) ARMY ENGINEER WATERWAYS
EXPERIMENT STATION VICKSBURG MS HYDRA.. R E JENSEN
UNCLASSIFIED MAR 85 WES/TR/HL-82-15/10 F/G 8/3 NL

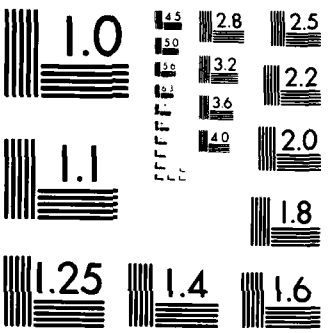

MICROCOPY RESOLUTION TEST CHART

Table B1 (Concluded)

Storm Number	Date Year, Month Day, Hour	Wind Speed knots	Wind Direction deg azimuth
3A	81122215	11.3	164.3
	81122218	5.9	202.7
	81122221	9.5	176.3
	81122300	9.8	192.0
4A	82010200	9.3	95.7
	82010203	10.4	94.2
	82010206	11.0	104.6
	82010209	10.6	102.7
	82010212	10.6	116.0
	82010215	9.7	152.3
	82010218	8.6	152.3
	82010221	9.1	162.3
	82010300	10.2	176.8
	82010303	10.2	169.0
	82010306	9.8	158.0
	82010309	9.7	150.4
	82010312	9.1	165.8
	82010315	8.1	176.5
	82010318	11.3	192.9
	82010321	11.1	207.3
	82010400	10.6	250.6
5A	82010515	9.6	139.9
	82010518	8.6	137.2
	82010521	8.0	118.3
	82010600	8.0	152.3
	82010603	9.8	172.3
	82010606	6.9	173.4
	82010609	4.8	176.6
	82010612	6.0	165.7
	82010615	3.7	171.0
	82010618	6.0	170.3
	82010621	7.2	170.8
	82010700	9.1	176.9

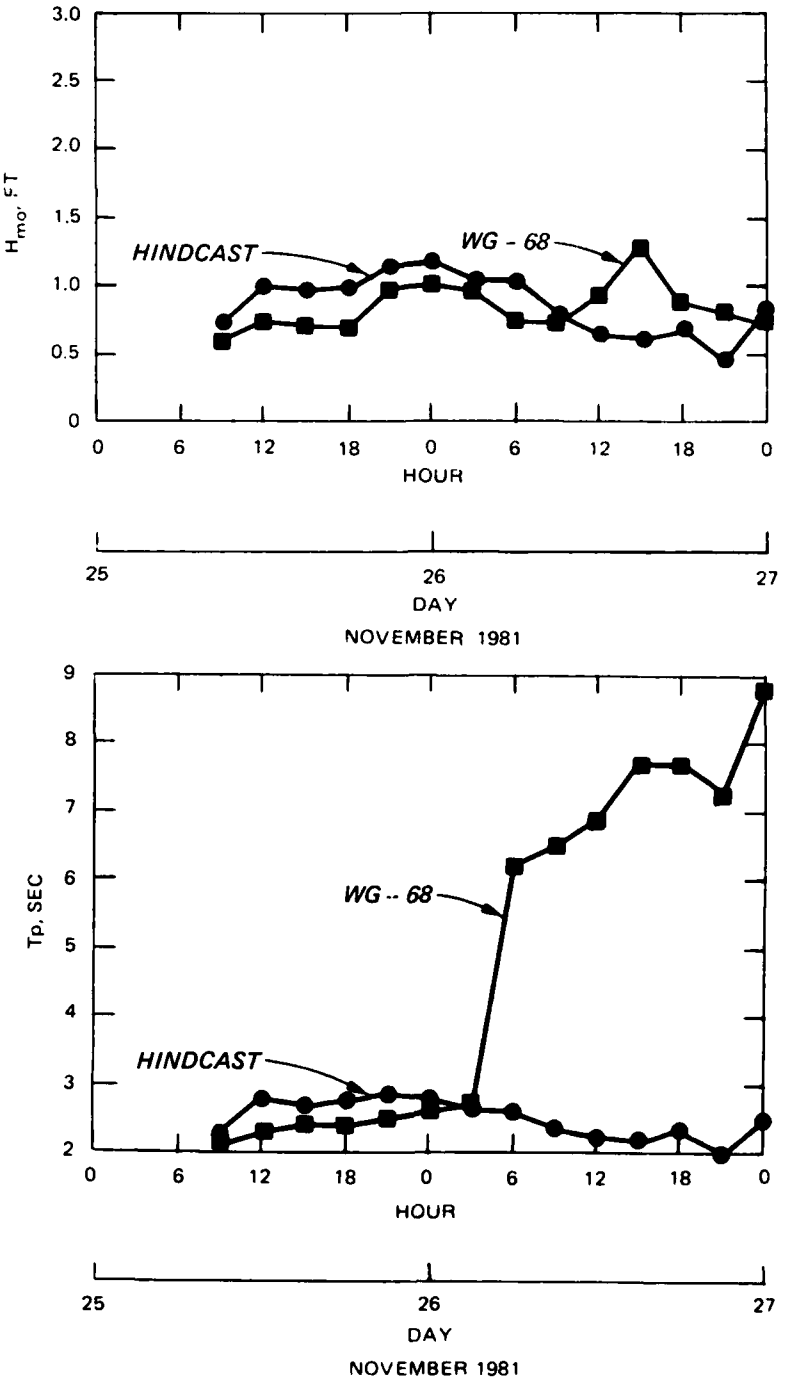

Figure B1. Wave comparisons for Storm 1A at WG-68

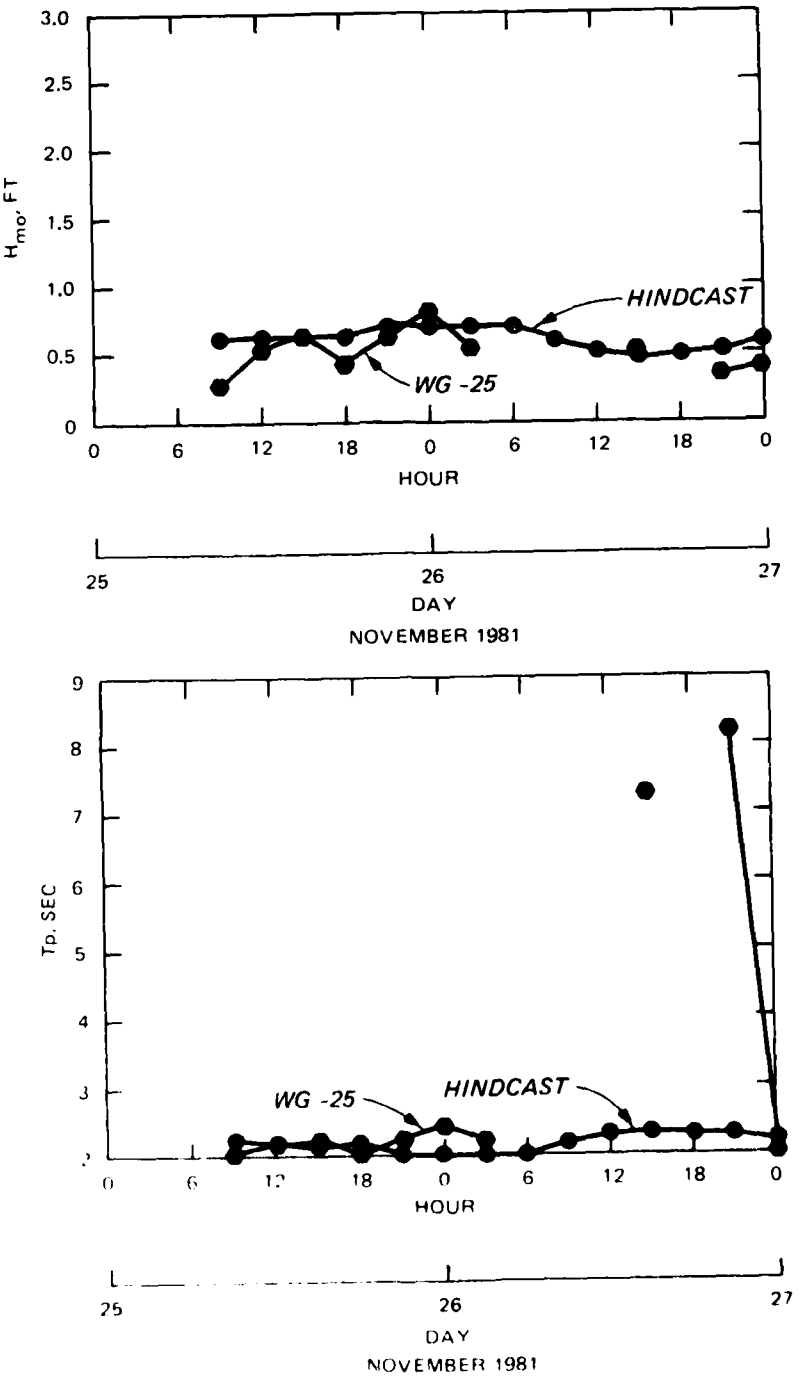

Figure B2. Wave comparisons for Storm 1A at WG-25

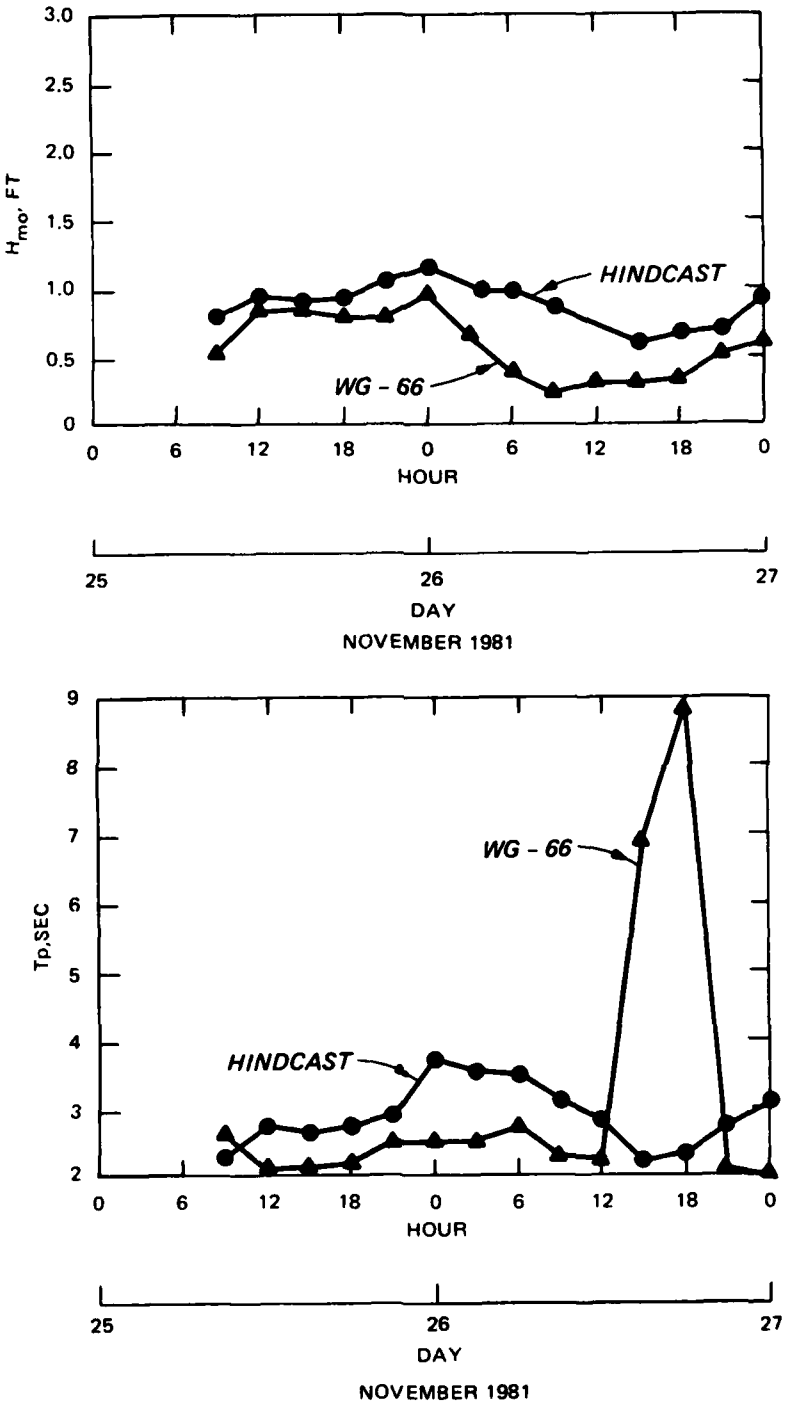

Figure B3. Wave comparisons for Storm 1A at WG-66

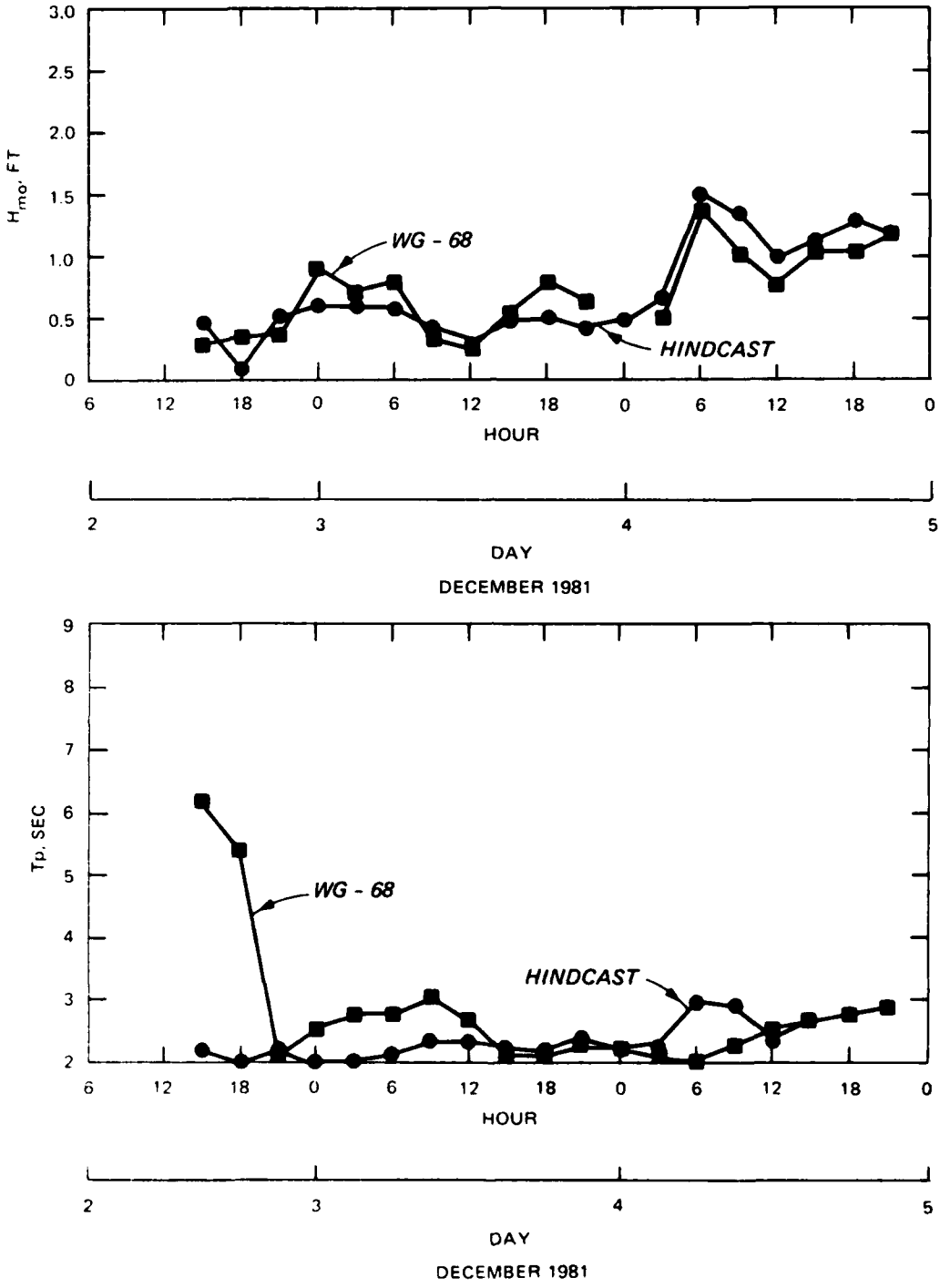

Figure B4. Wave comparisons for Storm 2A at WG-68

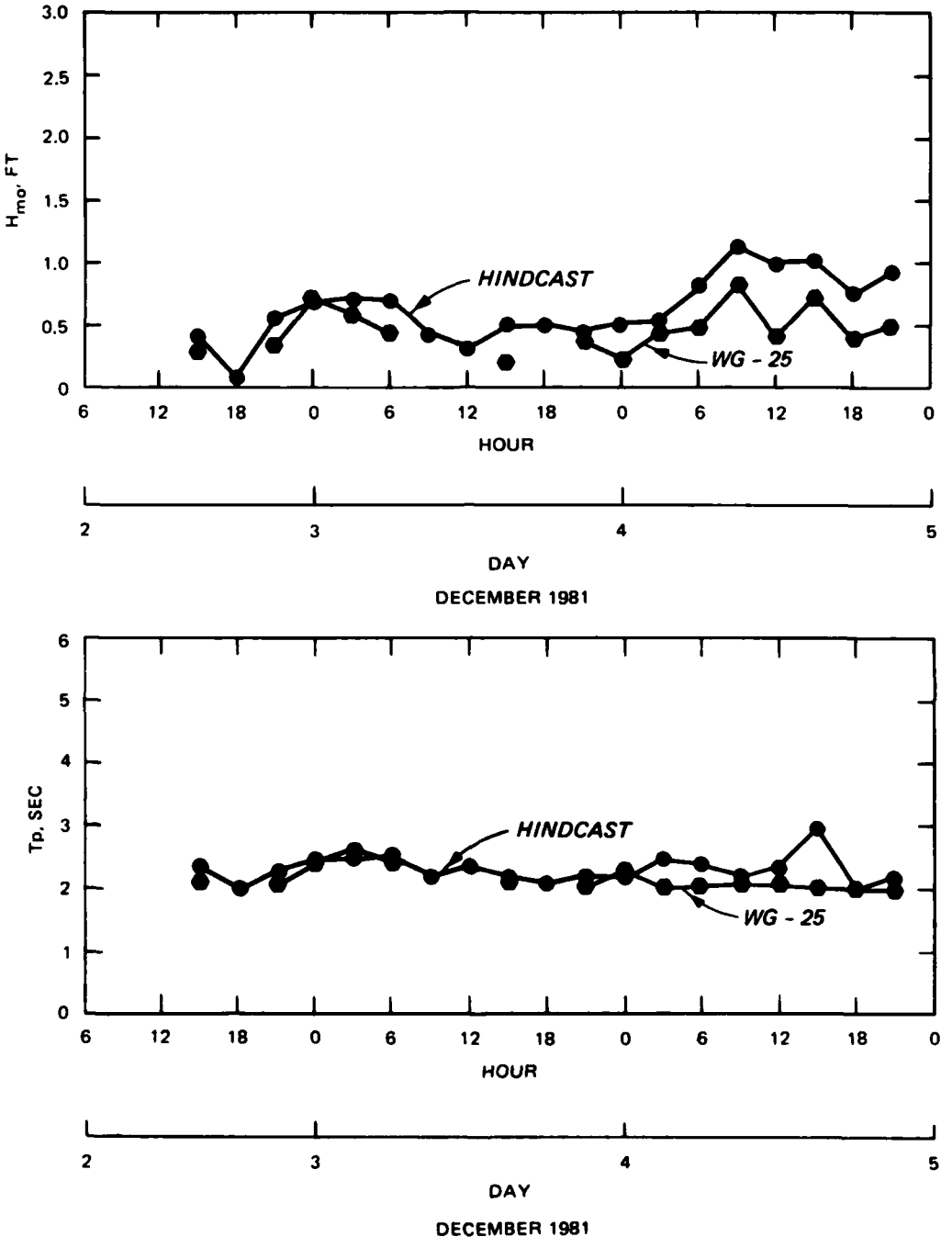

Figure B5. Wave comparisons for Storm 2A at WG-25

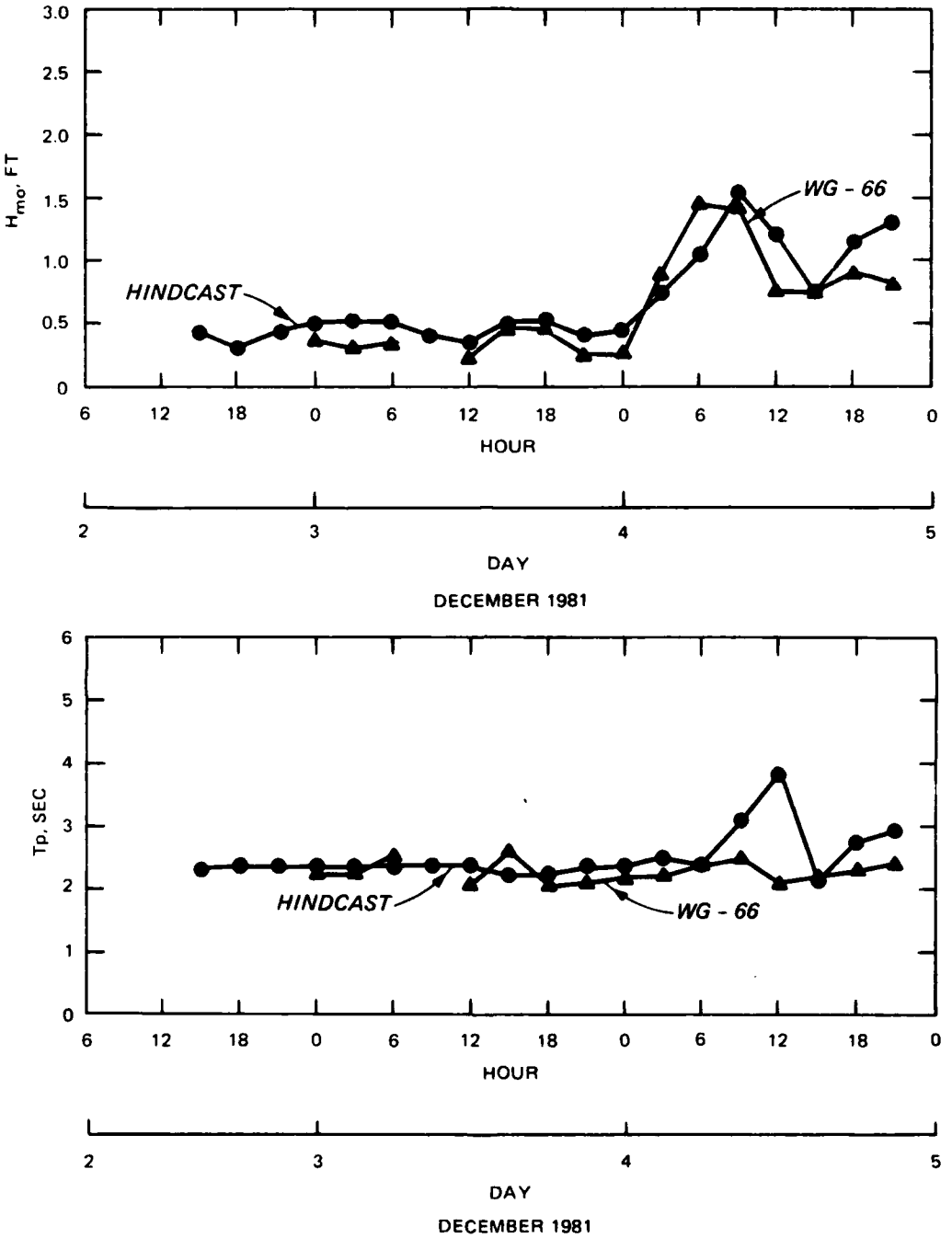

Figure B6. Wave comparisons for Storm 2A at WG-66

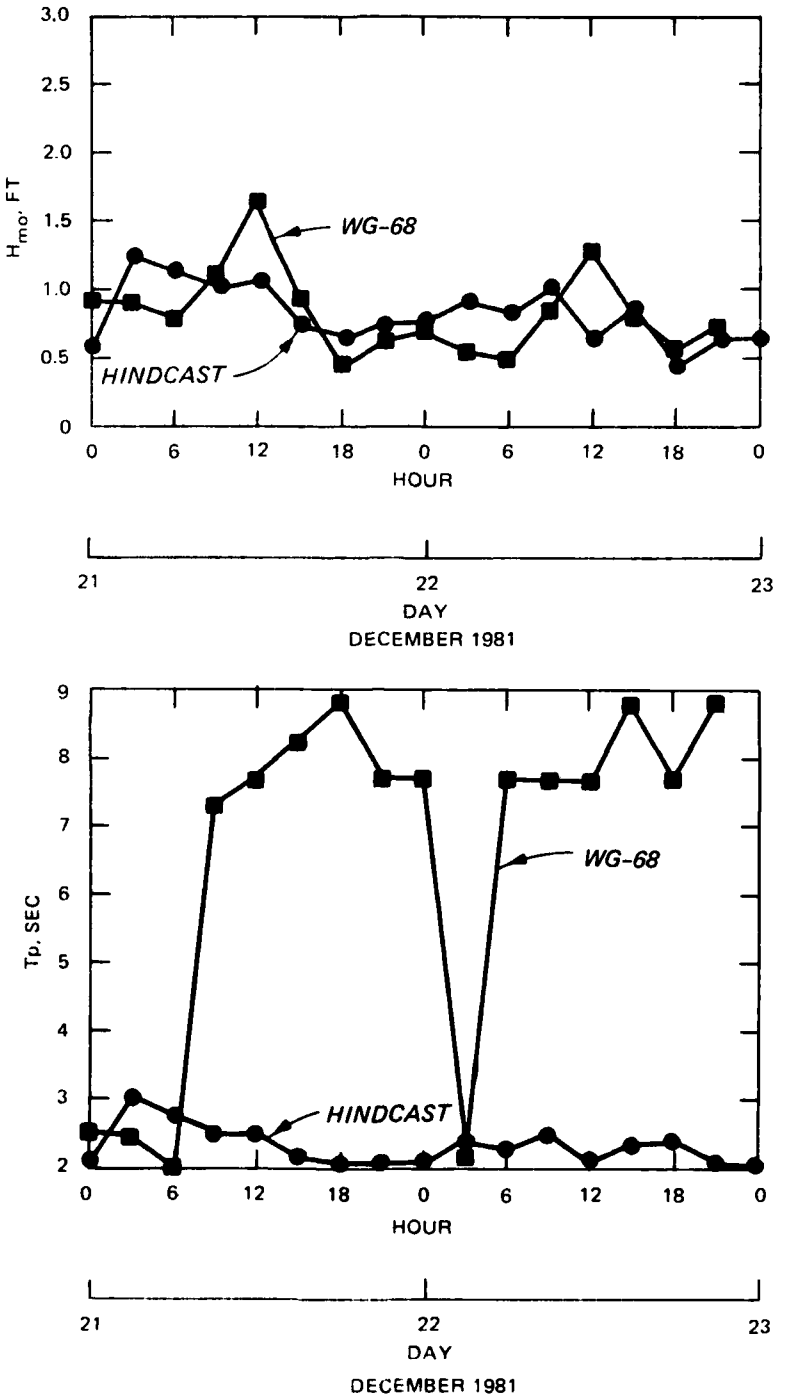

Figure B7. Wave comparisons for Storm 3A at WG-68

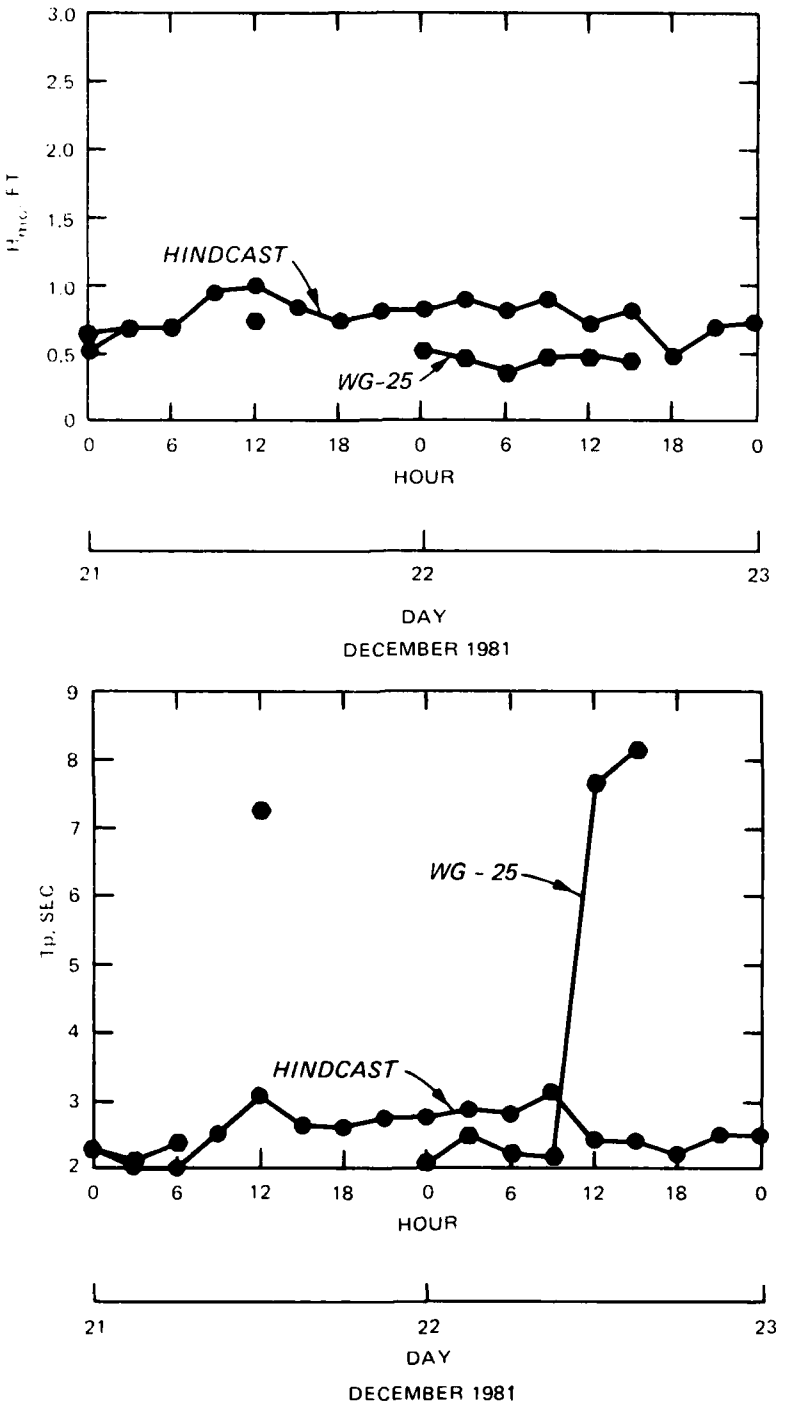

Figure B8. Wave comparisons for Storm 3A at WG-25

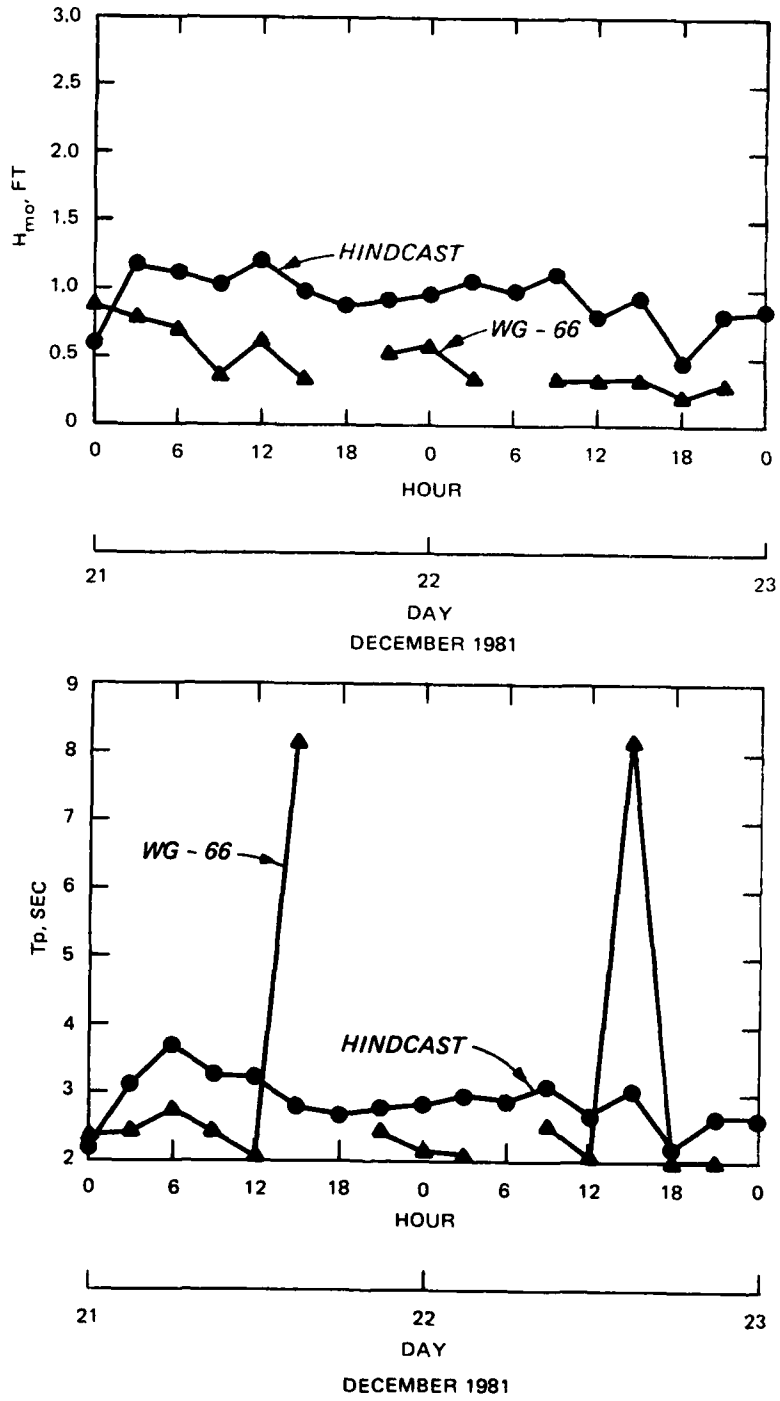

Figure B9. Wave comparisons for Storm 3A at WG-66

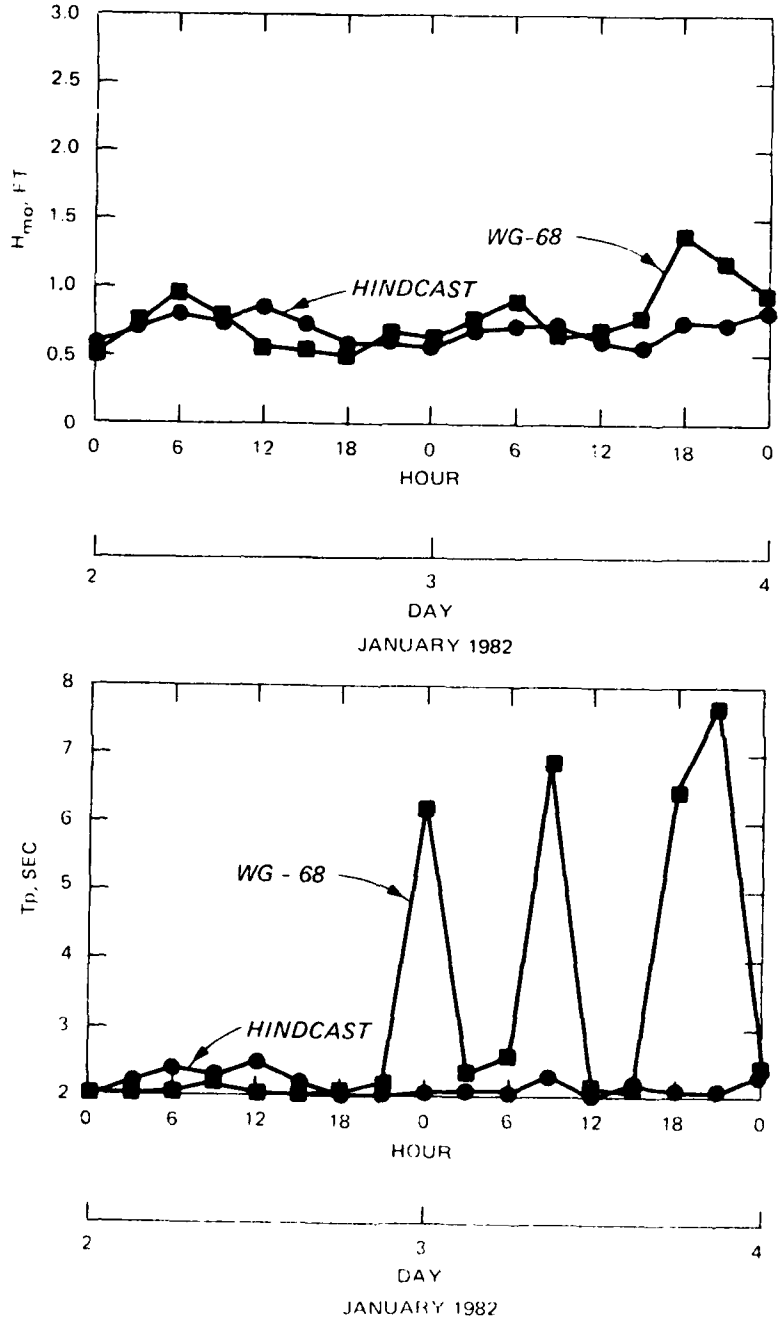

Figure B10. Wave comparisons for Storm 4A at WG-68

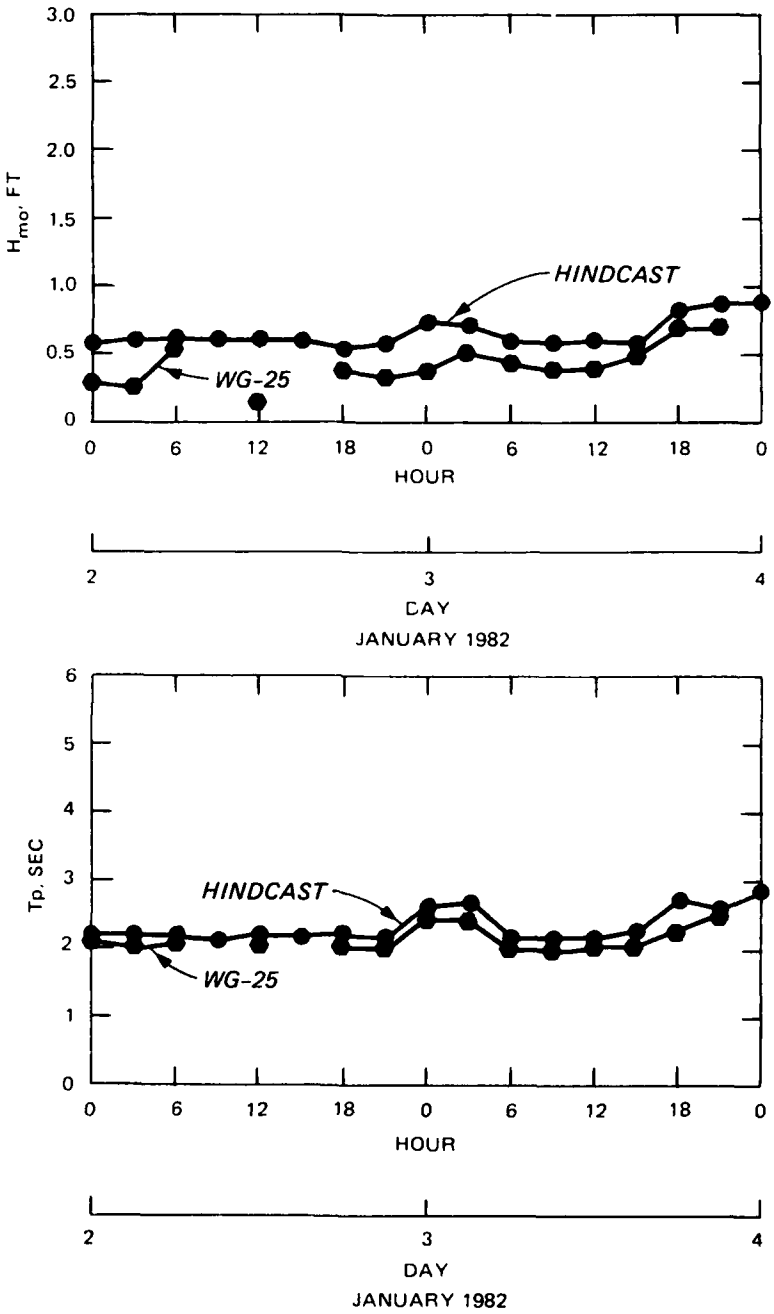

Figure B11. Wave comparisons for Storm 4A at WG-25

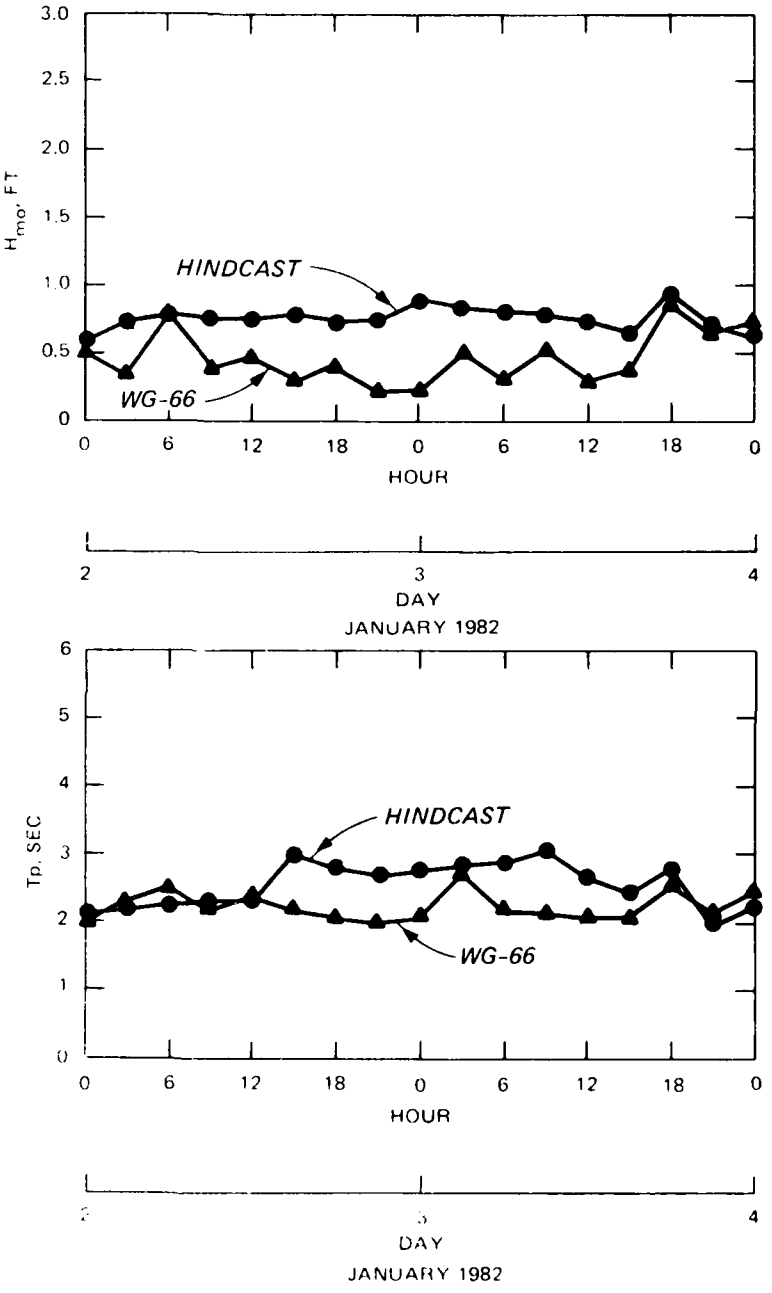

Figure B12. Wave comparisons for Storm 4A at WG-66

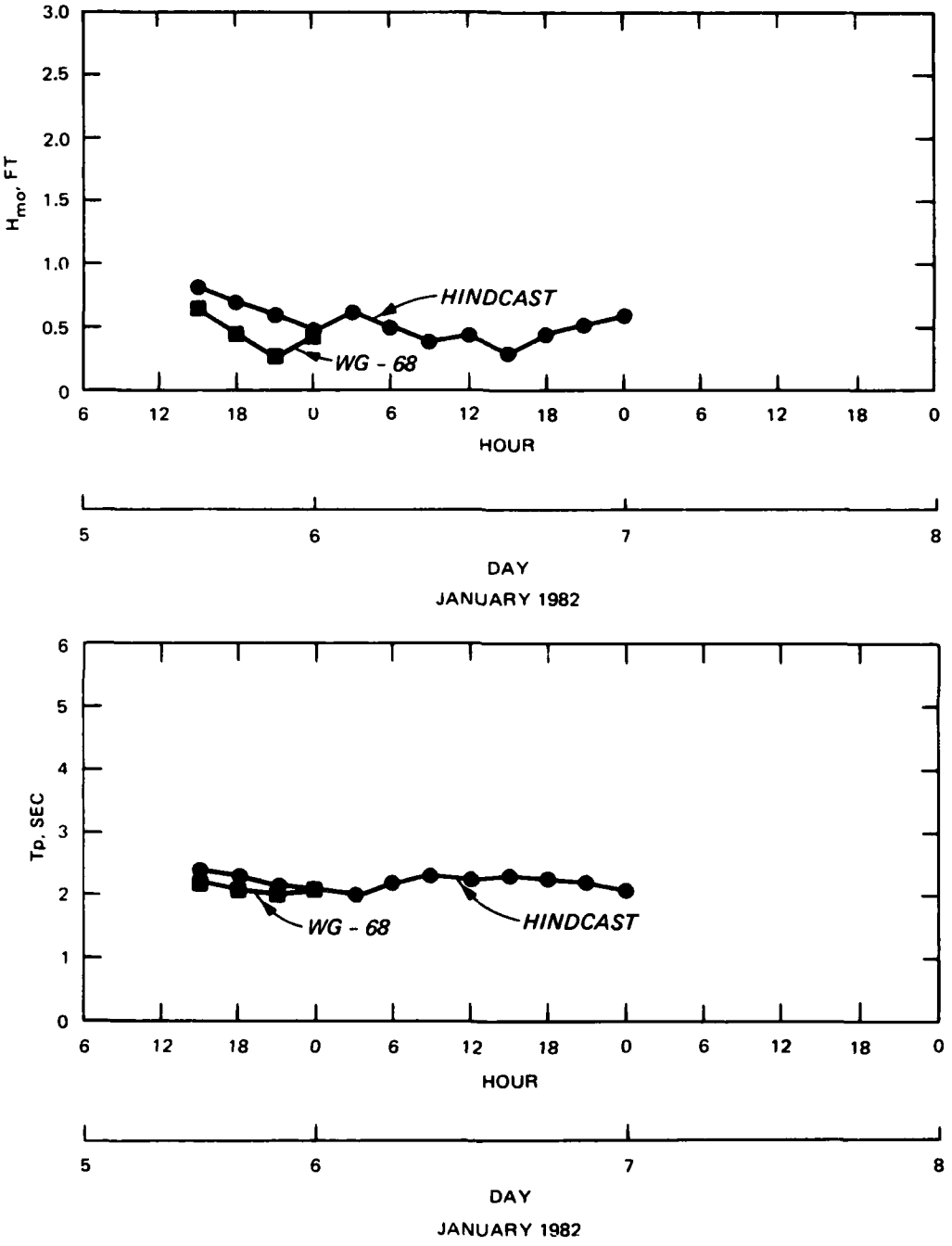

Figure B13. Wave comparisons for Storm 5A at WG-68

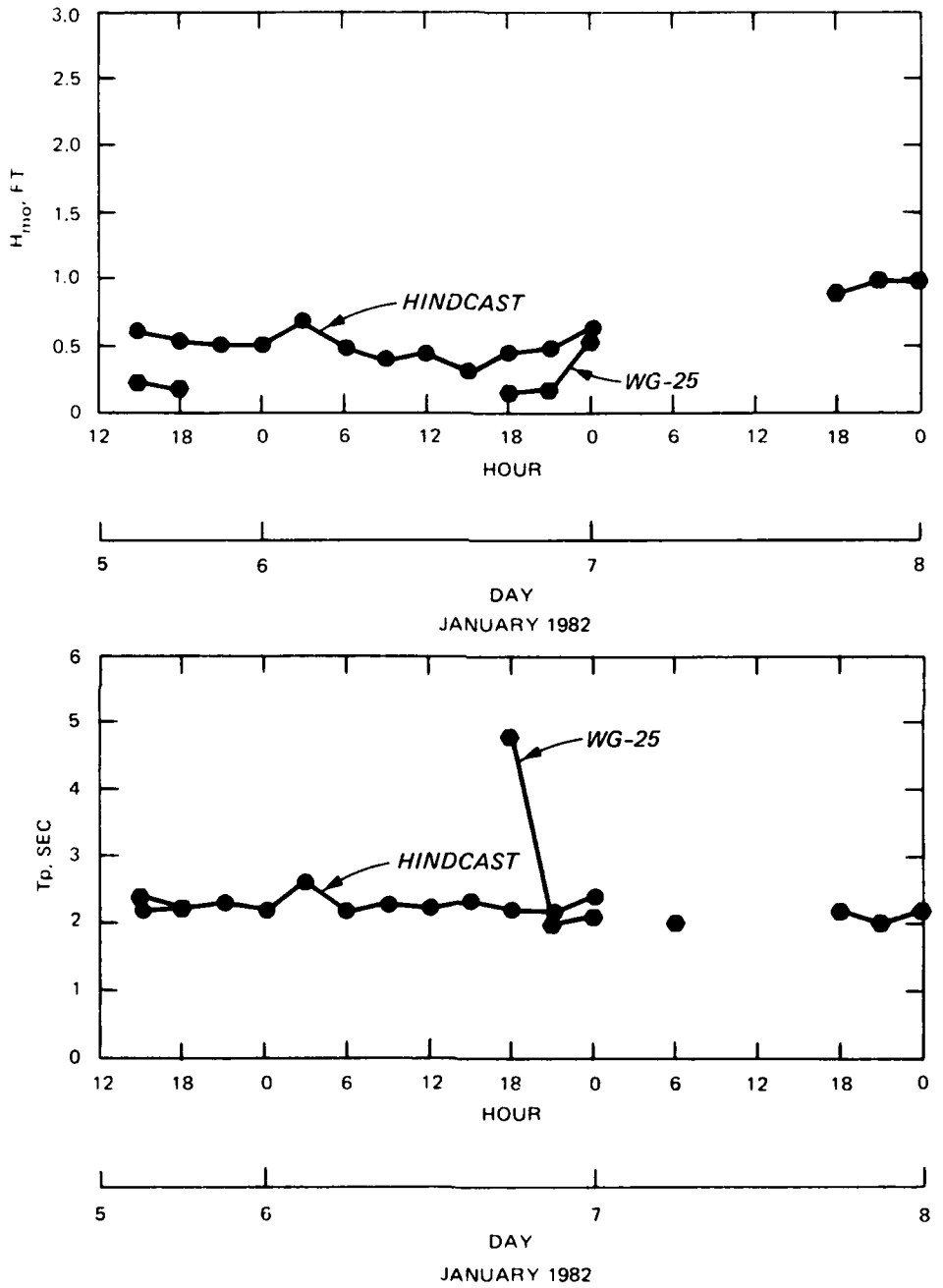

Figure B14. Wave comparisons for Storm 5A at WG-25

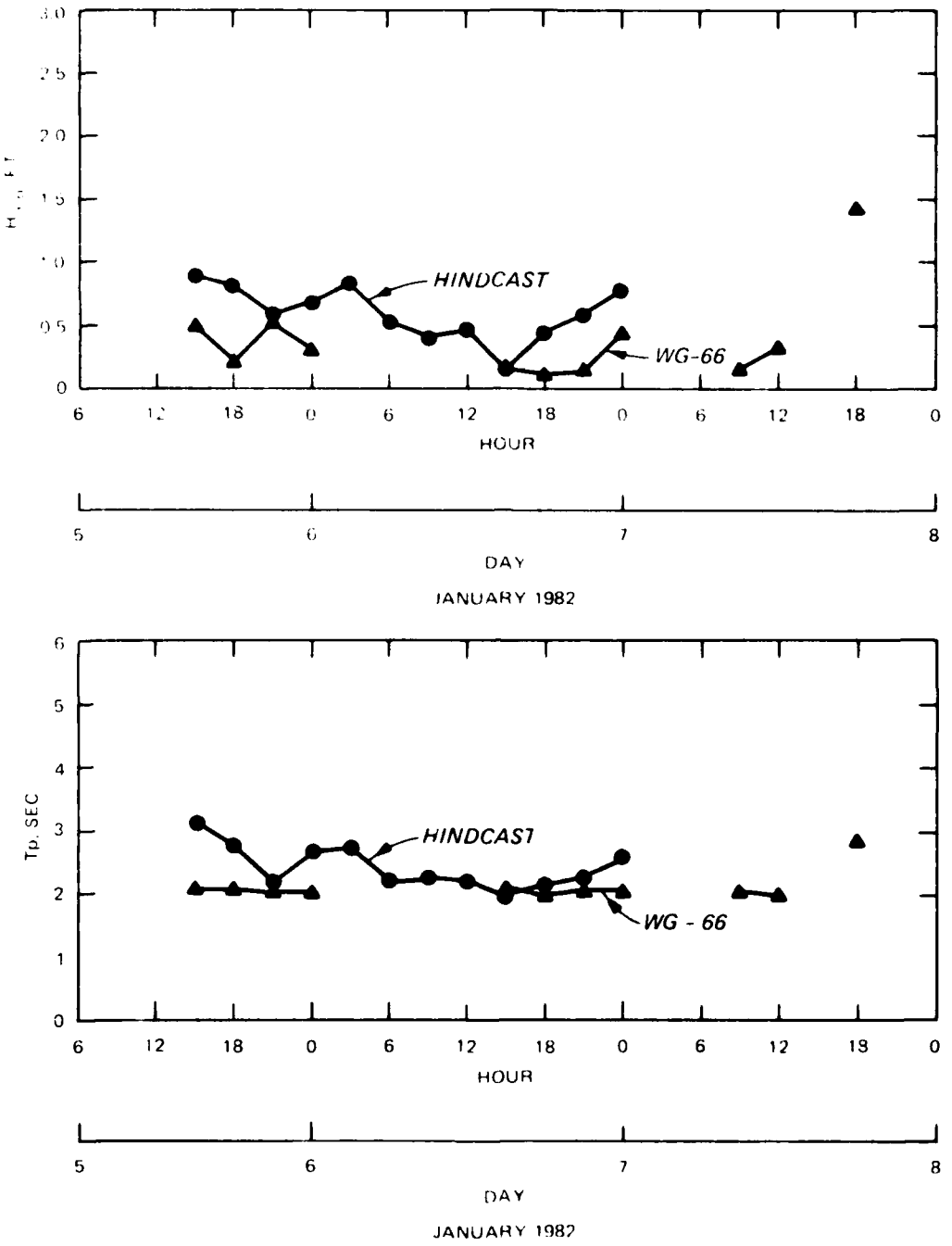

Figure B15. Wave comparisons for Storm 5A at WG-66

END

FILMED

8-85

DTIC